Univerza v Ljubljani
Fakulteta za elektrotehniko

Edi Bulić

Izračun kvazistatičnega magnetnega polja ob dolgih kovinskih zaslonih z metodo robnih elementov

DOKTORSKA DISERTACIJA

Mentor: doc. dr. Anton R. Sinigoj

Ljubljana, 2009

Kazalo

Povzetek

Doktorska disertacija se ukvarja z metodo, ki omogoča analizo učinkovitosti zastiranja magnetnega polja s kovinskimi zasloni v 2D strukturah. Viri primarnega polja so harmonični toki v ravnih vzporednih vodnikih. To polje v delih prostora zastrejo vodnikom vzporedni prevodni in/ali magnetni zasloni. V zaslonih se inducirajo električni toki in v njih se odvija magnetenje. Oba procesa imata reakcijski vpliv na primarno polje – da se slednje s sekundarnim dopolni v novo, rezultančno polje. V disertaciji privzemamo vodnike in zaslone kot linearne cilindre znanih specifičnih električnih prevodnosti in permeabilnosti, okoliški prostor kot prazen, prečne izmere zaslonske strukture pa kot majhne v primerjavi z njeno dolžino, da je upravičena 2D analiza, in neznatne v primerjavi z valovno dolžino, da je zadoščeno pogoju kvazistatičnosti.

Vektorski magnetni potencial v in ob vzporednih prevodnih in/ali magnetnih zaslonih in vodnikih je zapisan kot vsota polj linijskih virov in oblog enojnega in dvojnega sloja na površinah vodnikov in zaslonov. Ti oblogi se izračuna iz sistema sklopljenih robnih integralskih enačb (2.18), izpeljanih z uporabo lastnosti potencialov enojnega in dvojnega sloja, ter enačb tipa (2.21), (2.22), (2.23) in/ali (2.24), ki zajemajo napetostno-tokovne razmere v vodnikih in zaslonih. Za numerični izračun sistema enačb sta uporabljeni metoda robnih elementov oziroma momentna metoda.

V nadaljevanju je podana vrsta verifikacij predlagane metode. Na konkretnih primerih so predstavljene primerjave rezultatov predlagane metode z rezultati analitične metode, hibridne metode, metode tokovnih niti pri nemagnetnih zaslonih, metode ploskovnih tokov pri neprevodnih magnetnih zaslonih in primerjave z rezultati različnih meritev. Pri tem je pomembna predvsem krajevna porazdelitev rezultančnega polja ali faktorja zastiranja, ki je definiran kot razmerje absolutnih vrednosti gostote magnetnega pretoka primarnega in rezultančnega polja.

Analitični rešitvi za primer vodnika ali dvovoda v cevastem zaslonu krožnega preseka omogočata oceno natančnosti predlagane metode. Iz primerjav na slikah 3.2, 3.3 in 3.6

je razvidno odlično ujemanje rezultatov predlagane metode z analitičnima; edina omembe vredna odstopanja so tik ob površinah zaslona. Analitični rešitvi omogočata tudi oceno vpliva velikosti robnih elementov na natančnost predlagane metode (sliki 3.4 in 3.7).

Analitična rešitev obstoja tudi za neskončno širok raven zaslon. Z njo so primerjani rezultati predlagane metode za primer zelo širokega zaslona. Iz diagramov na sliki 3.10 je razvidno dobro ujemanje ob sredini zaslona, odstopanje pa pričakovano narašča s približevanjem krajiščem zaslona.

Pri končno širokem ravnem nemagnetnem zaslonu je opravljena primerjava z rezultati meritev iz literature, z rezultati hibridne metode in metode tokovnih niti (slika 3.12). Ujemanje je zelo dobro pri slednji, ujemanje z merilnimi rezultati pa je dokaj dobro. Pri magnetnem zaslonu je primerjava opravljena z rezultati hibridne metode ter metode ploskovnih tokov (slika 3.13). Pri zadnji je ujemanje pri zaslonih, ki so tudi prevodni, frekvenčno zelo odvisno: pri nizkih frekvencah je izvrstno, pri višjih pa ne, saj metoda ploskovnih tokov ne upošteva induciranih tokov.

V sklepnem delu je podanih nekaj izračunov zastiranja, ki nakažejo tudi možnosti uporabe predlagane metode. Posebej zanimiva je možnost analize povratnega učinka na primarno strukturo, ki je pri problemih zastiranja v literaturi ni zaslediti. Povratni učinek se kaže predvsem v povečanju notranjih izgub primarnih vodov in je izdatnejši, če so zasloni bliže primarnih virov.

Izbrali smo zaslon profila U, ki je prevoden nemagneten ali neprevoden magneten ali prevoden magneten in zastira polje tokovodnika ali dvovoda ali polje trifaznega voda. Na prikazu magnetnih polj okrog zaslona pri tokovodniku na sliki 4.2 in dvovodu na sliki 4.5 sta lepo razvidna osnovna principa zastiranja, indukcija in magnetizacija, ter njun kombiniran učinek. Učinkovitost zaslonov je prikazana na sliki 4.3, v primeru zaslanjanja polja trifaznega voda, ter podobno na sliki 4.4, kjer dodatni vodoravni del sestavljenega zaslona skoraj zapre odprtino profila U. V bližini zaslona je boljši učinek magnetnega, dlje stran prevodnega, povsod pa je od obeh izdatno učinkovitejši prevodni magnetni. Pri zadnjem je še najbolj očitno izboljšanje, ki ga prinese dodatni vodoravni del.

Abstract

In this dissertation we present a method that enables the analysis of the magnetic field shielding efficiency of metal shields in 2D structures. The primary magnetic field source is time-harmonic currents in straight parallel conductors. This field is shielded in some regions by conducting and/or magnetic shields that run parallel to the conductors. Eddy currents are induced in the shields that can also become magnetized. Both processes impact the primary field. The resultant field is a superposition of the primary field and the secondary field. We assume that: 1) the conductors and shields are linear cylinders with known electric conductivities and magnetic permeabilities; 2) the surrounding medium is empty; 3) transverse dimensions of the structure which are small compared to the structure length justify a 2D approach; and 4) these dimensions are negligible compared to the wave length and therefor fulfil quasi-static conditions.

The magnetic vector potential inside and outside the parallel conducting and/or magnetic shields and conductors is expressed by a sum of fields caused by line sources and by equivalent single- and double-layer surface sources on the conductors and the shields. A system of coupled integral equations ((2.18), (2.21), (2.22), (2.23), and/or (2.24)) for unknown distributions of these equivalent sources is derived by implementing the properties of single- and double-layer potentials, and by taking into account voltage-current relations in the conductors and the shields. This system is solved by using the boundary element method and the moment method.

Several verifications of the proposed method are given afterwards. The results obtained with this method on concrete examples are compared with the results of: 1) analytically solvable problems; 2) hybrid method; 3) multiconductor method in the case of the nonmagnetic shields; 4) surface-current method for analysis of the nonconducting magnetic shields; and 5) measurements. The space distributions of the resultant field and shielding factor (that is defined as a ratio between the primary and the resultant magnetic flux density magnitude) are the focus of these comparisons.

In the case of a conductor or bifilar pair of parallel conductors inside a cylindrical shield analytical solution can be used as an estimation of the accuracy of the proposed method. The comparisons in Figures 3.2, 3.3, and 3.6 clearly show that the results obtained with the proposed method are in great accordance with the analytical ones; the only significant deviation is detected close to the shield surfaces. These analytical solutions also enable the estimation of the impact of the length of the boundary elements on the accuracy of the proposed method (Figures 3.4 and 3.7).

The analytical solution is also possible in the case of an infinite planar shield. The results of the proposed method in the case of an exceedingly wide shield are compared with the results of the analytical solution. From the diagrams in Figure 3.10 it is clear that: 1) good accordance in the vicinity of the shield centre is obtained, and 2) discrepancy increases rapidly when approaching either end of the shield.

In the case of the finite-width flat nonmagnetic shield (Figure 3.12) we compare the results with: 1) measurements reported in literature; 2) the hybrid method; and 3) the multiconductor method. The best agreement is achieved with the multiconductor method. The agreement with the measurements is also good. In the case of the magnetic shield the comparison is made with the results of the hybrid method and the surface-current method (Figure 3.13). The agreement with the surface-current method when the shield is conducting depends on the frequency: at low frequencies it is excellent, but at higher frequencies it is not because this method does not consider the induced eddy currents.

Some computations of shielding that demonstrate the possibilities of usage of the proposed method are given in the final part. The possibility of the analysis of the reactive effect on the primary structure, which has not yet been considered in literature for the problems of shielding, can be of great interest. The reactive effect is evident in the increase of the power dissipation and even more if the shields are closer to the conductors.

The shield of a U-shape is chosen. It is either nonmagnetic conducting, magnetic nonconducting, or magnetic conducting, and it shields the field of either one conductor, a pair of conductors, or three-phase conductors. The presentation of the magnetic field around the shield in the vicinity of the conductor (Figure 4.2) or the pair of conductors (Figure 4.5) shows two basic principles of shielding, i.e. induction and magnetization, and their combined effect. The efficiency of shielding is demonstrated in Figure 4.3 for the case of three-phase system, while in Figure 4.4 when an additional shield is placed horizontally below the first one, almost closing the aperture of the first one. The magnetic shield has

better performance in the vicinity of the shield while the conducting shield has better performance farther away. The magnetic conducting shield is more efficient than the first two in either region. The additional shield improves the shielding factor most significantly in the case of a magnetic conducting type of a shield.

Poglavje 1

Uvod

Pričujoča disertacija sodi v področji elektromagnetne kompatibilnosti in numeričnih metod v elektromagnetiki, še natančneje, v področji zaslanjanja magnetnega polja in metode robnih elementov.

1.1 Zaslanjanje magnetnega polja

Zanimanje za zaslanjanje magnetnega polja presega 100 let [1] in je še vedno aktualno. Pomembnost problematike potrjujeta tudi posebni številki revije *IEEE Transactions on Electromagnetic Compatibility* na temo elektromagnetne zaščite v letih 1968 in 1988. Danes narekujejo potrebe po zaslanjanju predvsem kriteriji elektromagnetne kompatibilnosti in standardi za neionizirajoča sevanja.

Zmanjšanje motečega magnetnega polja v določenem območju se v praksi doseže s prestavljanjem virov polja ali/in z nameščanjem ustreznih kovinskih zaslonov [2, 3, 4, 5]. Kadar na vire polja ni možno vplivati, ostanejo zasloni edini izhod. Učinkovitost zaslonov pogojujejo frekvenca, položaj, oblika, velikost, debelina, elektromagnetne lastnosti in električna povezovanja. Zaradi velikega števila vplivnih parametrov je dobro dizajniranje zaslonov možno le z usrezno metodo, ki omogoča izračun magnetnega polja v njihovi okolici, s tem pa tudi oceno učinkovitosti zaslanjanja. V nadaljevanju so v kratkem opisane značilnosti metod, ki jih zasledimo v literaturi.

Najprej so se uporabljale različne analitične ocene učinkovitosti zaslanjanja [1, 6, 7, 8, 9, 10, 11, 12, 13]; te so uporabljive za enostavne geometrije ter postavitve virov in zaslonov. Analitični pristopi kasneje seveda niso zamrli, ampak so se še naprej razvijali in dopolnjevali [14, 15, 2, 16, 17, 18, 19, 20, 21]; njihova prednost je v relativno hitrem izračunu učinkovitosti zaslanjanja. Kot takšni slonijo na določenih privzetkih, poenostavitvah in

omejitvah (npr. okrogli ali ravninski zasloni, idealizirane elektromagnetne lastnosti, nizke frekvence itn.), ki jim v resnici ožajo domeno uporabnosti in mejo natančnosti.

Pomanjkljivosti analitičnih pristopov odpravljajo primerne numerične metode. V elektromagnetiki nasploh je zelo uveljavljena metoda končnih elementov [22, 23]. Pri uporabi te v problemih zastiranja [24] izstopata težavi odprtih mej in tankih zaslonov, ki posledično terjata razmeroma veliko število elementov, obsežen spomin in dolg računalniški čas [17, 5, 25], zato jo v literaturi zasledimo bolj v vlogi verifikacije kakšnega drugačnega pristopa [17, 20, 26, 5, 27]. Podobne ugotovitve veljajo tudi za metodo končnih diferenc [28].

Težave metode končnih elementov rešijo ali omilijo metode, ki slonijo na konceptu virov. Te spadajo v skupino integralskih metod in so pri problemih zaslanjanja dokaj pogosto uporabljene. Primer takšne je metoda tokovnih niti [29, 30, 31], ki je primerna za prevodne, vendar nemagnetne zaslone [3, 26, 32, 33, 34, 27, 35]. Ker se pri njej diskretizira le notranjost zaslonov (ne pa tudi ostalega prostora), je potrebno število neznank precej manjše kot pri metodi končnih elementov. Pri zelo nizkih frekvencah je za magnetne zaslone možno uporabiti tudi magnetostatično aproksimacijo, ki sloni na tokih magnetizacije po površinah zaslonov [36, 31, 32, 33].

Poleg načinov, ki obravnavajo zastiranje polja z dolgimi zasloni, omenimo še nekaj tistih, ki omogočajo analizo 3D problemov. Dela [26, 5, 37] obravnavajo zaslanjanje polja z nemagnetno prevodno ploščo, ki je tako tanka, da se ji sme prirediti žični model. Zastiranje polja s tanko kovinsko steno, na kateri se lahko uporabi impedančni mejni pogoj, obravnava z metodo robnih elementov delo [38], z metodo končnih pa delo [25].

Razen metode končnih elementov, ki ni najbolj primerna za analizo zaslanjanja, je poglavitna pomanjkljivost ostalih pristopov v tem, da so vezani na določene posebne skupine primerov, pri katerih so postavljene kakšne omejitve glede geometrije in/ali snovnih lastnosti zaslonov, medsebojne lege zaslonov in virov polja, frekvence virov in podobno. V praksi se dogaja, da je zaslonov več [2, 17, 39] in da ti ne sodijo nujno v isto skupino, vendar zaenkrat ni zaslediti načina, ki bi bil primeren za vse. Še najbližji temu je kombiniran način [32, str. 31], ki v področju zelo nizkih frekvenc združuje magnetostatično aproksimacijo in koncept tokovnih niti; kot takšen omogoča analizo prevodnih nemagnetnih zaslonov in neprevodnih magnetnih zaslonov.

1.2 Obravnavane zaslonske strukture

Problema zastiranja se bomo lotili na splošni 2D strukturi žic, tokovodnikov in zaslonov (slika 1.1). Viri primarnega magnetnega polja so harmonični toki v vzporednih tokovodnikih in/ali tankih žicah (žice sprejmimo kot tako tanke, da jih smemo obravnavati kot tokovne premice), njim vzporedni pa so prevodni in/ali permeabilni zasloni, ki primarno magnetno polje delno popačijo. Obravnava tokovodnikov in zaslonov (oziroma valjev ali cilindrov) bo pri predlagani metodi poenotena. Nadalje predpostavimo, da so cilindri iz linearnih snovi, kar pomeni, da bomo analizo elektromagnetnega polja opravili v kompleksnem prostoru, vse poljske količine pa razumeli kot kompleksne. Prečne izmere zaslonske strukture so praviloma neznatne v primerjavi z valovno dolžino in dolžino strukture l_0, kar vse govori v prid kvazistatičnega opisa polja v 2D prostoru [40, razdelek 3.3].

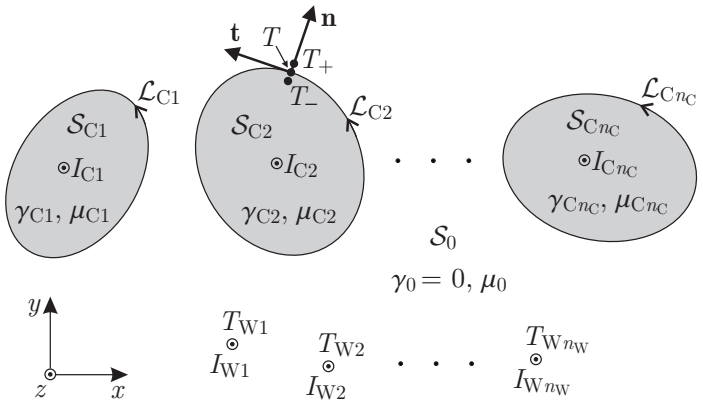

Slika 1.1: Presek splošne strukture zaslonov, tokovodnikov in tankih žic.

Pomeni oznak na sliki 1.1 so sledeči:

- n_W – število žic,
- n_C – število cilindrov,
- $T_{\mathrm{W}1}$, $T_{\mathrm{W}2}$, …, $T_{\mathrm{W}n_\mathrm{W}}$ – točke osi žic,
- $\mathcal{S}_{\mathrm{C}1}$, $\mathcal{S}_{\mathrm{C}2}$, …, $\mathcal{S}_{\mathrm{C}n_\mathrm{C}}$ – preseki cilindrov,
- $\mathcal{L}_{\mathrm{C}1}$, $\mathcal{L}_{\mathrm{C}2}$, …, $\mathcal{L}_{\mathrm{C}n_\mathrm{C}}$ – robovi cilindrov,
- $\mathcal{S}_0$ – zunanjost valjev,
- $\gamma_{\mathrm{C}1}$, $\gamma_{\mathrm{C}2}$, …, $\gamma_{\mathrm{C}n_\mathrm{C}}$ in $\mu_{\mathrm{C}1}$, $\mu_{\mathrm{C}2}$, …, $\mu_{\mathrm{C}n_\mathrm{C}}$ – specifične prevodnosti in permeabilnosti cilindrov,

- $\gamma_0 = 0$ in μ_0 – snovni konstanti zunanjosti valjev,
- $I_{\mathrm{W}1}$, $I_{\mathrm{W}2}$, …, $I_{\mathrm{W}n_{\mathrm{W}}}$ – toki v žicah,
- $I_{\mathrm{C}1}$, $I_{\mathrm{C}2}$, …, $I_{\mathrm{C}n_{\mathrm{C}}}$ – toki v cilindrih,
- $\mathbf{n}$ – eksterna normala cilindra in
- $\mathbf{t}$ – enotski tangentni vektor cilindra, da velja $\mathbf{n} \times \mathbf{t} = \mathbf{e}_z$.

Če je T robna točka nekega cilindra, potem oznaki T_- in T_+ pomenita točki, ki sta njej infinitezimalno blizu: prva še znotraj in druga že zunaj cilindra. Unijo presekov cilindrov označimo s $\mathcal{S} = \mathcal{S}_{\mathrm{C}1} \cup \mathcal{S}_{\mathrm{C}2} \cup \cdots \cup \mathcal{S}_{\mathrm{C}n_{\mathrm{C}}}$, unijo njih robov pa z $\mathcal{L} = \mathcal{L}_{\mathrm{C}1} \cup \mathcal{L}_{\mathrm{C}2} \cup \cdots \cup \mathcal{L}_{\mathrm{C}n_{\mathrm{C}}}$.

1.2.1 Vrednotenje učinka zastiranja

V tem delu je za merljivost učinka zastiranja izbran tako imenovan faktor zastiranja s_B, ki je v splošni točki T definiran [27] s kvocientom absolutnih vrednosti vektorjev gostot pretoka primarnega $\mathbf{B}_0$ in rezultančnega magnetnega polja $\mathbf{B}$:

$$s_B(T) = \frac{|\mathbf{B}_0(T)|}{|\mathbf{B}(T)|}. \tag{1.1}$$

Omenjeno razmerje se pogosto podaja v logaritemski skali; v [17] ga imenujejo učinkovitost zaslanjanja.

1.3 Metoda robnih elementov

Glede na pristop k problemu moremo numerične metode v elektromagnetiki razdeliti na tiste, ki slonijo na diferencialnem, in tiste, ki slonijo na integralskem pristopu. Najbolj znani predstavnici prvega sta metodi končnih elementov in končnih diferenc, zelo razširjena predstavnica drugega pristopa pa je metoda robnih elementov [41, 42, 30, poglavje 9]. V tem delu je prikazana uporaba metode robnih elementov pri problemih zastiranja magnetnega polja. Prvi korak metode je izpeljava robnih integralskih enačb, temu sledi razdelitev integracijskega območja oziroma robov opazovanega področja na množico kratkih segmentov, imenovanih robni elementi, in zapis aproksimacij iskanih robnih funkcij z interpolacijskimi funkcijami. Z uporabo momentne metode [43] se robno integralsko enačbo nato prevede v sistem algebrskih enačb. Za določitev koeficientov matrične enačbe je potrebno izračunati množico integralov po posameznih elementih. Rešitev matrične enačbe da aproksimacijo

iskanih funkcij na robovih opazovanega območja. Iz njih se nadalje izračuna polje kjerkoli v opazovanem območju.

V monografiji [44] iz leta 1978 je C. A. Brebbia prvi vpeljal izraz *metoda robnih elementov* in metodo tudi formaliziral. Od takrat naprej se je začela hitro razvijati in tudi vse bolj uporabljati. Metoda ima v primerjavi z drugimi, ki slonijo na diferencialnem pristopu, kar nekaj prednosti:

- dimenzija problema se zmanjša (diskretizirani so le robovi območij),
- pisana je na kožo problemov odprtih mej,
- natančnost izračuna polja na mejah je ponavadi večja,
- ni potrebno računati polja v celotnem prostoru in
- napake zaradi aproksimacij se v integralnem smislu delno kompenzirajo,

ima pa tudi nekaj pomanjkljivosti:

- uporabljane Greenove funkcije so v nekaterih primerih težko določljive,
- potrebno je veliko število časovno potratnih numeričnih integracij,
- integrali singularnih funkcij terjajo posebno obravnavo,
- rezultirajoče matrike so polne in včasih slabo pogojene ter
- težje je uporabljiva pri kompleksnejših in nelinearnih problemih.

Poglavje 2

Koncept ekvivalentnih ploskovnih virov

Poglavje predstavlja implementacijo metode robnih elementov pri problemih zaslanjanja iz razdelka 1.2. V prvih dveh razdelkih je postavljen matematični model, ki opisuje obravnavan elektromagnetni problem, v tretjem je opisan numerični postopek reševanja integralskih enačb oziroma njihovega preoblikovanja v sistem algebrskih enačb, v zadnjem pa je prikazan način izračuna polja v željenem delu prostora in joulskih moči v cilindrih.

2.1 Robni integralski enačbi

Začnimo z izpeljavo robnih integralskih enačb za porazdelitve gostot ekvivalentnih virov polja na robovih cilindrov ($\mathcal{L}$). Koordinatni sistem (glej sliko 1.1) orientiramo tako, da je os z vzporedna s cilindri. Električni toki vdolž žic, vodnikov in zaslonov določajo z komponento vektorskega magnetnega potenciala: $\mathbf{J} = \mathbf{e}_z J_z(x,y) \Longrightarrow \mathbf{A} = \mathbf{e}_z A_z(x,y)$.

V kvazistatičnih razmerah velja za potencial Poissonova enačba [40, razdelek 8.1],

$$\triangle A_z(T) = \begin{cases} -\mu(T) J_z(T), & T \in \mathcal{S} \\ -\sum\limits_{i=1}^{n_\mathrm{W}} \mu_0 I_{\mathrm{W}i} \delta_{\mathrm{2D}}\big(\overline{TT_{\mathrm{W}i}}\big)\,, & T \in \mathcal{S}_0 \end{cases}, \tag{2.1}$$

kjer so μ permeabilnost, μ_0 permeabilnost praznega prostora, $T(x,y)$ splošna točka, $\overline{TT_{\mathrm{W}i}} = \sqrt{(x_{\mathrm{W}i}-x)^2 + (y_{\mathrm{W}i}-y)^2}$ razdalja med točkama T in $T_{\mathrm{W}i}$ v (prerezni) ravnini x-y in δ_{2D} Diracova 2D funkcija, za katero velja [42, str. 12]

$$\int\limits_{\mathcal{S}_{xy}} \delta_{\mathrm{2D}}\big(\overline{TT'}\big)\mathrm{d}s = \begin{cases} 1, & T' \in \mathcal{S}_{xy} \\ 0, & T' \notin \mathcal{S}_{xy} \end{cases}, \tag{2.2}$$

$\mathcal{S}_{xy}$ je poljubna ploskev v ravnini x-y, T pa integracijska točka. Tokovno gostoto izrazimo z električno poljsko jakostjo $\mathbf{E}$, to pa z vektorskim magnetnim $\mathbf{A}$ ter skalarnim električnim

potencialom V [45],

$$J_z(T) = \gamma(T)E_z(T) = -\mathrm{j}\omega\gamma(T)A_z(T) - \gamma(T)\frac{\partial V(T)}{\partial z}, \tag{2.3}$$

kjer so γ specifična električna prevodnost, $\mathrm{j} = \sqrt{-1}$ imaginarna enota in ω krožna frekvenca harmoničnega polja. Zaradi neodvisnosti polja od koordinate z je $\partial V(T)/\partial z = -U(T)/l_0$. $U(T)$ je razlika električnih potencialov med začetkom in koncem cilindra v $T \in \mathcal{S}$ in je lastna posameznemu cilindru, l_0 pa je razdalja med koncema. Za tokovno gostoto dobimo izraz

$$J_z(T) = -\mathrm{j}\omega\gamma(T)A_z(T) + \gamma(T)\frac{U(T)}{l_0}. \tag{2.4}$$

Ko enačbo (2.4) zanesemo v Poissonovo enačbo (2.1), dobimo

$$\triangle A_z(T) + k^2(T)A_z(T) = -\mu(T)\gamma(T)\frac{U(T)}{l_0}, \quad T \in \mathcal{S} \tag{2.5a}$$

$$\triangle A_z(T) = -\sum_{i=1}^{n_\mathrm{W}} \mu_0 I_{\mathrm{W}i}\delta_{2\mathrm{D}}\big(\overline{TT_{\mathrm{W}i}}\big), \quad T \in \mathcal{S}_0, \tag{2.5b}$$

kjer je $k = \sqrt{-\mathrm{j}\omega\mu\gamma}$ valovno število cilindra, ki je v vlogi tokovodnika ali zaslona.

Reševanja diferencialnih enačb (2.5) se lotimo z metodo robnih elementov [41, 42, 30]. V ta namen uporabimo Greenovi funkciji za notranjost in zunanjost cilindrov[1]

$$g(T,T') = \frac{1}{4\mathrm{j}}H_0^{(2)}\big(k_T\overline{TT'}\big) \tag{2.7a}$$

$$g_0(T,T') = -\frac{1}{2\pi}\ln\overline{TT'}, \tag{2.7b}$$

kjer je $H_0^{(2)}$ Hankelova funkcija druge vrste ničtega reda. Da bi Greenove funkcije tipa (2.7a) ne pisali posebej za vsak cilinder, smo uporabili kar oznako k_T, ki naj pomeni valovno število tistega cilindra, ki mu pripada točka T. Greenovi funkciji v (2.7) sta rešitvi Helmholtzove oziroma Poissonove enačbe za polje linijskega vira $\delta_{2\mathrm{D}}\big(\overline{TT'}\big)$ v točki T' [47, razdelek 1.6]:

$$\triangle g(T,T') + k_T^2 g(T,T') = -\delta_{2\mathrm{D}}\big(\overline{TT'}\big) \tag{2.8a}$$

$$\triangle g_0(T,T') = -\delta_{2\mathrm{D}}\big(\overline{TT'}\big)\,. \tag{2.8b}$$

[1] V primeru zaslonske strukture, ki je vzporedna s površino zemlje, upoštevamo vpliv zemlje z naslednjo Greenovo funkcijo [46], [31, razdelek 30]:

$$g_{\mathrm{g}0}(T,T') \simeq \frac{1}{2\pi}\ln\frac{d_\mathrm{C}e^{-\mathrm{j}\pi/4}}{\overline{TT'}}, \tag{2.6}$$

kjer je $d_\mathrm{C} \simeq 1{,}85/|k_\mathrm{g}|$ Carsonova razdalja, k_g pa je valovno število zemlje. Kadar d_C močno presega razdaljo $\overline{TT'}$, je vpliv zemlje zanemarljiv. Pri nižjih frekvencah je ta pogoj vsekakor izpoljen.

V drugo Greenovo formulo za območje valjev ($\mathcal{S}$) vstavimo Greenovo funkcijo g in z-komponento A_z magnetnega potenciala, za območje zunanjosti valjev ($\mathcal{S}_0$) pa funkciji g_0 in A_z,

$$\int\limits_{\mathcal{S}} \Big(g(T,T')\triangle A_z(T) - A_z(T)\triangle g(T,T') \Big) \mathrm{d}s = \oint\limits_{\mathcal{L}} \left(g(T,T')\frac{\partial A_z(T_-)}{\partial n} - A_z(T_-)\frac{\partial g(T,T')}{\partial n} \right) \mathrm{d}l \quad (2.9a)$$

$$\int\limits_{\mathcal{S}_0} \Big(g_0(T,T')\triangle A_z(T) - A_z(T)\triangle g_0(T,T') \Big) \mathrm{d}s = \oint\limits_{\mathcal{L}} \left(-g_0(T,T')\frac{\partial A_z(T_+)}{\partial n} + A_z(T_+)\frac{\partial g_0(T,T')}{\partial n} \right) \mathrm{d}l, \quad (2.9b)$$

kjer je T integracijska, T' pa splošna točka[2]. Na levih straneh enačb (2.9) upoštevajmo enačbi (2.5) in (2.8) in dobimo:

$$\int\limits_{\mathcal{S}} \left(A_z(T)\delta_{2\mathrm{D}}\big(\overline{TT'}\big) - \mu(T)\gamma(T)\frac{U(T)}{l_0} g(T,T') \right) \mathrm{d}s = \oint\limits_{\mathcal{L}} \left(g(T,T')\frac{\partial A_z(T_-)}{\partial n} - A_z(T_-)\frac{\partial g(T,T')}{\partial n} \right) \mathrm{d}l \quad (2.11a)$$

$$-\sum_{i=1}^{n_\mathrm{W}} g_0(T_{\mathrm{W}i},T')\mu_0 I_{\mathrm{W}i} + \int\limits_{\mathcal{S}_0} A_z(T)\delta_{2\mathrm{D}}\big(\overline{TT'}\big)\,\mathrm{d}s = \oint\limits_{\mathcal{L}} \left(-g_0(T,T')\frac{\partial A_z(T_+)}{\partial n} + A_z(T_+)\frac{\partial g_0(T,T')}{\partial n} \right) \mathrm{d}l. \quad (2.11b)$$

Nadalje upoštevajmo še mejna pogoja za tangencialni komponenti magnetne, $H_t = B_t/\mu = (-\partial A_z/\partial n)/\mu$, in električne poljske jakosti, $E_z = -\mathrm{j}\omega A_z - \partial V/\partial z = -\mathrm{j}\omega A_z + U/l_0$, na robovih valjev,

$$H_t(T_+) = H_t(T_-) \quad \Longrightarrow \quad -\frac{\partial A_z(T_+)}{\partial n} = -\frac{1}{\mu_\mathrm{r}(T_-)}\frac{\partial A_z(T_-)}{\partial n} = \alpha_1(T) \quad (2.12a)$$

$$E_z(T_+) = E_z(T_-) \quad \Longrightarrow \quad A_z(T_+) = A_z(T_-) = \alpha_2(T), \quad (2.12b)$$

[2]Greenovi funkciji in njuna normalna odvoda so čez rob $\mathcal{L}$ zvezni,

$$\lim_{T_-\to T} g(T_-,T') = g(T,T') \qquad \lim_{T_+\to T} g_0(T_+,T') = g_0(T,T') \quad (2.10a)$$

$$\lim_{T_-\to T} \frac{\partial g(T_-,T')}{\partial n} = \frac{\partial g(T,T')}{\partial n} \qquad \lim_{T_+\to T} \frac{\partial g_0(T_+,T')}{\partial n} = \frac{\partial g_0(T,T')}{\partial n}, \quad (2.10b)$$

kar smo v enačbah tudi upoštevali.

kjer je μ_r relativna permeabilnost, pa dobimo:

$$\int\limits_{\mathcal{S}} \left(A_z(T)\delta_{2\mathrm{D}}\big(\overline{TT'}\big) - \mu(T)\gamma(T)\frac{U(T)}{l_0}g(T,T') \right) \mathrm{d}s = \oint\limits_{\mathcal{L}} \left(-\mu_\mathrm{r}(T_-)\alpha_1(T)g(T,T') - \alpha_2(T)\frac{\partial g(T,T')}{\partial n} \right) \mathrm{d}l \quad (2.13a)$$

$$-\sum_{i=1}^{n_\mathrm{W}} g_0(T_{\mathrm{W}i},T')\mu_0 I_{\mathrm{W}i} + \int\limits_{\mathcal{S}_0} A_z(T)\delta_{2\mathrm{D}}\big(\overline{TT'}\big)\,\mathrm{d}s = \oint\limits_{\mathcal{L}} \left(\alpha_1(T)g_0(T,T') + \alpha_2(T)\frac{\partial g_0(T,T')}{\partial n} \right) \mathrm{d}l. \quad (2.13b)$$

Zatem točko T' v enačbi (2.13a) limitirajmo proti robu $\mathcal{L}$ od zunaj ($T' \to T'_+$), v enačbi (2.13b) pa od znotraj ($T' \to T'_-$). Pri tem upoštevajmo rezultate[3] iz [47, razdelek 3.1] oziroma lastnosti potenciala enojnega in dvojnega sloja [42, str. 20-21] iz [31, razdelka 11 in 15]. Končno dobimo

$$\alpha_2(T') + 2\oint\limits_{\mathcal{L}} \left(\mu_\mathrm{r}(T_-)\alpha_1(T)g(T,T') + \alpha_2(T)\frac{\partial g(T,T')}{\partial n} \right) \mathrm{d}l - 2\int\limits_{\mathcal{S}} \mu(T)\gamma(T)\frac{U(T)}{l_0}g(T,T'_+)\mathrm{d}s = 0, \quad T' \in \mathcal{L} \quad (2.15a)$$

$$\alpha_2(T') - 2\oint\limits_{\mathcal{L}} \left(\alpha_1(T)g_0(T,T') + \alpha_2(T)\frac{\partial g_0(T,T')}{\partial n} \right) \mathrm{d}l = 2\sum_{i=1}^{n_\mathrm{W}} g_0(T_{\mathrm{W}i},T')\mu_0 I_{\mathrm{W}i}, \quad T' \in \mathcal{L}. \quad (2.15b)$$

Integrale po presekih valjev ($\mathcal{S} = \mathcal{S}_{\mathrm{C}1} \cup \mathcal{S}_{\mathrm{C}2} \cup \cdots \cup \mathcal{S}_{\mathrm{C}n_\mathrm{C}}$) preoblikujmo v krivuljne po njih robovih s pomočjo Gaussovega stavka in z upoštevanjem enačbe (2.8a). Za j-ti valj

[3]

$$\oint\limits_{\mathcal{L}} \left(\mu_\mathrm{r}(T_-)\alpha_1(T)g(T,T'_+) + \alpha_2(T)\frac{\partial g(T,T'_+)}{\partial n} \right) \mathrm{d}l = \frac{\alpha_2(T')}{2} + \oint\limits_{\mathcal{L}} \left(\mu_\mathrm{r}(T_-)\alpha_1(T)g(T,T') + \alpha_2(T)\frac{\partial g(T,T')}{\partial n} \right) \mathrm{d}l, \quad T' \in \mathcal{L}$$

$$\oint\limits_{\mathcal{L}} \left(\alpha_1(T)g_0(T,T'_-) + \alpha_2(T)\frac{\partial g_0(T,T'_-)}{\partial n} \right) \mathrm{d}l = -\frac{\alpha_2(T')}{2} + \oint\limits_{\mathcal{L}} \left(\alpha_1(T)g_0(T,T') + \alpha_2(T)\frac{\partial g_0(T,T')}{\partial n} \right) \mathrm{d}l, \quad T' \in \mathcal{L}.$$

dobimo

$$\begin{aligned}\int\limits_{\mathcal{S}_{\mathrm{C}j}} \mu(T)\gamma(T)\frac{U(T)}{l_0}g(T,T'_+)\mathrm{d}s =& \mu_{\mathrm{C}j}\gamma_{\mathrm{C}j}\frac{U_{\mathrm{C}j}}{l_0}\int\limits_{\mathcal{S}_{\mathrm{C}j}} g(T,T'_+)\mathrm{d}s \\ =& \mu_{\mathrm{C}j}\gamma_{\mathrm{C}j}\frac{U_{\mathrm{C}j}}{l_0}\int\limits_{\mathcal{S}_{\mathrm{C}j}} \frac{1}{k_T^2}\left(-\boldsymbol{\nabla}\cdot\boldsymbol{\nabla}g(T,T'_+) - \delta_{\mathrm{2D}}\big(\overline{TT'_+}\big)\right)\mathrm{d}s \\ =& \mu_{\mathrm{C}j}\gamma_{\mathrm{C}j}\frac{U_{\mathrm{C}j}}{l_0}\frac{-1}{k_{\mathrm{C}j}^2}\oint\limits_{\mathcal{L}_{\mathrm{C}j}} \frac{\partial g(T,T'_+)}{\partial n}\mathrm{d}l \\ =& \frac{1}{\mathrm{j}\omega}\oint\limits_{\mathcal{L}_{\mathrm{C}j}} \frac{U(T)}{l_0}\frac{\partial g(T,T'_+)}{\partial n}\mathrm{d}l, \end{aligned} \tag{2.16}$$

$U_{\mathrm{C}j}$ je razlika električnega potenciala med začetkom in koncem j-tega valja, $k_{\mathrm{C}j} = \sqrt{-\mathrm{j}\omega\mu_{\mathrm{C}j}\gamma_{\mathrm{C}j}}$ pa njegovo valovno število. Kar velja za en cilinder, velja tudi za presek $\mathcal{S}$ z robom $\mathcal{L}$:

$$\int\limits_{\mathcal{S}} \mu(T)\gamma(T)\frac{U(T)}{l_0}g(T,T'_+)\mathrm{d}s = \frac{1}{\mathrm{j}\omega}\oint\limits_{\mathcal{L}} \frac{U(T)}{l_0}\frac{\partial g(T,T'_+)}{\partial n}\mathrm{d}l. \tag{2.17}$$

Z upoštevanjem tega v enačbi (2.15) dobimo končni sklopljeni robni integralski enačbi za funkciji α_1 in α_2:

$$\begin{aligned}\alpha_2(T') + 2\oint\limits_{\mathcal{L}} \left(\mu_{\mathrm{r}}(T_-)\alpha_1(T)g(T,T') + \alpha_2(T)\frac{\partial g(T,T')}{\partial n}\right)\mathrm{d}l \\ + \frac{2\mathrm{j}}{\omega}\oint\limits_{\mathcal{L}} \frac{U(T)}{l_0}\frac{\partial g(T,T'_+)}{\partial n}\mathrm{d}l = 0, \quad T' \in \mathcal{L}\end{aligned} \tag{2.18a}$$

$$\begin{aligned}\alpha_2(T') - 2\oint\limits_{\mathcal{L}} \left(\alpha_1(T)g_0(T,T') + \alpha_2(T)\frac{\partial g_0(T,T')}{\partial n}\right)\mathrm{d}l \\ = 2\sum_{i=1}^{n_{\mathrm{W}}} g_0(T_{\mathrm{W}i},T')\mu_0 I_{\mathrm{W}i}, \quad T' \in \mathcal{L}.\end{aligned} \tag{2.18b}$$

Funkciji α_1 in α_2 sta gostoti oblog enojnega in dvojnega sloja in predstavljata nekakšna ekvivalentna ploskovna vira. Skozi njiju se odražajo vplivi konduktivnih tokov in magnetizacij v cilindrih.

2.1.1 Matrična oblika robnih integralskih enačb

Enačbi (2.18) moremo v jedrnatejši obliki zapisati z matrično notacijo. V ta namen vpeljimo okrajšave za matriko jeder integralskih enačb ($\underline{\mathbf{K}}$) in za stolpčne vektorje gostot

ekvivalentnih ploskovnih virov ($\underline{\boldsymbol{\alpha}}$), jeder integralov ($\underline{\mathbf{K}}_U$), ki vsebujejo potencialno razliko U, in desnih strani ($\underline{\mathbf{G}}_\mathrm{W}$):

$$\underline{\mathbf{K}}(T,T') = \begin{bmatrix} K_{11}(T,T') & K_{12}(T,T') \\ K_{21}(T,T') & K_{22}(T,T') \end{bmatrix} = \begin{bmatrix} 2\mu_\mathrm{r}(T_-)g(T,T') & 2\partial g(T,T')/\partial n \\ -2g_0(T,T') & -2\partial g_0(T,T')/\partial n \end{bmatrix} \tag{2.19a}$$

$$\underline{\boldsymbol{\alpha}}(T) = \begin{bmatrix} \alpha_1(T) & \alpha_2(T) \end{bmatrix}^\mathrm{T} \tag{2.19b}$$

$$\underline{\mathbf{K}}_U(T,T'_+) = \begin{bmatrix} K_{U1}(T,T'_+) & 0 \end{bmatrix}^\mathrm{T} = \begin{bmatrix} \dfrac{2\mathrm{j}}{\omega l_0}\dfrac{\partial g(T,T'_+)}{\partial n} & 0 \end{bmatrix}^\mathrm{T} \tag{2.19c}$$

$$\underline{\mathbf{G}}_\mathrm{W}(T') = \begin{bmatrix} 0 & G_\mathrm{W2}(T') \end{bmatrix}^\mathrm{T} = \begin{bmatrix} 0 & 2\sum\limits_{i=1}^{n_\mathrm{W}} g_0(T_{\mathrm{W}i},T')\mu_0 I_{\mathrm{W}i} \end{bmatrix}^\mathrm{T}. \tag{2.19d}$$

Matrična oblika sklopljenih robnih integralskih enačb (2.18) je pri $\underline{\mathbf{C}}_{\alpha 2} = \begin{bmatrix} 0 & 1 \\ 0 & 1 \end{bmatrix}$ sledeča:

$$\underline{\mathbf{C}}_{\alpha 2}\cdot\underline{\boldsymbol{\alpha}}(T') + \oint_{\mathcal{L}} \underline{\mathbf{K}}(T,T')\cdot\underline{\boldsymbol{\alpha}}(T)\mathrm{d}l + \oint_{\mathcal{L}} \underline{\mathbf{K}}_U(T,T'_+)U(T)\mathrm{d}l = \underline{\mathbf{G}}_\mathrm{W}(T'), \quad T'\in\mathcal{L}. \tag{2.20}$$

Pridobljena matrična integralska enačba za vektor $\underline{\boldsymbol{\alpha}}$ gostot ekvivalentnih ploskovnih virov je Fredholmova druge vrste [48, str. 983].

2.2 Sistem sklopljenih integralskih enačb

V integralski enačbi (2.20) so razen vektorja gostot ekvivalentnih ploskovnih virov $\underline{\boldsymbol{\alpha}}$ neznanke tudi potencialne razlike U oziroma $U_{\mathrm{C}1}, U_{\mathrm{C}2}, \ldots, U_{\mathrm{C}n_\mathrm{C}}$ med začetki in konci posameznih valjev. Za enolično rešitev potrebujemo še n_C dodatnih enačb. Te zapišemo glede na to, kako so cilindri ozemljeni [49, razdelek 3.20] in/ali med seboj električno povezani.

Če je npr. j-ti cilinder v vlogi zaslona, ki ima konca odprta ali je le enostransko ozemljen, je inducirani tok (kot integral tokovne gostote v njem) enak nič. Po Ampèrovem zakonu ga izrazimo z integralom tangencialne komponente magnetne poljske jakosti po obodu cilindra (glej enačbi (2.12a) in (2.19b)),

$$I_{\mathrm{C}j} = \frac{1}{\mu_0}\oint_{\mathcal{L}_{\mathrm{C}j}} \alpha_1(T)\mathrm{d}l = \frac{1}{\mu_0}\oint_{\mathcal{L}_{\mathrm{C}j}} \underline{\mathbf{C}}_{\alpha 1}\cdot\underline{\boldsymbol{\alpha}}(T)\mathrm{d}l = 0, \tag{2.21}$$

in je $\underline{\mathbf{C}}_{\alpha 1} = \begin{bmatrix} 1 & 0 \end{bmatrix}$ vrstični vektor. Kadar pa je cilinder dvostransko ozemljen [16], je tok sorazmeren potencialni razliki $U_{\mathrm{C}j}$ med koncema cilindra,

$$I_{\mathrm{C}j} = \frac{1}{\mu_0}\oint_{\mathcal{L}_{\mathrm{C}j}} \alpha_1(T)\mathrm{d}l = \frac{1}{\mu_0}\oint_{\mathcal{L}_{\mathrm{C}j}} \underline{\mathbf{C}}_{\alpha 1}\cdot\underline{\boldsymbol{\alpha}}(T)\mathrm{d}l = -U_{\mathrm{C}j}/Z_{\mathrm{g,C}j}, \tag{2.22}$$

pri čemer je $Z_{\mathrm{g,C}j}$ vsota ozemljitvenih impedanc tega cilindra. Če je impedanca $Z_{\mathrm{g,C}j}$ majhna v primerjavi z impedanco cilindra, lahko ozemljitev smatramo za idealno. V tem primeru je potencialna razlika med koncema cilindra zanemarljiva ($U_{\mathrm{C}j} \to 0$) in tudi ni več neznanka, zato v takem primeru tudi enačbe (2.22) ne potrebujemo.[4].

Kadar je j-temu vodniku tok $I_{\mathrm{C}j}$ vsiljen, je

$$\frac{1}{\mu_0} \oint\limits_{\mathcal{L}_{\mathrm{C}j}} \alpha_1(T)\mathrm{d}l = \frac{1}{\mu_0} \oint\limits_{\mathcal{L}_{\mathrm{C}j}} \underline{\mathbf{C}}_{\alpha 1} \cdot \underline{\alpha}(T)\mathrm{d}l = I_{\mathrm{C}j}, \tag{2.23}$$

kadar pa je med koncema vodnika vsiljena potencialna razlika $U_{\mathrm{C}j}$, dodatne enačbe pač ne potrebujemo.

Zasloni ali tokovodniki so lahko med seboj tudi električno povezani. Če sta j-ti in i-ti valj na konceh med seboj povezana, imata na dolžini l_0 enaki potencialni razliki ($U_{\mathrm{C}j} = U_{\mathrm{C}i}$). Potencialna razlika je le ena in potrebujemo le eno dodatno enačbo. Če sta valja tudi enostransko ozemljena, je njun skupen tok enak nič:

$$I_{\mathrm{C}j} + I_{\mathrm{C}i} = \frac{1}{\mu_0} \oint\limits_{\mathcal{L}_{\mathrm{C}j} \cup \mathcal{L}_{\mathrm{C}i}} \alpha_1(T)\mathrm{d}l = \frac{1}{\mu_0} \oint\limits_{\mathcal{L}_{\mathrm{C}j} \cup \mathcal{L}_{\mathrm{C}i}} \underline{\mathbf{C}}_{\alpha 1} \cdot \underline{\alpha}(T)\mathrm{d}l = 0. \tag{2.24}$$

Za enolično rešitev matrične integralske enačbe (2.20) potrebujemo dodatne enačbe tipa (2.21), (2.22), (2.23) in/ali (2.24), ki izhajajo iz načinov povezav in priključitev cilindrov. Na ta način dobimo sistem sklopljenih robnih integralskih enačb za

- vektor gostot ekvivalentnih ploskovnih virov $\underline{\alpha}$ na robu $\mathcal{L}$ in
- neznane potencialne razlike $U_{\mathrm{C}1}, U_{\mathrm{C}2}, \ldots, U_{\mathrm{C}n_{\mathrm{C}}}$ med krajišči valjev.

2.3 Numerično reševanje sistema integralskih enačb

Sistem sklopljenih integralskih enačb smo reševali numerično z momentno metodo [43, 30]. Za poskusne funkcije smo izbrali pravokotne impulze [50] (zaradi relativno enostavno izračunljivih integralov [47, str. 239]), za testne funkcije pa Diracove [47, str. 235], kar je tudi sicer najpogostejša izbira in spominja na metodo kolokacije. Pri takšni izbiri se izognemo računanju skalarnih produktov s testnimi funkcijami [30, str. 55]. Reševanje sistema integralskih enačb se prevede na sistem linearnih algebrskih enačb. Postopku

[4] Primarni viri polja so v praksi praviloma uravnoteženi: da je vsota tokov enaka nič (dvovod, trifazni vod). V tem primeru sta inducirani tok v zaslonu in potencialna razlika med koncema zaslona zanemarljiva. Ta okoliščina deluje na računski ravni enako kot idealna dvostranska ozemljitev.

pravimo diskretizacija integralskih enačb [47, razdelek 4.1], njegove podrobnosti pa si oglejmo v nadaljevanju.

Rob $\mathcal{L}$ valjev aproksimiramo z množico kratkih segmentov, robnih elementov, ki naj so ravni (slika 2.1). Z $\delta\mathcal{L}_m$ smo označili m-ti element, s T_m pa njegovo središčno točko. Dolžine robnih elementov naj so δl_1, δl_2, …, δl_{n_E}, kjer je n_E število vseh elementov. S takšno diskretizacijo smo robu $\mathcal{L}$ priredili odsekoma raven rob[5]:

$$\mathcal{L} \approx \tilde{\mathcal{L}} = \bigcup_{m=1}^{n_\mathrm{E}} \delta\mathcal{L}_m. \tag{2.25}$$

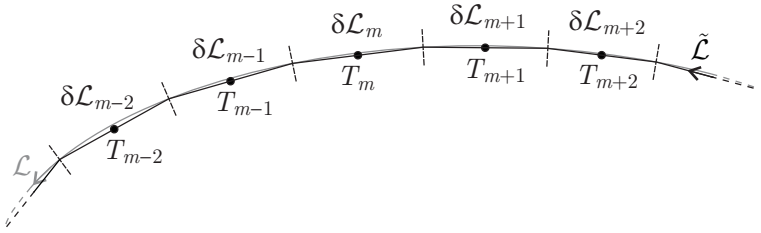

Slika 2.1: Del odsekoma ravne aproksimacije $\tilde{\mathcal{L}}$ roba cilindrov $\mathcal{L}$.

Pravokotni impulz oziroma poskusna funkcija φ_m naj ima vrednost 1 na m-tem segmentu, na vseh ostalih pa vrednost 0:

$$\varphi_m(T) = \begin{cases} 1, & T \in \delta\mathcal{L}_m \\ 0, & T \notin \delta\mathcal{L}_m \end{cases}, \quad m = 1, 2, \ldots, n_\mathrm{E}. \tag{2.26}$$

S temi poskusnimi funkcijami aproksimiramo iskani vektor (2.19b) gostot ekvivalentnih ploskovnih virov z vektorjem stopničastih funkcij,

$$\underline{\alpha}(T) \approx \underline{\tilde{\alpha}}(T) = \left[\sum_{m=1}^{n_\mathrm{E}} \tilde{\alpha}_{1,m}\varphi_m(T) \quad \sum_{m=1}^{n_\mathrm{E}} \tilde{\alpha}_{2,m}\varphi_m(T) \right]^\mathrm{T} = \sum_{m=1}^{n_\mathrm{E}} \underline{\tilde{\alpha}}_m \varphi_m(T), \tag{2.27}$$

kjer je $\underline{\tilde{\alpha}}_m = \left[\tilde{\alpha}_{1,m} \quad \tilde{\alpha}_{2,m} \right]^\mathrm{T}$ in sta $\tilde{\alpha}_{1,m}$ in $\tilde{\alpha}_{2,m}$ približni vrednosti iskanih gostot enojnega in dvojnega sloja na m-tem robnem elementu.

V sistemu integralskih enačb je poleg vektorja $\underline{\alpha}$ neznana tudi funkcija potencialnih razlik U med konci valjev, ki je (zaradi konstantnih vrednosti na območjih posameznih valjev) na preseku $\mathcal{S}$ v resnici že stopničasta funkcija:

$$U(T) = \sum_{j=1}^{n_\mathrm{C}} U_{\mathrm{C}j}\varphi_{\mathrm{C}j}(T), \quad T \in \mathcal{S}, \tag{2.28}$$

[5]Kadar je rob $\mathcal{L}$ poligonalen, se original in aproksimacija ujemata, $\mathcal{L} = \tilde{\mathcal{L}}$.

kjer so $\varphi_{\mathrm{C}j}$ pravokotni impulzi:

$$\varphi_{\mathrm{C}j}(T) = \begin{cases} 1, & T \in \mathcal{S}_{\mathrm{C}j} \\ 0, & T \notin \mathcal{S}_{\mathrm{C}j} \end{cases}, \quad j = 1, 2, \ldots, n_{\mathrm{C}}. \tag{2.29}$$

Če v matrični integralski enačbi (2.20) rob $\mathcal{L}$ in iskani vektor $\underline{\alpha}$ nadomestimo z njunima aproksimacijama (2.25) in (2.27) ter upoštevamo (2.28), dobimo približno enačbo:

$$\underline{\mathbf{C}}_{\alpha 2} \cdot \sum_{m=1}^{n_{\mathrm{E}}} \underline{\tilde{\alpha}}_m \varphi_m(T') + \oint_{\tilde{\mathcal{L}}} \underline{\mathbf{K}}(T, T') \cdot \left(\sum_{m=1}^{n_{\mathrm{E}}} \underline{\tilde{\alpha}}_m \varphi_m(T) \right) \mathrm{d}l + \oint_{\tilde{\mathcal{L}}} \underline{\mathbf{K}}_U(T, T'_+) \left(\sum_{j=1}^{n_{\mathrm{C}}} U_{\mathrm{C}j} \varphi_{\mathrm{C}j}(T) \right) \mathrm{d}l \approx \underline{\mathbf{G}}_{\mathrm{W}}(T'), \quad T' \in \tilde{\mathcal{L}}. \tag{2.30}$$

Zamenjajmo vrstni red vsot in integralov ter upoštevajmo, da se integracijsko območje integralov skrči le na tiste podintervale, na katerih imajo pravokotni impulzi od nič različno vrednost. V ta namen vpeljimo še koeficiente pripadnosti robnih elementov posameznim cilindrom,

$$\zeta_{\mathrm{C}j,m} = \begin{cases} 1, & \delta\mathcal{L}_m \in \tilde{\mathcal{L}}_{\mathrm{C}j} \\ 0, & \delta\mathcal{L}_m \notin \tilde{\mathcal{L}}_{\mathrm{C}j} \end{cases}, \quad m = 1, 2, \ldots, n_{\mathrm{E}};\ j = 1, 2, \ldots, n_{\mathrm{C}}. \tag{2.31}$$

Enačba (2.30) se preoblikuje v

$$\sum_{m=1}^{n_{\mathrm{E}}} \left(\underline{\mathbf{C}}_{\alpha 2} \varphi_m(T') + \int_{\delta\mathcal{L}_m} \underline{\mathbf{K}}(T, T') \mathrm{d}l \right) \cdot \underline{\tilde{\alpha}}_m + \sum_{m=1}^{n_{\mathrm{E}}} \left(\sum_{j=1}^{n_{\mathrm{C}}} U_{\mathrm{C}j} \zeta_{\mathrm{C}j,m} \right) \int_{\delta\mathcal{L}_m} \underline{\mathbf{K}}_U(T, T'_+) \mathrm{d}l \approx \underline{\mathbf{G}}_{\mathrm{W}}(T'), \quad T' \in \tilde{\mathcal{L}}. \tag{2.32}$$

Izbira Diracovih funkcij [51, poglavje 1] $\delta_{1\mathrm{D}}\big(\overline{TT_m}\big)$, $m = 1, 2, \ldots, n_{\mathrm{E}}$, kot testnih funkcij, za katere velja

$$\int_{\delta\mathcal{L}_p} \delta_{1\mathrm{D}}\big(\overline{TT_m}\big)\, \mathrm{d}l = \begin{cases} 1, & m = p \\ 0, & m \neq p \end{cases}, \quad p, m = 1, 2, \ldots, n_{\mathrm{E}}, \tag{2.33}$$

pomeni zahtevo, da približna enačba (2.32) natančno velja v središčnih točkah T_1, T_2, …, $T_{n_{\mathrm{E}}}$ segmentov (metoda kolokacije):

$$\underline{\mathbf{C}}_{\alpha 2} \cdot \underline{\tilde{\alpha}}_p + \sum_{m=1}^{n_{\mathrm{E}}} \left(\int_{\delta\mathcal{L}_m} \underline{\mathbf{K}}(T, T_p) \mathrm{d}l \cdot \underline{\tilde{\alpha}}_m + \left(\sum_{j=1}^{n_{\mathrm{C}}} U_{\mathrm{C}j} \zeta_{\mathrm{C}j,m} \right) \int_{\delta\mathcal{L}_m} \underline{\mathbf{K}}_U(T, T_{p+}) \mathrm{d}l \right) = \underline{\mathbf{G}}_{\mathrm{W}}(T_p), \quad p = 1, 2, \ldots, n_{\mathrm{E}}. \tag{2.34}$$

Dobili smo sistem linearnih algebrskih enačb za:

- vektorje $\underline{\tilde{\alpha}}_m$, $m = 1, 2, \ldots, n_\mathrm{E}$, približnih vrednosti gostot ekvivalentnih ploskovnih virov na posameznih robnih elementih in
- potencialne razlike $U_{\mathrm{C}j}$, $j = 1, 2, \ldots, n_\mathrm{C}$, med začetki in konci valjev.

Sistem enačb (2.34) še ni dokončen, saj vsebuje n_E matričnih enačb oziroma $2n_\mathrm{E}$ skalarnih in $2n_\mathrm{E} + n_\mathrm{C}$ skalarnih neznank[6] (vsak od neznanih vektorjev $\underline{\tilde{\alpha}}_m$ vsebuje dve skalarni neznanki). Glede na vezavo zaslonov je potrebno sistemu enačb dodati še integralske enačbe tipa (2.21), (2.22), (2.23) in/ali (2.24), ki jih z upoštevanjem stopničaste aproksimacije (2.27) ter koeficientov pripadnosti (2.31) diskretiziramo v algebrske:

$$\frac{1}{\mu_0}\sum_{m=1}^{n_\mathrm{E}} \zeta_{\mathrm{C}j,m}\delta l_m \underline{\mathbf{C}}_{\alpha 1}\cdot\underline{\tilde{\alpha}}_m \approx I_{\mathrm{C}j} = 0 \tag{2.35a}$$

$$\frac{1}{\mu_0}\sum_{m=1}^{n_\mathrm{E}} \zeta_{\mathrm{C}j,m}\delta l_m \underline{\mathbf{C}}_{\alpha 1}\cdot\underline{\tilde{\alpha}}_m \approx I_{\mathrm{C}j} = -U_{\mathrm{C}j}/Z_{\mathrm{g,C}j} \tag{2.35b}$$

$$\frac{1}{\mu_0}\sum_{m=1}^{n_\mathrm{E}} \zeta_{\mathrm{C}j,m}\delta l_m \underline{\mathbf{C}}_{\alpha 1}\cdot\underline{\tilde{\alpha}}_m \approx I_{\mathrm{C}j} \tag{2.35c}$$

$$\frac{1}{\mu_0}\sum_{m=1}^{n_\mathrm{E}} (\zeta_{\mathrm{C}j,m} + \zeta_{\mathrm{C}i,m})\delta l_m \underline{\mathbf{C}}_{\alpha 1}\cdot\underline{\tilde{\alpha}}_m \approx I_{\mathrm{C}j} + I_{\mathrm{C}i} = 0. \tag{2.35d}$$

Tako dobljen (kompleten) sistem linearnih algebrskih enačb rešujemo z algoritmom Gaussove eliminacije z delnim pivotiranjem, ki je vgrajen v programski paket MATLAB® [52, str. 2-2249].

Elementi matrik $\underline{\mathbf{K}}$ (2.19a) in $\underline{\mathbf{K}}_U$ (2.19c), ki nastopata v sistemu (2.34), vsebujejo tudi normalna odvoda Greenovih funkcij (2.7). Argument teh funkcij je razdalja med točkama T in T', ki jo krajše označimo s $P = \overline{TT'} = \sqrt{(x'-x)^2 + (y'-y)^2}$. Določimo najprej normalni odvod te razdalje:

$$\frac{\partial P}{\partial n} = \mathbf{n}\cdot\boldsymbol{\nabla}P = \mathbf{n}\cdot\boldsymbol{\nabla}\sqrt{(x'-x)^2+(y'-y)^2} = \mathbf{n}\cdot\frac{(x-x', y-y')}{\sqrt{(x-x')^2+(y-y')^2}} = -\frac{\mathbf{n}\cdot\mathbf{P}}{P}, \tag{2.36}$$

kjer je $\mathbf{P} = \overrightarrow{TT'} = (x'-x, y'-y)$ distančni vektor od točke T k T'. Analitična izraza za normalna odvoda Greenovih funkcij sta

$$\frac{\partial g_0(T,T')}{\partial n} = \mathbf{n}\cdot\boldsymbol{\nabla}g_0(T,T') = -\frac{1}{2\pi}\mathbf{n}\cdot\boldsymbol{\nabla}\ln P = -\frac{1}{2\pi P}\mathbf{n}\cdot\boldsymbol{\nabla}P = \frac{\mathbf{n}\cdot\mathbf{P}}{2\pi P^2} \tag{2.37a}$$

[6] Če je potencialna razlika med koncema kakšnega valja znana ali so te za več električno povezanih valjev enake, se število neznank temu ustrezno zmanjša.

$$\begin{aligned}\frac{\partial g(T,T')}{\partial n} &= \mathbf{n}\cdot\boldsymbol{\nabla} g(T,T') = \frac{1}{4\mathrm{j}}\mathbf{n}\cdot\boldsymbol{\nabla} H_0^{(2)}(k_T P) = -\frac{1}{4\mathrm{j}}H_1^{(2)}(k_T P)\mathbf{n}\cdot\boldsymbol{\nabla}(k_T P)\\ &= \frac{k_T\mathbf{n}\cdot\mathbf{P}}{4\mathrm{j}P}H_1^{(2)}(k_T P),\end{aligned} \tag{2.37b}$$

pri slednjem smo upoštevali [53, str. 463], da je

$$\frac{\mathrm{d}H_0^{(2)}(u)}{\mathrm{d}u} = -H_1^{(2)}(u). \tag{2.38}$$

Pri določanju koeficientov sistema (2.34) je največ dela z računanjem integralov elementov matrik $\underline{\mathbf{K}}$ (2.19a) in $\underline{\mathbf{K}}_U$ (2.19c) vzdolž posameznih segmentov. Te integrale računamo numerično; uporabljamo adaptivni rekurzivni Simpsonov kvadraturni algoritem [54], ki je vgrajen v programski paket MATLAB® [55, str. 2-2694]. Posebno obravnavo terjajo tako imenovani lastni prispevki, ko je $m = p$. Pri njih so integrandi, ki vsebujejo Greenovi funkciji in njuna normalna odvoda, singularni v središčnih točkah segmentov, zaradi česar numerična integracija odpove. Te singularnosti so integrabilne in o njih bo tekla beseda v nadaljevanju.

2.3.1 Lastni prispevki

Lastni prispevki v sistemu enačb (2.34) so (glej enačbi (2.19a) in (2.19c)):

$$\begin{aligned}&\int\limits_{\delta\mathcal{L}_p} K_{11}(T,T_p)\mathrm{d}l = 2\int\limits_{\delta\mathcal{L}_p}\mu_{\mathrm{r}}(T_-)g(T,T_p)\mathrm{d}l \qquad \int\limits_{\delta\mathcal{L}_p} K_{12}(T,T_p)\mathrm{d}l = 2\int\limits_{\delta\mathcal{L}_p}\frac{\partial g(T,T_p)}{\partial n}\mathrm{d}l\\ &\int\limits_{\delta\mathcal{L}_p} K_{21}(T,T_p)\mathrm{d}l = -2\int\limits_{\delta\mathcal{L}_p} g_0(T,T_p)\mathrm{d}l \qquad \int\limits_{\delta\mathcal{L}_p} K_{22}(T,T_p)\mathrm{d}l = -2\int\limits_{\delta\mathcal{L}_p}\frac{\partial g_0(T,T_p)}{\partial n}\mathrm{d}l\\ &\int\limits_{\delta\mathcal{L}_p} K_{U1}(T,T_{p+})\mathrm{d}l = \frac{2\mathrm{j}}{\omega l_0}\int\limits_{\delta\mathcal{L}_p}\frac{\partial g(T,T_{p+})}{\partial n}\mathrm{d}l.\end{aligned} \tag{2.39}$$

Pri prvem je v integrandu razen Greenove funkcije ali njenega odvoda še relativna permeabilnost μ_{r}, ki je tudi, podobno kot potencialna razlika (2.28), stopničasta funkcija:

$$\mu_{\mathrm{r}}(T) = \sum_{j=1}^{n_{\mathrm{C}}}\frac{\mu_{\mathrm{C}j}}{\mu_0}\varphi_{\mathrm{C}j}(T), \quad T\in\mathcal{S}. \tag{2.40}$$

Če upoštevamo to v prvem od lastnih prispevkov (2.39) ter uporabimo koeficiente pripadnosti (2.31), dobimo

$$\begin{aligned}\int\limits_{\delta\mathcal{L}_p} K_{11}(T,T_p)\mathrm{d}l &= \frac{2}{\mu_0}\int\limits_{\delta\mathcal{L}_p}\left(\sum_{j=1}^{n_{\mathrm{C}}}\mu_{\mathrm{C}j}\varphi_{\mathrm{C}j}(T_-)\right)g(T,T_p)\mathrm{d}l\\ &= \frac{2}{\mu_0}\left(\sum_{j=1}^{n_{\mathrm{C}}}\mu_{\mathrm{C}j}\zeta_{\mathrm{C}j,p}\right)\int\limits_{\delta\mathcal{L}_p} g(T,T_p)\mathrm{d}l.\end{aligned} \tag{2.41}$$

Za izračun lastnih prispevkov je potrebno izračunati integrale Greenovih funkcij (2.7) oziroma njunih normalnih odvodov[7]:

$$\int_{\delta\mathcal{L}_p} g(T,T_p)\mathrm{d}l = \frac{1}{4\mathrm{j}}\int_{\delta\mathcal{L}_p} H_0^{(2)}\big(k_T\overline{TT_p}\big)\,\mathrm{d}l \qquad \int_{\delta\mathcal{L}_p} \frac{\partial g(T,T_p)}{\partial n}\mathrm{d}l = \frac{1}{4\mathrm{j}}\int_{\delta\mathcal{L}_p} \frac{\partial H_0^{(2)}\big(k_T\overline{TT_p}\big)}{\partial n}\mathrm{d}l$$
$$\int_{\delta\mathcal{L}_p} g_0(T,T_p)\mathrm{d}l = -\frac{1}{2\pi}\int_{\delta\mathcal{L}_p} \ln\overline{TT_p}\mathrm{d}l \qquad \int_{\delta\mathcal{L}_p} \frac{\partial g_0(T,T_p)}{\partial n}\mathrm{d}l = -\frac{1}{2\pi}\int_{\delta\mathcal{L}_p} \frac{\partial \ln\overline{TT_p}}{\partial n}\mathrm{d}l$$
$$\int_{\delta\mathcal{L}_p} \frac{\partial g(T,T_{p+})}{\partial n}\mathrm{d}l = \frac{1}{4\mathrm{j}}\int_{\delta\mathcal{L}_p} \frac{\partial H_0^{(2)}\big(k_T\overline{TT_{p+}}\big)}{\partial n}\mathrm{d}l. \tag{2.42}$$

V ta namen vpeljimo lokalni koordinatni sistem s koordinatami (η,ξ) in izhodiščem v središčni točki T_p, kot je to prikazano na sliki 2.2. Integracijsko območje $\delta\mathcal{L}_p$ je simetrično okrog točke T_p, funkcije pa sode, saj sta razdalji $\overline{TT_p} = |\xi|$ in $\overline{TT_{p+}} = \sqrt{\eta_{p+}^2+\xi^2}$. Diferencial dolžine $\mathrm{d}l$ segmenta $\delta\mathcal{L}_p$, po katerem integriramo, je enak diferencialu koordinate ξ, $\mathrm{d}l = \mathrm{d}\xi$.

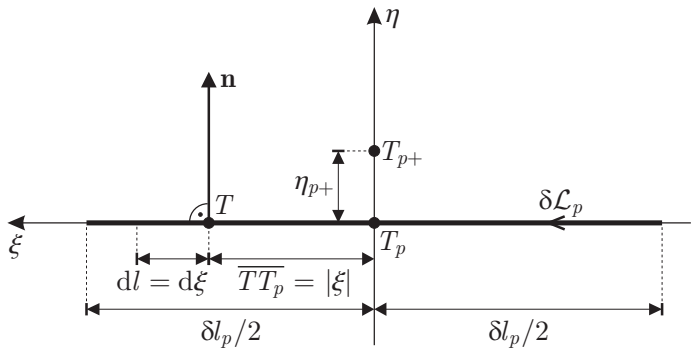

Slika 2.2: Robni element $\delta\mathcal{L}_p$.

Začnimo z določanjem tretjega integrala v (2.42) (glej [50, str. 889]):

$$\int_{\delta\mathcal{L}_p} g_0(T,T_p)\mathrm{d}l = -2\frac{1}{2\pi}\lim_{\varepsilon\to 0}\int_{\varepsilon}^{\delta l_p/2} \ln\xi\mathrm{d}\xi = -\lim_{\varepsilon\to 0}\frac{\xi}{\pi}\ln\frac{\xi}{\mathrm{e}}\bigg|_{\varepsilon}^{\delta l_p/2} = -\frac{\delta l_p}{2\pi}\ln\frac{\delta l_p}{2\mathrm{e}}, \tag{2.43}$$

kjer je e osnova naravnega logaritma.

Nadaljujmo s prvim integralom v (2.42). Pri njem smo ubrali sledeč postopek. Integracijsko območje $\delta\mathcal{L}_p$ razdelimo na bližnji interval $\delta^2\mathcal{L}_p$ središčne točke T_p in preostali

[7] Ker so integrandi v središčni točki T_p singularni, je potrebno integrale razumeti kot posplošene. Njihove vrednosti se določijo tako, da se iz integracijskega območja izvzame bližnjo okolico singularne točke ter opravi limito, ko gre širina te okolice proti nič [50, str. 339].

del. Integral na bližnjem intervalu določimo analitično, če za Hankelovo funkcijo $H_0^{(2)}$ uporabimo aproksimacijo pri majhnih argumentih [53, str. 462]

$$H_0^{(2)}(ku) \doteq 1 - \mathrm{j}\frac{2}{\pi}\ln\frac{\gamma_\mathrm{e} ku}{2} = C_H + \frac{2}{\mathrm{j}\pi}\ln u, \quad |ku| \ll 1, \tag{2.44}$$

kjer sta $C_H = 1 - (2\mathrm{j}/\pi)\ln(\gamma_\mathrm{e} k/2)$ in $\gamma_\mathrm{e} = \mathrm{e}^{C_\mathrm{e}} \doteq 1,78107$, C_e pa je Eulerjeva konstanta [50]. Valovno število k_T cilindra, ki mu pripada integracijska točka $T \in \delta\mathcal{L}_p$, lahko z upoštevanjem koeficientov pripadnosti (2.31) izrazimo kot

$$k_T = \sum_{j=1}^{n_\mathrm{C}} k_{\mathrm{C}j}\zeta_{\mathrm{C}j,p} = k_p, \tag{2.45}$$

kjer je k_p okrajšava za valovno število cilindra, ki mu pripada p-ti robni element. Integral Greenove funkcije (2.7a) po bližnjem intervalu $\delta^2\mathcal{L}_p$ je (glej izpeljavo (2.43))

$$\begin{aligned}\int_{\delta^2\mathcal{L}_p} g(T,T_p)\mathrm{d}l &= \frac{1}{2\mathrm{j}}\lim_{\varepsilon\to 0}\int_\varepsilon^{\delta^2 l_p/2} H_0^{(2)}(k_p\xi)\,\mathrm{d}\xi \doteq \frac{1}{2\mathrm{j}}\left(\frac{\delta^2 l_p}{2} - \frac{2\mathrm{j}}{\pi}\lim_{\varepsilon\to 0}\int_\varepsilon^{\delta^2 l_p/2}\ln\frac{\gamma_\mathrm{e} k_p\xi}{2}\mathrm{d}\xi\right)\\ &\doteq \frac{\delta^2 l_p}{4}\left(-\mathrm{j} - \frac{2}{\pi}\ln\frac{\gamma_\mathrm{e} k_p \delta^2 l_p}{4\mathrm{e}}\right),\end{aligned} \tag{2.46}$$

kjer je $\delta^2 l_p$ dolžina bližnjega intervala. Bližnji interval $\delta^2\mathcal{L}_p$ smo izbrali tako, da največja absolutna vrednost argumenta Hankelove funkcije na njem ne presega $1/10$, kar upravičuje uporabo aproksimacije te funkcije pri majhnih argumentih. Integral v preostalem delu segmenta $\delta\mathcal{L}_p$ izračunamo numerično.

Lotimo se sedaj četrtega integrala v (2.42). Njegov integrand je enak nič (glej (2.37a)),

$$\frac{\partial g_0(T,T_p)}{\partial n} = \frac{\mathbf{n}\cdot\mathbf{P}_p}{2\pi P_p^2} = \frac{\mathbf{n}\cdot\mathbf{P}_p}{2\pi\xi^2} = 0, \tag{2.47}$$

saj sta $\mathbf{n}$ in $\mathbf{P}_p$ pravokotna na integracijskem intervalu $\varepsilon \le \xi \le \delta l_p/2$, $\varepsilon \to 0$ (glej sliko 2.2), zato je

$$\int_{\delta\mathcal{L}_p}\frac{\partial g_0(T,T_p)}{\partial n}\mathrm{d}l = 2\lim_{\varepsilon\to 0}\int_\varepsilon^{\delta l_p/2}\frac{\mathbf{n}\cdot\mathbf{P}_p}{2\pi\xi^2}\mathrm{d}\xi = 0. \tag{2.48}$$

Enako velja tudi za drugi integral v (2.42),

$$\int_{\delta\mathcal{L}_p}\frac{\partial g(T,T_p)}{\partial n}\mathrm{d}l = 0, \tag{2.49}$$

kajti tudi njegov integrand vsebuje skalarni produkt $\mathbf{n}\cdot\mathbf{P}_p$ (glej (2.37b)).

Preostal je še zadnji integral v (2.42) (glej [47, razdelek 3.1.2]). Tudi pri njem razdelimo integracijsko območje na bližnji interval $\delta^2\mathcal{L}_p$ točke T_p, kjer je upravičena aproksimacija (2.44) Hankelove funkcije pri majhnih argumentih, in preostali del $\delta\mathcal{L}_p \setminus \delta^2\mathcal{L}_p$.

Pri integralu na preostalem delu integrand ni singularen. Ker je točka T_{p+} infinitezimalno blizu točke T, velja

$$\int\limits_{\delta\mathcal{L}_p\setminus\delta^2\mathcal{L}_p} \frac{\partial g(T,T_{p+})}{\partial n}\mathrm{d}l = \int\limits_{\delta\mathcal{L}_p\setminus\delta^2\mathcal{L}_p} \frac{\partial g(T,T_p)}{\partial n}\mathrm{d}l. \tag{2.50}$$

Pri izračunu integrala na bližnjem intervalu $\delta^2\mathcal{L}_p$ upoštevajmo, da je normalni odvod $\partial/\partial n = \partial/\partial\eta$ (glej sliko 2.2), in dobimo

$$\begin{aligned}\int\limits_{\delta^2\mathcal{L}_p} \frac{\partial g(T,T_{p+})}{\partial n}\mathrm{d}l &\doteq -\frac{1}{2\pi}\int\limits_{\delta^2\mathcal{L}_p} \frac{\partial \ln\left(\overline{TT_{p+}}\right)}{\partial n}\mathrm{d}l \\ &\doteq -\frac{1}{\pi}\lim_{\eta_{p+}\to 0}\lim_{\varepsilon\to 0}\int\limits_{\varepsilon}^{\delta^2 l_p/2}\lim_{\eta\to 0}\frac{\partial \ln\sqrt{(\eta-\eta_{p+})^2+\xi^2}}{\partial\eta}\mathrm{d}\xi \\ &\doteq \frac{1}{\pi}\lim_{\eta_{p+}\to 0}\lim_{\varepsilon\to 0}\int\limits_{\varepsilon}^{\delta^2 l_p/2}\frac{\eta_{p+}}{\eta_{p+}^2+\xi^2}\mathrm{d}\xi = \frac{1}{\pi}\lim_{\eta_{p+}\to 0}\arctan\frac{\delta^2 l_p}{2\eta_{p+}} = \frac{1}{2}.\end{aligned} \tag{2.51}$$

Velja tudi

$$\int\limits_{\delta^2\mathcal{L}_p} \frac{\partial g(T,T_{p+})}{\partial n}\mathrm{d}l \doteq \int\limits_{\delta^2\mathcal{L}_p} \frac{\partial g(T,T_p)}{\partial n}\mathrm{d}l + \frac{1}{2}, \tag{2.52}$$

saj je desni integral enak nič (glej enačbo (2.49)). Če združimo rezultate (2.50) in (2.52) ter upoštevamo še (2.49), dobimo

$$\int\limits_{\delta\mathcal{L}_p} \frac{\partial g(T,T_{p+})}{\partial n}\mathrm{d}l \doteq \int\limits_{\delta\mathcal{L}_p} \frac{\partial g(T,T_p)}{\partial n}\mathrm{d}l + \frac{1}{2} = \frac{1}{2}. \tag{2.53}$$

2.4 Izračun magnetnega polja

Ko enkrat rešimo sistem sklopljenih robnih integralskih enačb in izračunamo ekvivalentne ploskovne vire ter potencialne razlike, se lahko lotimo izračuna polja kjerkoli v prostoru.

2.4.1 Izračun vektorskega magnetnega potenciala

Izraza za vektorski magnetni potencial znotraj ($T' \in \mathcal{S}$) ali izven valjev ($T' \in \mathcal{S}_0$) sledita iz enačb (2.13a) in (2.13b):

$$\begin{aligned} A_z(T' \in \mathcal{S}) = &- \oint_{\mathcal{L}} \left(\alpha_2(T) \frac{\partial g(T,T')}{\partial n} + \mu_\mathrm{r}(T_-)\alpha_1(T) g(T,T') \right) \mathrm{d}l \\ &+ \int_{\mathcal{S}} \mu(T)\gamma(T) \frac{U(T)}{l_0} g(T,T') \mathrm{d}s \end{aligned} \tag{2.54a}$$

$$A_z(T' \in \mathcal{S}_0) = \oint_{\mathcal{L}} \left(\alpha_2(T) \frac{\partial g_0(T,T')}{\partial n} + \alpha_1(T) g_0(T,T') \right) \mathrm{d}l + \sum_{i=1}^{n_\mathrm{W}} g_0(T_{\mathrm{W}i}, T') \mu_0 I_{\mathrm{W}i}. \tag{2.54b}$$

Ploskovni integral v zgornji enačbi preoblikujemo v krivuljnega, podobno kot smo to storili v razdelku 2.1, in upoštevamo, da je $T' \in \mathcal{S}$. Na preseku npr. j-tega valja dobimo

$$\begin{aligned} \int_{\mathcal{S}_{\mathrm{C}j}} \mu(T)\gamma(T) \frac{U(T)}{l_0} g(T,T') \mathrm{d}s =& \mu_{\mathrm{C}j}\gamma_{\mathrm{C}j} \frac{U_{\mathrm{C}j}}{l_0} \int_{\mathcal{S}_{\mathrm{C}j}} g(T,T') \mathrm{d}s \\ =& \mu_{\mathrm{C}j}\gamma_{\mathrm{C}j} \frac{U_{\mathrm{C}j}}{l_0} \int_{\mathcal{S}_{\mathrm{C}j}} \frac{1}{k_T^2} \left(-\boldsymbol{\nabla} \cdot \boldsymbol{\nabla} g(T,T') - \delta_{2\mathrm{D}}\big(\overline{TT'}\big) \right) \mathrm{d}s \\ =& \mu_{\mathrm{C}j}\gamma_{\mathrm{C}j} \frac{U_{\mathrm{C}j}}{l_0} \frac{-1}{k_{\mathrm{C}j}^2} \left(\oint_{\mathcal{L}_{\mathrm{C}j}} \frac{\partial g(T,T')}{\partial n} \mathrm{d}l + \int_{\mathcal{S}_{\mathrm{C}j}} \delta_{2\mathrm{D}}\big(\overline{TT'}\big) \, \mathrm{d}s \right) \\ =& \frac{1}{\mathrm{j}\omega} \left(\oint_{\mathcal{L}_{\mathrm{C}j}} \frac{U(T)}{l_0} \frac{\partial g(T,T')}{\partial n} \mathrm{d}l + \int_{\mathcal{S}_{\mathrm{C}j}} \frac{U(T)}{l_0} \delta_{2\mathrm{D}}\big(\overline{TT'}\big) \, \mathrm{d}s \right), \end{aligned} \tag{2.55}$$

za celoten presek $\mathcal{S}$ valjev pa velja

$$\begin{aligned} \int_{\mathcal{S}} \mu(T)\gamma(T) \frac{U(T)}{l_0} g(T,T') \mathrm{d}s =& \frac{1}{\mathrm{j}\omega} \left(\oint_{\mathcal{L}} \frac{U(T)}{l_0} \frac{\partial g(T,T')}{\partial n} \mathrm{d}l + \int_{\mathcal{S}} \frac{U(T)}{l_0} \delta_{2\mathrm{D}}\big(\overline{TT'}\big) \, \mathrm{d}s \right) \\ =& \frac{1}{\mathrm{j}\omega} \oint_{\mathcal{L}} \frac{U(T)}{l_0} \frac{\partial g(T,T')}{\partial n} \mathrm{d}l + \frac{1}{\mathrm{j}\omega} \frac{U(T')}{l_0}. \end{aligned} \tag{2.56}$$

Če to upoštevamo v enačbi (2.54), dobimo[8]

$$\begin{aligned} A_z(T' \in \mathcal{S}) = &- \oint_{\mathcal{L}} \left(\alpha_2(T) \frac{\partial g(T,T')}{\partial n} + \mu_\mathrm{r}(T_-)\alpha_1(T) g(T,T') \right) \mathrm{d}l \\ &+ \frac{1}{\mathrm{j}\omega} \oint_{\mathcal{L}} \frac{U(T)}{l_0} \frac{\partial g(T,T')}{\partial n} \mathrm{d}l + \frac{1}{\mathrm{j}\omega} \frac{U(T')}{l_0} \end{aligned} \tag{2.57a}$$

$$A_z(T' \in \mathcal{S}_0) = \oint_{\mathcal{L}} \left(\alpha_2(T) \frac{\partial g_0(T,T')}{\partial n} + \alpha_1(T) g_0(T,T') \right) \mathrm{d}l + \sum_{i=1}^{n_\mathrm{W}} g_0(T_{\mathrm{W}i}, T') \mu_0 I_{\mathrm{W}i}. \tag{2.57b}$$

Ti enačbi lahko jedrnato zapišemo v matrični obliki podobno, kot smo to že počeli v razdelku 2.1.1. V ta namen vpeljimo naslednje okrajšave:

$$\underline{\widehat{\mathbf{K}}}(T,T') = \begin{bmatrix} -\mu_\mathrm{r}(T_-) g(T,T') & -\partial g(T,T')/\partial n \\ g_0(T,T') & \partial g_0(T,T')/\partial n \end{bmatrix} \tag{2.58a}$$

$$\underline{\widehat{\mathbf{K}}}_U(T,T') = \begin{bmatrix} \dfrac{1}{\mathrm{j}\omega l_0} \dfrac{\partial g(T,T')}{\partial n} & 0 \end{bmatrix}^\mathrm{T} \tag{2.58b}$$

$$\underline{\widehat{\mathbf{C}}}_U = \begin{bmatrix} \dfrac{1}{\mathrm{j}\omega l_0} & 0 \end{bmatrix}^\mathrm{T} \tag{2.58c}$$

$$\underline{\widehat{\mathbf{G}}}_\mathrm{W}(T') = \begin{bmatrix} 0 & \displaystyle\sum_{i=1}^{n_\mathrm{W}} g_0(T_{\mathrm{W}i}, T') \mu_0 I_{\mathrm{W}i} \end{bmatrix}^\mathrm{T}. \tag{2.58d}$$

Matrična oblika enačb (2.57) je

$$\begin{bmatrix} A_z(T' \in \mathcal{S}) \\ A_z(T' \in \mathcal{S}_0) \end{bmatrix} = \oint_{\mathcal{L}} \underline{\widehat{\mathbf{K}}}(T,T') \cdot \underline{\alpha}(T) \mathrm{d}l + \oint_{\mathcal{L}} \underline{\widehat{\mathbf{K}}}_U(T,T') U(T) \mathrm{d}l + \underline{\widehat{\mathbf{C}}}_U U(T') + \underline{\widehat{\mathbf{G}}}_\mathrm{W}(T'). \tag{2.59}$$

Če krivuljne integrale diskretiziramo na podoben način, kot smo to storili v razdelku 2.3, dobimo sledeče:

$$\begin{aligned} \begin{bmatrix} A_z(T' \in \tilde{\mathcal{S}}) \\ A_z(T' \in \tilde{\mathcal{S}}_0) \end{bmatrix} \approx \sum_{m=1}^{n_\mathrm{E}} \left(\int_{\delta\mathcal{L}_m} \underline{\widehat{\mathbf{K}}}(T,T') \mathrm{d}l \cdot \underline{\tilde{\alpha}}_m + \left(\sum_{j=1}^{n_\mathrm{C}} U_{\mathrm{C}j} \zeta_{\mathrm{C}j,m} \right) \int_{\delta\mathcal{L}_m} \underline{\widehat{\mathbf{K}}}_U(T,T') \mathrm{d}l \right) \\ + \underline{\widehat{\mathbf{C}}}_U \sum_{j=1}^{n_\mathrm{C}} U_{\mathrm{C}j} \varphi_{\mathrm{C}j}(T') + \underline{\widehat{\mathbf{G}}}_\mathrm{W}(T'), \end{aligned} \tag{2.60}$$

[8] Enačbo (2.13a) bi lahko pisali tudi za vsak cilinder posebej. Izraz za potencial v j-tem cilindru je podoben izrazu (2.57a), le da je integracijski interval zgolj rob $\mathcal{L}_{\mathrm{C}j}$ tega cilindra. V primeru strukture z več cilindri na ta način skrajšamo izračun integralov. Zaradi kompaktnosti zapisa smo enačbo (2.57a) zapisali v obliki, veljavni za vse cilindre.

kjer sta $\tilde{\mathcal{S}}$ območje znotraj odsekoma ravnega robu $\tilde{\mathcal{L}}$, $\tilde{\mathcal{S}}_0$ pa območje izven tega roba. Integrale elementov matrik $\underline{\widehat{\mathbf{K}}}$ in $\underline{\widehat{\mathbf{K}}}_U$ vzdolž posameznih robnih elementov izračunamo brez težav numerično, saj integrandi takrat niso singularni, $T' \notin \tilde{\mathcal{L}}$.

Na robu $\mathcal{L}$ valjev je potencial enak gostoti dvojnega sloja (glej enačbo (2.12b)), zato velja zanj na $\tilde{\mathcal{L}}$ naslednji približek (glej enačbo (2.27)):

$$A_z(T' \in \tilde{\mathcal{L}}) \approx \underline{\widehat{\mathbf{C}}}_{\alpha 2} \cdot \sum_{m=1}^{n_\mathrm{E}} \underline{\tilde{\alpha}}_m \varphi_m(T'), \tag{2.61}$$

kjer je vrstični vektor $\underline{\widehat{\mathbf{C}}}_{\alpha 2} = \begin{bmatrix} 0 & 1 \end{bmatrix}$.

2.4.2 Izračun vektorja gostote magnetnega pretoka

Vektor gostote magnetnega pretoka je enak rotorju vektorskega potenciala:

$$\mathbf{B}(T') = \boldsymbol{\nabla}' \times \mathbf{A}(T') = \boldsymbol{\nabla}' \times \mathbf{e}_z A_z(x', y') = \mathbf{e}_x \frac{\partial A_z}{\partial y'} - \mathbf{e}_y \frac{\partial A_z}{\partial x'}, \tag{2.62}$$

kjer smo z $\boldsymbol{\nabla}'$ označili operator nabla, ki se nanaša na koordinate točke $T'(x', y')$. Pri določanju parcialnih odvodov sta dve možnosti. Pri prvi jih aproksimiramo z diferenčnima kvocientoma,

$$\frac{\partial A_z}{\partial x'} \simeq \frac{A_z(x' + \delta x', y') - A_z(x', y')}{\delta x'} \tag{2.63a}$$

$$\frac{\partial A_z}{\partial y'} \simeq \frac{A_z(x', y' + \delta y') - A_z(x', y')}{\delta y'}, \tag{2.63b}$$

vrednosti potencialov pa določamo po enačbi (2.60) ali (2.61). Slabost načina je, da moramo vrednosti potenciala izračunati v vsaj treh točkah, (x', y'), $(x' + \delta x', y')$ in $(x', y' + \delta y')$, in v tem, da je treba skrbno izbrati diferenci $\delta x'$ in $\delta y'$. Če sta premajhni, sta diferenci potenciala lahko celo znotraj numerične napake, če pa sta diferenci preveliki, sta preveliki tudi odstopanji diferenčnih kvocientov od odvodov.

Druga možnost je, da parcialne odvode komponente A_z določimo z odvajanjem izraza (2.60):

$$\begin{bmatrix} \dfrac{\partial A_z(T' \in \tilde{\mathcal{S}})}{\partial w'} & \dfrac{\partial A_z(T' \in \tilde{\mathcal{S}}_0)}{\partial w'} \end{bmatrix}^\mathrm{T} \approx \frac{\partial \underline{\widehat{\mathbf{G}}}_\mathrm{W}(T')}{\partial w'} + \sum_{m=1}^{n_\mathrm{E}} \left(\int_{\delta\mathcal{L}_m} \frac{\partial \underline{\widehat{\mathbf{K}}}(T, T')}{\partial w'} \mathrm{d}l \cdot \underline{\tilde{\alpha}}_m + \left(\sum_{j=1}^{n_\mathrm{C}} U_{\mathrm{C}j} \zeta_{\mathrm{C}j,m} \right) \int_{\delta\mathcal{L}_m} \frac{\partial \underline{\widehat{\mathbf{K}}}_U(T, T')}{\partial w'} \mathrm{d}l \right), \tag{2.64}$$

kjer je spremenljivka w' ali x' ali y'. Odvod predzadnjega člena v enačbi (2.60) je enak nič, saj so potencialne razlike (2.28) konstante na območju valjev. Integrale v enačbi (2.64) izračunamo numerično tudi tokrat.

Odvodi Greenovih funkcij

V izrazu (2.64) nastopajo odvodi elementov matrik $\underline{\widehat{\mathbf{K}}}$, $\underline{\widehat{\mathbf{K}}}_U$ in $\underline{\widehat{\mathbf{G}}}_{\mathrm{W}}$, v njih (glej enačbo (2.58)) pa Greenove funkcije (2.7); določiti je torej potrebno parcialne odvode prvega oziroma drugega reda teh funkcij:

$$\begin{aligned} \frac{\partial g(T,T')}{\partial w'} &= \frac{1}{4\mathrm{j}}\frac{\partial H_0^{(2)}\left(k_T\overline{TT'}\right)}{\partial w'} \qquad \frac{\partial^2 g(T,T')}{\partial w'\partial n} = \frac{1}{4\mathrm{j}}\frac{\partial^2 H_0^{(2)}\left(k_T\overline{TT'}\right)}{\partial w'\partial n} \\ \frac{\partial g_0(T,T')}{\partial w'} &= -\frac{1}{2\pi}\frac{\partial \ln \overline{TT'}}{\partial w'} \qquad \frac{\partial^2 g_0(T,T')}{\partial w'\partial n} = -\frac{1}{2\pi}\frac{\partial^2 \ln \overline{TT'}}{\partial w'\partial n}, \end{aligned} \tag{2.65}$$

kjer je w' ali x' ali y'. Argument funkcij je razdalja $P = \overline{TT'} = \sqrt{(x'-x)^2+(y'-y)^2}$ med točkama $T(x,y)$ in $T'(x',y')$. Določimo najprej njen odvod po koordinati w':

$$\frac{\partial P}{\partial w'} = \frac{\partial}{\partial w'}\sqrt{(x'-x)^2+(y'-y)^2} = \frac{w'-w}{P}, \tag{2.66}$$

kjer je $w = x$, če je $w' = x'$, in $w = y$, če je $w' = y'$.

Tretji odvod v (2.65) je

$$\frac{\partial g_0(T,T')}{\partial w'} = -\frac{1}{2\pi}\frac{\partial \ln P}{\partial w'} = -\frac{1}{2\pi P}\frac{\partial P}{\partial w'} = -\frac{w'-w}{2\pi P^2}. \tag{2.67}$$

Nadaljujmo s prvim (glej enačbo (2.38)):

$$\frac{\partial g(T,T')}{\partial w'} = \frac{1}{4\mathrm{j}}\frac{\partial H_0^{(2)}(k_T P)}{\partial w'} = -\frac{1}{4\mathrm{j}}H_1^{(2)}(k_T P)\frac{\partial (k_T P)}{\partial w'} = -\frac{k_T(w'-w)}{4\mathrm{j}P}H_1^{(2)}(k_T P). \tag{2.68}$$

Lotimo se odvoda normalnega odvoda (2.37a):

$$\begin{aligned} \frac{\partial^2 g_0(T,T')}{\partial w'\partial n} &= \frac{1}{2\pi}\left(\frac{1}{P^2}\frac{\partial(\mathbf{n}\cdot\mathbf{P})}{\partial w'} + \mathbf{n}\cdot\mathbf{P}\frac{\partial(1/P^2)}{\partial w'}\right) \\ &= \frac{1}{2\pi}\left(\frac{1}{P^2}\frac{\partial(n_x(x'-x)+n_y(y'-y))}{\partial w'} - 2\frac{\mathbf{n}\cdot\mathbf{P}}{P^3}\frac{\partial P}{\partial w'}\right) \\ &= \frac{1}{2\pi}\left(\frac{n_w}{P^2} - 2(w'-w)\frac{\mathbf{n}\cdot\mathbf{P}}{P^4}\right) = \frac{1}{\pi P^2}\left(\frac{n_w}{2} - (w'-w)\frac{\mathbf{n}\cdot\mathbf{P}}{P^2}\right), \end{aligned} \tag{2.69}$$

kjer je $\mathbf{P} = \overrightarrow{TT'} = (x'-x, y'-y)$ distančni vektor od točke T k T'.

Za konec ostaja še odvod normalnega odvoda (2.37b):

$$\begin{aligned} \frac{\partial^2 g(T,T')}{\partial w'\partial n} &= \frac{k_T}{4\mathrm{j}}\left(\frac{\partial(\mathbf{n}\cdot\mathbf{P})}{\partial w'}\frac{H_1^{(2)}(k_T P)}{P} + \mathbf{n}\cdot\mathbf{P}\frac{\partial(1/P)}{\partial w'}H_1^{(2)}(k_T P) + \frac{\mathbf{n}\cdot\mathbf{P}}{P}\frac{\partial H_1^{(2)}(k_T P)}{\partial w'}\right) \\ &= \frac{k_T}{4\mathrm{j}}\left(\frac{n_w H_1^{(2)}(k_T P)}{P} - \frac{\mathbf{n}\cdot\mathbf{P}}{P^2}\frac{\partial P}{\partial w'}H_1^{(2)}(k_T P)\right. \\ &\quad \left. + \frac{\mathbf{n}\cdot\mathbf{P}}{P}\left(H_0^{(2)}(k_T P) - \frac{1}{k_T P}H_1^{(2)}(k_T P)\right)\frac{\partial(k_T P)}{\partial w'}\right) \\ &= \frac{k_T}{4\mathrm{j}P}\left(k_T(w'-w)\frac{\mathbf{n}\cdot\mathbf{P}}{P}H_0^{(2)}(k_T P) + \left(n_w - 2(w'-w)\frac{\mathbf{n}\cdot\mathbf{P}}{P^2}\right)H_1^{(2)}(k_T P)\right), \end{aligned} \tag{2.70}$$

kjer smo upoštevali [53, str. 463], da je

$$\frac{\mathrm{d}H_1^{(2)}(u)}{\mathrm{d}u} = H_0^{(2)}(u) - \frac{1}{u}H_1^{(2)}(u). \tag{2.71}$$

2.4.3 Izračun joulske moči v cilindru

Pri računanju joulske oziroma delovne moči v posameznem cilindru izhajamo iz Poyntingovega stavka v kompleksnem prostoru [45, razdelek 2.20]. Iskano moč na dolžinsko enoto v j-tem cilindru določa integracija Poyntingovega vektorja po njegovem obodu,

$$p_{\mathrm{J,C}j} = -\oint_{\mathcal{L}_{\mathrm{C}j}} \mathrm{Re}[S_n]\mathrm{d}l, \tag{2.72}$$

kjer je $\mathrm{Re}[S_n]$ realni del normalne komponente Poyntingovega vektorja[9] $\mathbf{S} = \mathbf{E} \times \mathbf{H}^*$. Normalno komponento $S_n = -E_z H_t^*$ na robu $\mathcal{L}_{\mathrm{C}j}$ moremo po enačbi (2.12) izraziti z ekvivalentnimi viri in potencialno razliko $U_{\mathrm{C}j}$ na tale način:

$$\begin{aligned} S_n &= -\left(-\mathrm{j}\omega A_z - \frac{\partial V}{\partial z}\right)\left(-\frac{1}{\mu_{\mathrm{C}j}}\frac{\partial A_z}{\partial n}\right)^* = -\left(-\mathrm{j}\omega\alpha_2 + \frac{U_{\mathrm{C}j}}{l_0}\right)\left(\frac{\alpha_1}{\mu_0}\right)^* \\ &= -\frac{U_{\mathrm{C}j}}{l_0}\frac{\alpha_1^*}{\mu_0} + \frac{\mathrm{j}\omega}{\mu_0}\alpha_1^*\alpha_2. \end{aligned} \tag{2.73}$$

Če upoštevamo še Ampèrov zakon (podobno kot v enačbi (2.21)), dobimo

$$p_{\mathrm{J,C}j} = \mathrm{Re}\left[\frac{U_{\mathrm{C}j}}{l_0}\oint_{\mathcal{L}_{\mathrm{C}j}}\frac{\alpha_1^*}{\mu_0}\mathrm{d}l - \frac{\mathrm{j}\omega}{\mu_0}\oint_{\mathcal{L}_{\mathrm{C}j}}\alpha_1^*\alpha_2\mathrm{d}l\right] = \frac{\mathrm{Re}[U_{\mathrm{C}j}I_{\mathrm{C}j}^*]}{l_0} + \frac{\omega}{\mu_0}\oint_{\mathcal{L}_{\mathrm{C}j}}\mathrm{Im}[\alpha_1^*\alpha_2]\mathrm{d}l. \tag{2.74}$$

Z upoštevanjem stopničaste aproksimacije (2.27) in koeficientov pripadnosti (2.31) se integral prevede v vsoto,

$$p_{\mathrm{J,C}j} \approx \frac{\mathrm{Re}[U_{\mathrm{C}j}I_{\mathrm{C}j}^*]}{l_0} + \frac{\omega}{\mu_0}\sum_{m=1}^{n_{\mathrm{E}}}\zeta_{\mathrm{C}j,m}\delta l_m \mathrm{Im}[\tilde{\alpha}_{1,m}^*\tilde{\alpha}_{2,m}], \tag{2.75}$$

tok $I_{\mathrm{C}j}$ v prvem sumandu pa izrazimo z enačbo (2.35c).

[9] Kadar se kompleksorji nanašajo na amplitude harmoničnih količin, je $\mathbf{S} = (\mathbf{E} \times \mathbf{H}^*)/2$.

Poglavje 3

Verifikacija predlagane metode

Rezultate predlagane metode smo primerjali z:

- rezultati analitično rešljivih primerov,
- rezultati meritev in
- rezultati dveh drugih numeričnih metod.

Iz primerjav sta razvidna natančnost in obseg uporabnosti predlagane metode.

3.1 Cevasti zaslon krožnega preseka

3.1.1 Vodnik v koaksialnem zaslonu

Na sliki 3.1 je prikazan primer žice znotraj zaslona, ki geometrijsko ustreza koaksialnemu kablu. Vir primarnega polja je harmoničen tok I_0 v žici oziroma žili. Oklop ima vlogo zaslona ter ima odprta konca. Rezultančno magnetno polje je v tem primeru analitično določljivo. Za funkcijo radialne porazdelitve inducirane tokovne gostote $\mathbf{J} = \mathbf{e}_z J_z$ v zaslonu velja Besselova diferencialna enačba ničtega reda [31, razdelek 28]

$$\triangle J_z(\rho) + k_{\mathrm{C}}^2 J_z(\rho) = \frac{\mathrm{d}^2 J_z}{\mathrm{d}\rho^2} + \frac{1}{\rho}\frac{\mathrm{d}J_z}{\mathrm{d}\rho} + k_{\mathrm{C}}^2 J_z(\rho) = 0, \quad \rho_1 \leq \rho \leq \rho_2, \tag{3.1}$$

kjer je k_{C} valovno število zaslona. Rešitev te enačbe se izraža z Besselovimi funkcijami prve in druge vrste ničtega reda,

$$J_z(\rho) = C_1 J_0(k_{\mathrm{C}}\rho) + C_2 N_0(k_{\mathrm{C}}\rho). \tag{3.2}$$

Jakost magnetnega polja v zaslonu izrazimo s tokovno gostoto. Upoštevamo Faradayev indukcijski zakon, $\boldsymbol{\nabla} \times \mathbf{E} = -\mathrm{j}\omega\mathbf{B} = -\mathrm{j}\omega\mu_{\mathrm{C}}\mathbf{H}$, $\mathbf{E} = \mathbf{J}/\gamma_{\mathrm{C}}$, in dobimo:

$$\mathbf{H} = \frac{-1}{\mathrm{j}\omega\mu_{\mathrm{C}}\gamma_{\mathrm{C}}}\boldsymbol{\nabla} \times \mathbf{J} = \frac{1}{k_{\mathrm{C}}^2}\boldsymbol{\nabla} \times (\mathbf{e}_z J_z(\rho)) = -\mathbf{e}_\varphi \frac{1}{k_{\mathrm{C}}^2}\frac{\mathrm{d}J_z(\rho)}{\mathrm{d}\rho}, \quad \rho_1 \leq \rho \leq \rho_2, \tag{3.3}$$

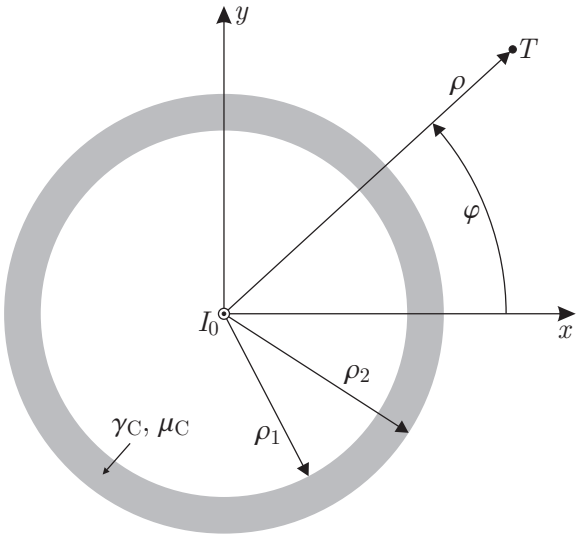

Slika 3.1: Vodnik v koaksialnem zaslonu.

kjer sta γ_C in μ_C specifična prevodnost in permeabilnost zaslona. Magnetno poljsko jakost izven zaslona določimo iz Ampèrovega zakona [56], $\oint \mathbf{H} \cdot \mathrm{d}\mathbf{l} = I$; upoštevamo, da je celotni inducirani tok v dvostransko odprtem zaslonu enak nič:

$$\mathbf{H} = \mathbf{e}_\varphi H_\varphi(\rho) = \mathbf{e}_\varphi \frac{I_0}{2\pi\rho}, \quad \rho < \rho_1 \text{ ali } \rho > \rho_2. \tag{3.4}$$

Če v enačbo (3.3) vstavimo nastavek (3.2) za tokovno gostoto in izračunamo njen odvod, dobimo nastavek za magnetno poljsko jakost oziroma komponento H_φ v zaslonu:

$$H_\varphi(\rho) = \left(C_1 J_1(k_\mathrm{C}\rho) + C_2 N_1(k_\mathrm{C}\rho)\right)/k_\mathrm{C}, \quad \rho_1 \le \rho \le \rho_2, \tag{3.5}$$

kjer sta J_1 in N_1 Besselovi funkciji prve in druge vrste prvega reda. Konstanti C_1 in C_2 se določi s pomočjo mejnega pogoja (2.12a) za tangencialno komponento magnetne poljske jakosti na površinah zaslona:

$$C_1 = \frac{k_\mathrm{C} I_0}{2\pi} \frac{N_1(k_\mathrm{C}\rho_2)/\rho_1 - N_1(k_\mathrm{C}\rho_1)/\rho_2}{J_1(k_\mathrm{C}\rho_1)N_1(k_\mathrm{C}\rho_2) - J_1(k_\mathrm{C}\rho_2)N_1(k_\mathrm{C}\rho_1)} \tag{3.6a}$$

$$C_2 = \frac{k_\mathrm{C} I_0}{2\pi} \frac{J_1(k_\mathrm{C}\rho_1)/\rho_2 - J_1(k_\mathrm{C}\rho_2)/\rho_1}{J_1(k_\mathrm{C}\rho_1)N_1(k_\mathrm{C}\rho_2) - J_1(k_\mathrm{C}\rho_2)N_1(k_\mathrm{C}\rho_1)}. \tag{3.6b}$$

Ta zaslon sicer ne služi zaslanjanju, ampak je zanimiv s stališča verifikacije numeričnih postopkov.

Primerjavi absolutnih vrednosti magnetnih poljskih jakosti, izračunanih po metodi robnih elementov (MRE) in analitično, sta za nemagnetni (Al) in magnetni (Fe) zaslon prikazani na slikah 3.2 in 3.3. Relativno odstopanje numerične od analitično izračunane

vrednosti je $\epsilon_\mathrm{r} = (H_\mathrm{num.} - H_\mathrm{anal.})/H_\mathrm{anal.}$. Številski podatki v primeru zaslona iz aluminijeve legure so: notranji in zunanji polmer zaslona sta $\rho_1 = 50\,\mathrm{mm}$ in $\rho_2 = 55\,\mathrm{mm}$, specifična prevodnost in permeabilnost sta $\gamma_\mathrm{C} = 30{,}5\,\mathrm{MS/m}$ in $\mu_\mathrm{C} = \mu_0$, harmonični tok v žici in frekvenca pa sta $I_0 = 100\,\mathrm{A}$ in $f = 5\,\mathrm{kHz}$. Pri zaslonu iz jekla so podatki spremenjeni pri prevodnosti, permeabilnosti in frekvenci (pri Al zaslonu je frekvenca večja zato, da bi ne bilo popačenje primarnega polja zanemarljivo): $\gamma_\mathrm{C} = 10\,\mathrm{MS/m}$, $\mu_\mathrm{C} = 1000\mu_0$ in $f = 50\,\mathrm{Hz}$. Kot je bilo pričakovati, je relativno odstopanje največje (do 3 %) ob površinah zaslona.

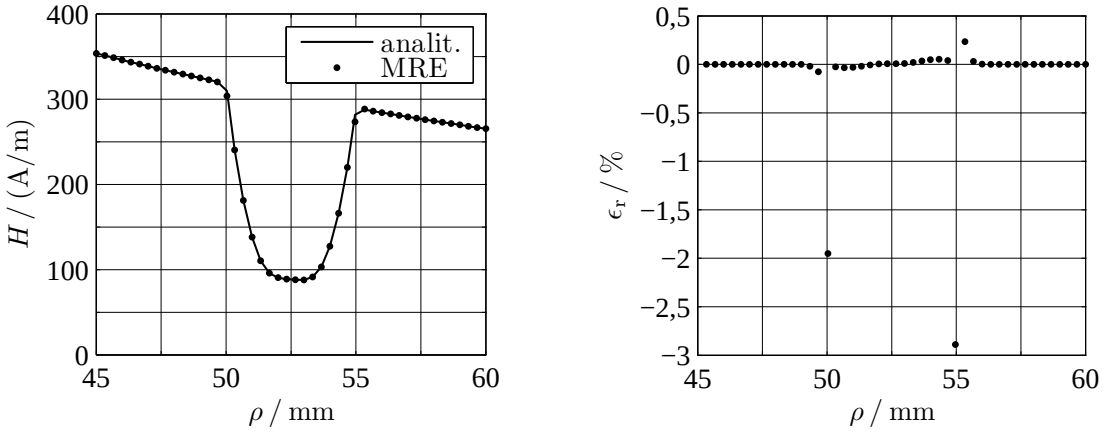

(a) Magnetna poljska jakost

(b) Relativna napaka

Slika 3.2: Primerjava numerične in analitične rešitve za primer vodnika v koaksialnem nemagnetnem zaslonu.

Primer koaksialnega zaslona lahko izkoristimo tudi za oceno točnosti predlagane numerične metode. Odstopanje je odvisno predvsem od razmerja med dolžino segmentov δl in vdorno globino $\delta_\mathrm{C} = \sqrt{2/(\omega\mu_\mathrm{C}\gamma_\mathrm{C})}$ v zaslonu. Odvisnost smo analizirali na primeru s podatki: $f = 250\,\mathrm{Hz}$, $\rho_1 = 10\,\mathrm{mm}$, $\rho_2 = 20\,\mathrm{mm}$, $\gamma_\mathrm{C} = 10\,\mathrm{MS/m}$ in $\mu_\mathrm{C} = 100\mu_0$. Slika 3.4 prikazuje absolutno vrednost relativnega odstopanja v zaslonu pri $\rho = 15\,\mathrm{mm}$. Ta vrednost narašča približno potenčno z razmerjem $\delta l/\delta_\mathrm{C}$ in pri $\delta l/\delta_\mathrm{C} = 1$ še ne doseže 1 %. Zadnja ugotovitev se ujema z napotkom v [47, str. 248], da naj bi širine segmentov ne presegale 70 % do 90 % vdorne globine.

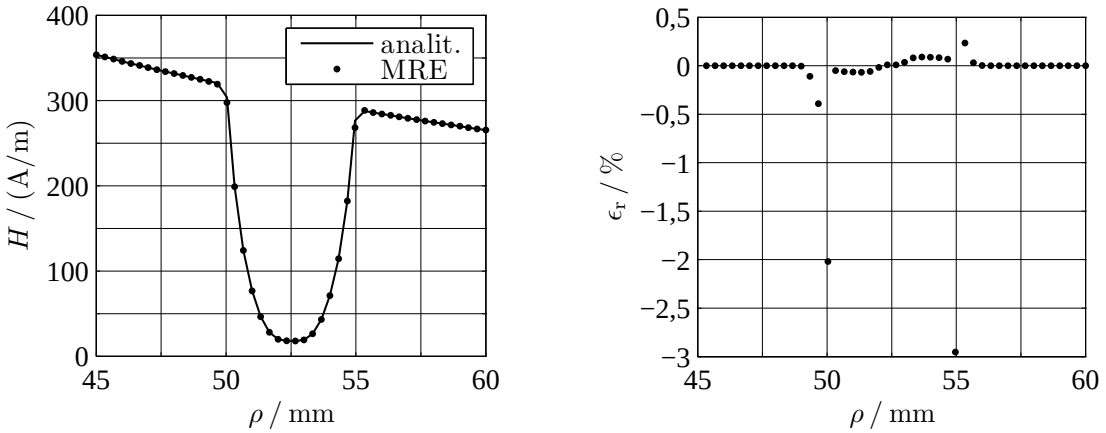

(a) Magnetna poljska jakost

(b) Relativna napaka

Slika 3.3: Primerjava numerične in analitične rešitve za vodnik v koaksialnem magnetnem zaslonu.

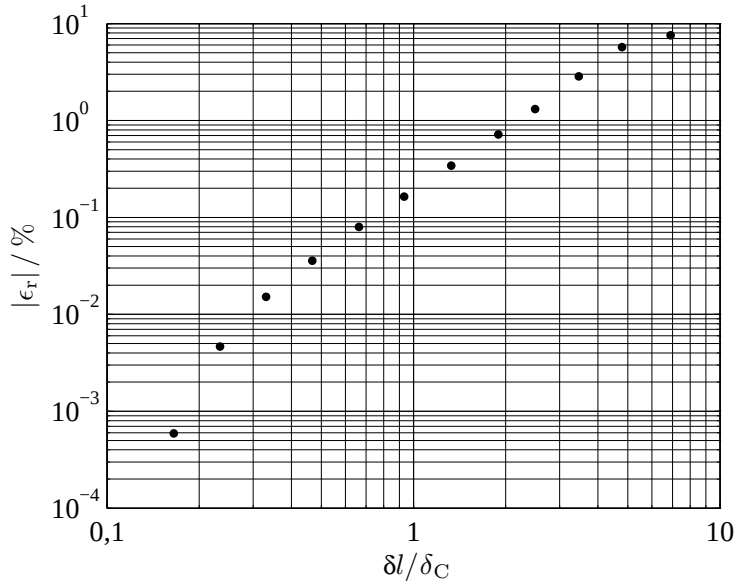

Slika 3.4: Relativno odstopanje v odvisnosti od razmerja dolžine robnih elementov in vdorne globine.

3.1.2 Oklopljen dvovod

Analitično rešljiv je tudi primer dvovoda tankih žic v cevastem zaslonu krožnega preseka (slika 3.5)[1]. Kratek opis izpeljave je v nadaljevanju [3]. Za z-komponento vektorskega

[1]Za tanek zaslon, $\rho_2 - \rho_1 \ll \delta_C$, je analitična rešitev predstavljena v [57, str. 142–145] in uporabljena v [58]. Kadar je medosna razdalja žic majhna, $2d \ll \rho_1$, moremo dvovod smatrati kot premi dipol. Analitična rešitev za ta primer je podana v [59] in uporabljena v [15, 2].

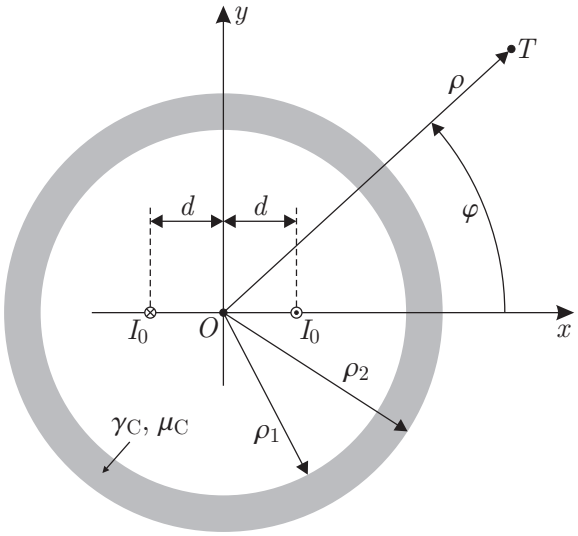

Slika 3.5: Dvovod v cevastem zaslonu krožnega preseka.

magnetnega potenciala velja enačba (2.5). Rešimo jo v valjnem koordinatnem sistemu z metodo ločitve spremenljivk: z-komponento $A_{0,z}$ potenciala primarnega polja razvijemo v Fourierevo vrsto,

$$A_{0,z}(\rho,\varphi) = \frac{\mu_0 I_0}{\pi} \sum_{n=1}^{\infty} \cos\left((2n-1)\varphi\right) \frac{1}{(2n-1)2^{2n-1}} \left(\frac{2d}{\rho}\right)^{2n-1}, \tag{3.7}$$

in oblikujemo nastavke za splošno rešitev,

$$A_z(\rho,\varphi) = \sum_{n=1}^{\infty} \cos\left((2n-1)\varphi\right) \left(C_{1,n}\rho^{2n-1} + \frac{\mu_0 I_0}{\pi} \frac{1}{(2n-1)2^{2n-1}} \left(\frac{2d}{\rho}\right)^{2n-1} \right), \quad \rho < \rho_1 \tag{3.8a}$$

$$A_z(\rho,\varphi) = \sum_{n=1}^{\infty} \cos\left((2n-1)\varphi\right) \left(C_{2,n} H^{(1)}_{2n-1}(k_{\mathrm{C}}\rho) + C_{3,n} H^{(2)}_{2n-1}(k_{\mathrm{C}}\rho) \right), \quad \rho_1 \le \rho \le \rho_2 \tag{3.8b}$$

$$A_z(\rho,\varphi) = \sum_{n=1}^{\infty} \cos\left((2n-1)\varphi\right) C_{4,n}\rho^{-(2n-1)}, \quad \rho > \rho_2, \tag{3.8c}$$

kjer so $H^{(1)}_{2n-1}$ in $H^{(2)}_{2n-1}$ Hankelovi funkciji prve oziroma druge vrste reda $(2n-1)$ ter k_{C} valovno število zaslona. Konstante $C_{1,n}$, $C_{2,n}$, $C_{3,n}$ in $C_{4,n}$, $n = 1, 2, \ldots$, se določi iz mejnih pogojev (2.12) na površinah zaslona. Vrste v enačbi (3.8) konvergirajo zelo hitro (razen v bližnji okolici žic, ko je $\rho \approx 2d$ ali $\rho < 2d$), zato je dovolj upoštevati le prvih nekaj členov. Pri izračunih smo upoštevali prvih deset členov.

Primerjava radialnih odvisnosti (vzdolž polpremice $\varphi = \pi/4$) absolutne vrednosti magnetne poljske jakosti, izračunanih po metodi robnih elementov (MRE) in analitično, je prikazana na sliki 3.6. Podatki za ta primer so: $I_0 = 100\,\mathrm{A}$, $f = 50\,\mathrm{Hz}$, $2d = 30\,\mathrm{mm}$,

$\rho_1 = 50\,\mathrm{mm}$, $\rho_2 = 55\,\mathrm{mm}$, $\gamma_\mathrm{C} = 10\,\mathrm{MS/m}$ in $\mu_\mathrm{C} = 10\mu_0$. Omembe vredna odstopanja je opaziti le ob površinah zaslona.

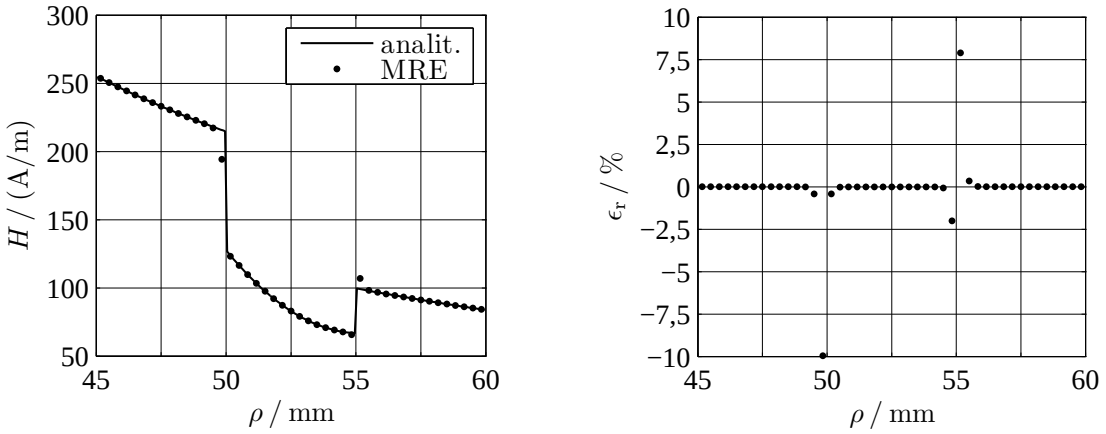

(a) Magnetna poljska jakost

(b) Relativna napaka

Slika 3.6: Primerjava numerične in analitične rešitve za primer dvovoda v cevastem zaslonu.

Diskrepanco med numerično in analitično izračunano absolutno vrednostjo magnetnega polja v odvisnosti od razmerja $\delta l/\delta_\mathrm{C}$ smo analizirali na enakem zaslonu in pri enaki frekvenci kot v prejšnjem primeru (glej razdelek 3.1.1). Primarni vir polja je tokrat tok v dvovodu medosne razdalje $2d = 10\,\mathrm{mm}$. Na sliki 3.7 so prikazani rezultati te analize v točki ($\rho = 15\,\mathrm{mm}, \varphi = \pi/4$). Absolutna vrednost relativnega odstopanja narašča spet približno potenčno z razmerjem $\delta l/\delta_\mathrm{C}$, pri $\delta l/\delta_\mathrm{C} \approx 1$ je okrog 1 %.

Hoburg in ostali [60] so merili magnetno polje dvovoda v cevastem zaslonu krožnega preseka. Primerjava vrednosti faktorjev zastiranja, ki so določene analitično, s predlagano metodo in z meritvijo, je za aluminijast zaslon prikazana na sliki 3.8a, za jeklen zaslon pa na sliki 3.8b. Številski podatki so $I_0 = 500\,\mathrm{A}$, $f = 60\,\mathrm{Hz}$, $2d = 6\,\mathrm{cm}$, $\rho_{1,\mathrm{Al}} = 25{,}435\,\mathrm{cm}$, $\rho_{1,\mathrm{Fe}} = 25{,}43\,\mathrm{cm}$, $\rho_2 = 25{,}5\,\mathrm{cm}$, $\gamma_{\mathrm{C,Al}} = 30{,}5\,\mathrm{MS/m}$, $\gamma_{\mathrm{C,Fe}} = 6{,}76\,\mathrm{MS/m}$ in $\mu_{\mathrm{C,Fe}} = 190\mu_0$[2]. Ostali podatki meritev so podrobno opisani v [60]. Vrednosti faktorjev zastiranja so izračunane na oddaljenosti $\rho = 0{,}62\,\mathrm{m}$ in kotih $0 \leq \varphi \leq \pi/2$, izmerjene pa le pri

[2]V [60] beremo: "Izmerjena relativna permeabilnost jekla je bila $\mu_\mathrm{r} = 182{,}5$ in je bila pod $\mu_\mathrm{r} = 190$ za gostote pretoka v jeklu pod $10^{-3}\,\mathrm{T}$". Ker pa je gostota pretoka v jeklenem zaslonu okrog 15 mT, smo pri izračunih za relativno permeabilnost uporabili vrednost 190, čeravno je verjetno še nekoliko večja in zaradi nelinearnosti jekla niti ni povsod v zaslonu enaka, kar najbrž tudi prispeva k diskrepanci med izmerjenimi in izračunanimi rezultati.

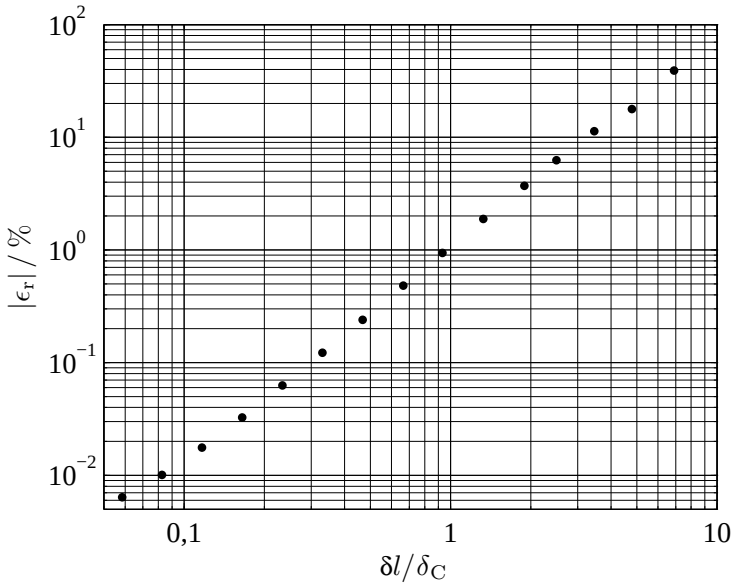

Slika 3.7: Natančnosti izračuna v odvisnosti od razmerja dolžine robnih elementov in vdorne globine za primer dvovoda.

kotih, $\varphi = 0$ in $\pi/2$. Iz diagramov na slikah 3.8a in 3.8b je razvidno izvrstno ujemanje numeričnih in analitičnih rezultatov (odstopanje je manj kot $0,02\,\%$). Ker je medosna razdalja dvovoda majhna, $2d < \rho_1/4$, je faktor zastiranja skoraj konstanten[3].

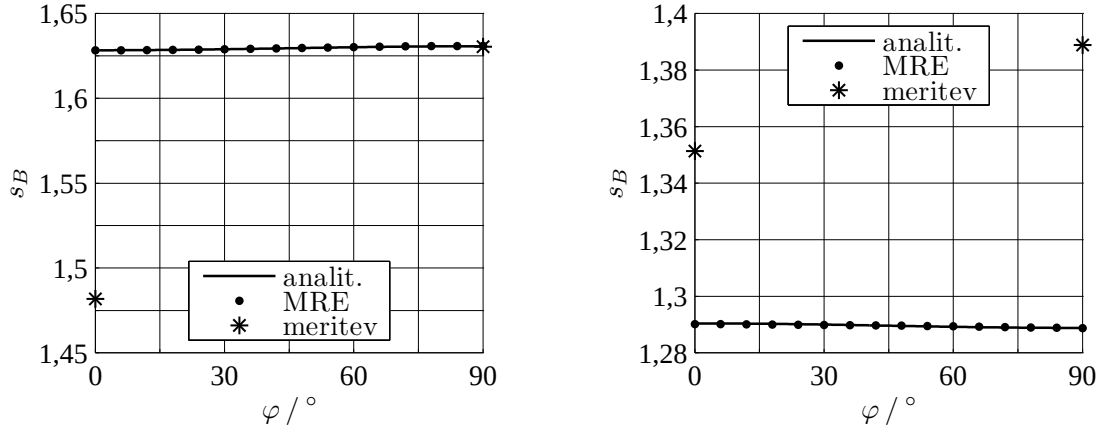

(a) Nemagnetni zaslon

(b) Magnetni zaslon

Slika 3.8: Primerjava numerične in analitične rešitve z rezultati meritev za primer dvovoda.

[3]V primeru premega dipola, $2d \ll \rho_1$, bi bil faktor zastiranja enak v vseh točkah zunaj cevastega zaslona [15, enačba (1)].

3.2 Zelo širok raven zaslon

Obravnavali smo tudi primer zelo širokega zaslona debeline t in širine l na višini y_C nad žico (slika 3.9), ki naj je idealno dvostransko ozemljen. Če je zaslon zelo širok, moremo za

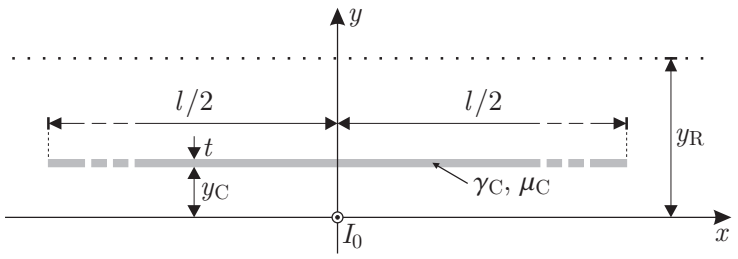

Slika 3.9: Zelo širok zaslon nad žico.

primerjavo uporabiti analitično rešitev za neskončno širok zaslon [46, 19, 31, razdelek 30]. Analitična rešitev za z-komponento A_z potenciala nad zaslonom se izraža s Fourierovim integralom [50, str. 579],

$$A_z(x, y > y_\mathrm{C} + t) = \int_0^\infty f(\xi)\mathrm{e}^{-\xi y}\cos(\xi x)\mathrm{d}\xi. \tag{3.9}$$

Funkcija $f(\xi)$ sledi iz mejnih pogojev (2.12) na površinah zaslona,

$$f(\xi) = \frac{I_0\mu_\mathrm{C}\mu_0^2}{\pi}\sqrt{\xi^2 - k_\mathrm{C}^2}\,\mathrm{e}^{t\xi}\left(2\mu_\mathrm{C}\mu_0\xi\sqrt{\xi^2 - k_\mathrm{C}^2}\cosh\left(t\sqrt{\xi^2 - k_\mathrm{C}^2}\right) + \left(\mu_\mathrm{C}^2\xi^2 + \mu_0^2\left(\xi^2 - k_\mathrm{C}^2\right)\right)\sinh\left(t\sqrt{\xi^2 - k_\mathrm{C}^2}\right)\right)^{-1}. \tag{3.10}$$

Z odvajanjem potenciala (3.9) pridobimo izraze za komponenti vektorja gostote magnetnega pretoka nad zaslonom (glej enačbo (2.62)):

$$B_x(x, y > y_\mathrm{C} + t) = \frac{\partial A_z(x, y > y_\mathrm{C} + t)}{\partial y} = -\int_0^\infty \xi f(\xi)\mathrm{e}^{-\xi y}\cos(\xi x)\mathrm{d}\xi \tag{3.11a}$$

$$B_y(x, y > y_\mathrm{C} + t) = -\frac{\partial A_z(x, y > y_\mathrm{C} + t)}{\partial x} = \int_0^\infty \xi f(\xi)\mathrm{e}^{-\xi y}\sin(\xi x)\mathrm{d}\xi. \tag{3.11b}$$

Integrale (3.9) in (3.11) računamo numerično, neskončno zgornjo mejo pa nadomestimo z ustrezno končno (v primerih, ki sta opisana v nadaljevanju, smo za zgornjo integracijsko mejo izbrali vrednost 10^4).

Absolutne vrednosti gostote magnetnega pretoka, izračunane po metodi robnih elementov in z analitično aproksimacijo, smo primerjali v nekaj točkah nad zaslonom (na

višini $y_R = 15\,\text{cm}$ nad žico). Za nemagnetni zaslon ($\gamma_C = 30{,}5\,\text{MS/m}$ in $\mu_C = \mu_0$) je primerjava prikazana na sliki 3.10a, za magnetnega ($\gamma_C = 10\,\text{MS/m}$ in $\mu_C = 10\mu_0$) pa na sliki 3.10b. Številski podatki so: $I_0 = 100\,\text{A}$, $f = 50\,\text{Hz}$, $t = 2\,\text{mm}$, $y_C = 5\,\text{cm}$ in $l = 4\,\text{m}$. Ob sredini zaslona je ujemanje solidno, proti robovom zaslona ($x = \pm l/2 = \pm 2\,\text{m}$) pa odstopanje pričakovano narašča.

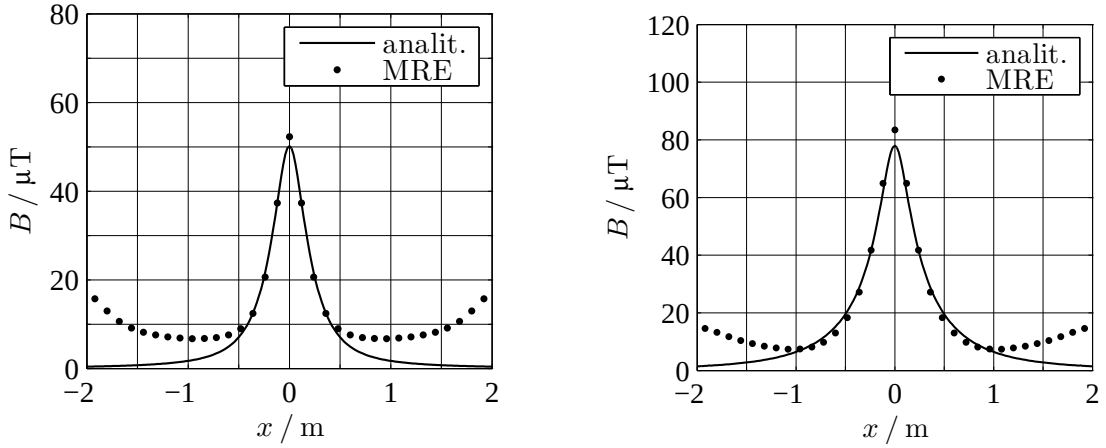

(a) Nemagnetni zaslon

(b) Magnetni zaslon

Slika 3.10: Primerjava numeričnih rezultatov z analitično aproksimacijo v primeru zelo širokega ravnega zaslona.

3.3 Raven zaslon

Rezultate predlagane metode smo primerjali z rezultati nekaterih drugih metod in meritev tudi na primeru ravnega zaslona nad žicami (slika 3.11).

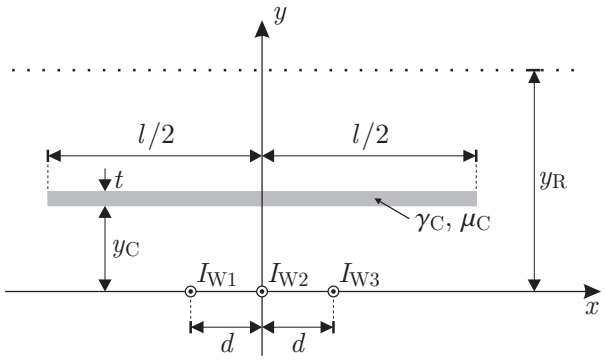

Slika 3.11: Raven zaslon nad žicami.

3.3.1 Hibridna metoda (HM)

V delih [20] in [21] je predstavljena metoda za izračun učinka zastiranja končno širokih ravnih kovinskih 2D zaslonov. Ta hibridna aproksimacija je kombinacija izraza za prodiranje polja skozi neskončno širok zaslon ter izraza za prepuščanje okrog končno širokega.

3.3.2 Metoda tokovnih niti (MTN)

Metoda tokovnih niti [29, 3, 26] je primerna le za analizo nemagnetnih cilindrov. Sloni na rešitvi integralske enačbe za porazdelitev gostote $\mathbf{J} = \mathbf{e}_z J_z$ toka v cilindrih.

Vir kvazistatičnega magnetnega polja so toki v žicah in cilindrih. Vzdolžno komponento vektorskega magnetnega potenciala izrazimo z vsoto prispevkov vseh tokov [40, razdelek 8.1]:

$$A_z(T) = -\frac{\mu_0}{2\pi} \sum_{i=1}^{n_\mathrm{W}} I_{\mathrm{W}i} \ln \overline{TT_{\mathrm{W}i}} - \frac{\mu_0}{2\pi} \int\limits_{\mathcal{S}} J_z(T') \ln \overline{TT'} \,\mathrm{d}s', \tag{3.12}$$

kjer je T opazovana, T' pa integracijska točka. Če je sistem vzporeden s površino zemlje, je treba Greenovo funkcijo (2.7b) nadomestiti s funkcijo (2.6). Po vstavljanju enačbe (3.12) v enačbo (2.4) sledi integralska enačba za gostoto toka v cilindrih,

$$\frac{J_z(T)}{\gamma(T)} - \frac{\mathrm{j}\omega\mu_0}{2\pi} \int\limits_{\mathcal{S}} J_z(T') \ln \overline{TT'} \,\mathrm{d}s' - \frac{U(T)}{l_0} = \frac{\mathrm{j}\omega\mu_0}{2\pi} \sum_{i=1}^{n_\mathrm{W}} I_{\mathrm{W}i} \ln \overline{TT_{\mathrm{W}i}}. \tag{3.13}$$

Tudi potencialne razlike U med konci posameznih valjev so v splošnem neznanke, podobno kot v razdelku 2.2, zato je potrebno tej pridružiti še enačbe tipa (2.21), (2.22), (2.23) in/ali (2.24), v katerih izrazimo tok z integralom tokovne gostote po preseku cilindra,

$$I_{\mathrm{C}j} = \int\limits_{\mathcal{S}_{\mathrm{C}j}} J_z(T') \mathrm{d}s', \quad j = 1, 2, \ldots, n_\mathrm{C}. \tag{3.14}$$

Dobimo sistem sklopljenih integralskih enačb. Tudi tega smo numerično reševali z momentno metodo, le da je bilo tokrat potrebno diskretizirati površine presekov cilindrov.

Frix in Karady [3] sta merila magnetno polje dvovoda, ki je zaslanjano z ravnim aluminijastim zaslonom. Struktura, ki sta jo uporabila, ustreza primeru na sliki 3.11, pri kateri je srednja žica odstranjena in sta toka v krajnih dveh nasprotna, $I_{\mathrm{W}1} = -I_{\mathrm{W}3} = I_0$. Uporabila sta dva različna aluminijasta zaslona. V prvem primeru so številski podatki: $I_0 = 100\,\mathrm{A}$, $f = 60\,\mathrm{Hz}$, $y_\mathrm{C} = 6{,}35\,\mathrm{cm}$, $2d = 7{,}62\,\mathrm{cm}$, $l = 30{,}48\,\mathrm{cm}$, $t = 3{,}175\,\mathrm{mm}$,

$\gamma_{\mathrm{C}} = (10^3/36{,}99)\,\mathrm{MS/m}$ in $\mu_{\mathrm{C}} = \mu_0$. Zaslon ima odprta konca in gostota magnetnega pretoka je merjena na višini $y_{\mathrm{R}} = 14{,}13\,\mathrm{cm}$ nad žicama dvovoda. V drugem primeru so podatki spremenjeni pri debelini zaslona, $t = 6{,}35\,\mathrm{mm}$, specifični prevodnosti, $\gamma_{\mathrm{C}} = (10^3/45)\,\mathrm{MS/m}$, in višini merilnih točk, $y_{\mathrm{R}} = 14{,}45\,\mathrm{cm}$. Preostali podatki meritev so podrobno opisani v [3]. Navajamo primerjavo rezultatov meritev, rezultatov metode robnih elementov (MRE), rezultatov metode tokovnih niti (MTN) in rezultatov hibridne metode (HM). Iz slike 3.12 je razvidno, da je ujemanje rezultatov MRE in MTN izvrstno (poprečje absolutnih vrednosti relativnega odstopanja je $|\epsilon_{\mathrm{r}}|_{\mathrm{sr.}} \doteq 0{,}03\,\%$) in da je ujemanje z rezultati eksperimenta pri teh dveh metodah ($|\epsilon_{\mathrm{r}}|_{\mathrm{sr.}} \doteq 5{,}1\,\%$) veliko boljše kot pri HM ($|\epsilon_{\mathrm{r}}|_{\mathrm{sr.}} \doteq 16{,}2\,\%$).

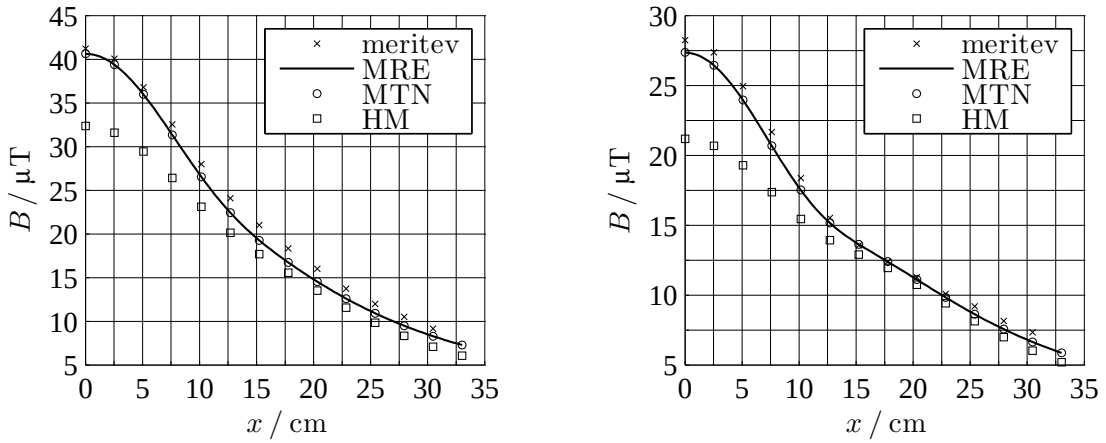

(a) Tanjši zaslon ($t = 3{,}175\,\mathrm{mm}$)

(b) Debelejši zaslon ($t = 6{,}35\,\mathrm{mm}$)

Slika 3.12: Primerjava rezultatov meritev, metode robnih elementov, metode tokovnih niti in hibridne metode pri ravnem aluminijastem zaslonu.

3.3.3 Metoda ploskovnih tokov (MPT)

Metoda ploskovnih tokov sloni na magnetostatični aproksimaciji in je primerna le za analizo magnetnih cilindrov. Na površinah magnetnih cilindrov je gostota ploskovnih tokov magnetizacije $\mathbf{K}$ sorazmerna tangencialni komponenti ($\mathbf{n} \times \mathbf{B}$) gostote magnetnega pretoka [36], [31, razdelek 22]:

$$\mathbf{K}(T) + \frac{2}{\mu_0}\beta(T)\mathbf{n}(T) \times \mathbf{B}(T) = \mathbf{0}, \tag{3.15}$$

kjer je $\beta(T) = (\mu(T_-) - \mu_0)\,/(\mu(T_-) + \mu_0)$. Če izrazimo vektor $\mathbf{B}$ z vsoto primarnega polja ($\mathbf{B_0}$) in prispevka gostote $\mathbf{K} = \mathbf{e}_z K_z$ ploskovnih tokov, dobimo integralsko enačbo

za porazdelitev le-te:

$$K_z(T) + \frac{\beta(T)}{\pi} \oint_{\mathcal{L}} K_z(T') \frac{\mathbf{n}(T) \cdot \mathbf{P}}{P^2} \mathrm{d}l' = -\frac{2\beta(T)}{\mu_0} \mathbf{e}_z \cdot (\mathbf{n}(T) \times \mathbf{B}_0(T)) \,, \tag{3.16}$$

kjer je $\mathbf{P} = \overrightarrow{TT'} = (x' - x, y' - y)$ distančni vektor med opazovano točko T in integracijsko T'.

Rezultate treh metod, metode robnih elementov, metode ploskovnih tokov in hibridne metode, smo podali za primer ravnega magnetnega zaslona, ki je idealno dvostransko ozemljen in se nahaja nad žicami trifaznega voda (slika 3.11): $I_{\mathrm{W1}} = I_0 \exp(\mathrm{j}2\pi/3)$, $I_{\mathrm{W2}} = I_0$ in $I_{\mathrm{W3}} = I_0 \exp(-\mathrm{j}2\pi/3)$. Na sliki 3.13 so prikazane izračunane vrednosti gostote magnetnega pretoka na višini $y_{\mathrm{R}} = 40\,\mathrm{cm}$ nad žicami. Številski podatki primera na sliki 3.13a so: $I_0 = 400\,\mathrm{A}$, $f = 50\,\mathrm{Hz}$, $y_{\mathrm{C}} = 10\,\mathrm{cm}$, $d = 8\,\mathrm{cm}$, $l = 40\,\mathrm{cm}$, $t = 2\,\mathrm{mm}$, $\gamma_{\mathrm{C}} = 10\,\mathrm{MS/m}$ in $\mu_{\mathrm{C}} = 1000\mu_0$. Ujemanje rezultatov HM z rezultati MRE ni prav dobro ($|\epsilon_{\mathrm{r}}|_{\mathrm{sr.}} \doteq 9{,}5\,\%$). Ujemanje rezultatov MPT z rezultati MRE je še slabše ($|\epsilon_{\mathrm{r}}|_{\mathrm{sr.}} \doteq 13{,}4\,\%$), saj magnetostatična aproksimacija ne upošteva induciranih vrtinčnih tokov v cilindrih. Opravili smo še izračun (glej sliko 3.13b) pri $f = 1\,\mathrm{Hz}$. Tokrat je ujemanje z rezultati MRE pri MPT izvrstno ($|\epsilon_{\mathrm{r}}|_{\mathrm{sr.}} \doteq 0{,}09\,\%$) in tudi boljše kot pri HM ($|\epsilon_{\mathrm{r}}|_{\mathrm{sr.}} \doteq 1{,}1\,\%$). Magnetostatična aproksimacija je očitno uporabljiva le, če so inducirani vrtinčni toki zanemarljivi, ti pa so pri zelo nizkih frekvencah [3] in pri lameliranih ali feritnih cilindrih.

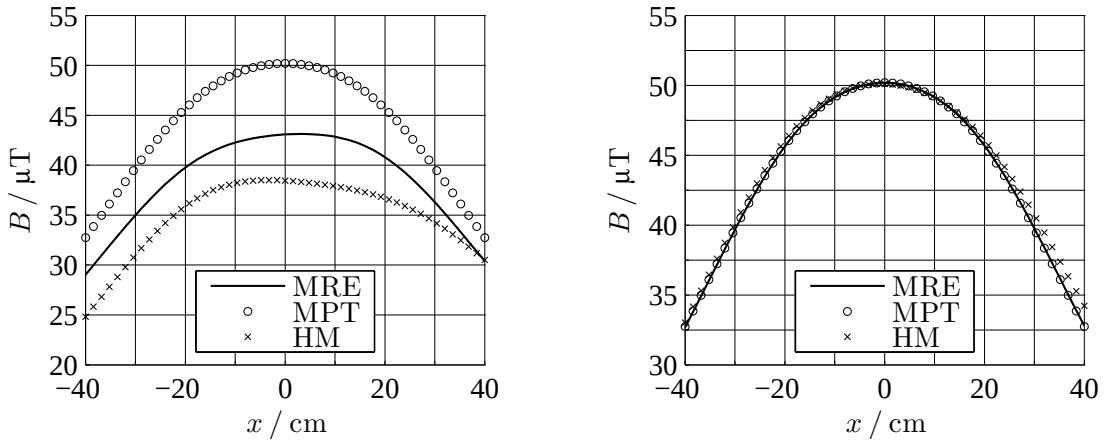

(a) $f = 50\,\mathrm{Hz}$ (b) $f = 1\,\mathrm{Hz}$

Slika 3.13: Primerjava rezultatov predlagane metode z rezultati metode ploskovnih tokov in hibridne metode v primeru ravnega magnetnega zaslona.

3.3.4 Meritev

Na Elektroinštitutu Milan Vidmar smo opravili meritve na primeru zaslona, ki je prikazan na sliki 3.11. Zaslon je bil širok $l = 1\,\mathrm{m}$ in dolg 8 m, dvostransko ozemljen in postavljen na višino $y_\mathrm{C} = 20\,\mathrm{cm}$ nad žicami trifaznega voda: $I_\mathrm{W1} = I_0 \exp(\mathrm{j}2\pi/3)$, $I_\mathrm{W2} = I_0$, $I_\mathrm{W3} = I_0 \exp(-\mathrm{j}2\pi/3)$, $I_0 = 100\,\mathrm{A}$, $f = 50\,\mathrm{Hz}$ in $d = 8\,\mathrm{cm}$. Dolžina trifaznega voda je bila 10 m. Eksperiment je bil opravljen za dva zaslona: za aluminijast zaslon ($\gamma_\mathrm{C} = 30{,}5\,\mathrm{MS/m}$, $\mu_\mathrm{C} = \mu_0$) debeline $t = 4\,\mathrm{mm}$ in jeklen zaslon ($\gamma_\mathrm{C} = 10\,\mathrm{MS/m}$, $\mu_\mathrm{C} = 100\mu_0$) debeline $t = 1{,}6\,\mathrm{mm}$. Zaslon je bil dvoslojen in iz plošč dimenzij $1\,\mathrm{m} \times 2\,\mathrm{m}$. Gostota magnetnega pretoka je bila merjena z Wandel & Goltermann EFA-3 EM poljskim analizatorjem. Ostali podatki eksperimenta so opisani v [32, razdelek 3.3.3].

Vrednosti gostote magnetnega pretoka, ki so bile izmerjene na višinah $y_\mathrm{R} = 30\,\mathrm{cm}$ in $y_\mathrm{R} = 70\,\mathrm{cm}$ nad žicami, smo primerjali z izračunanimi po metodi robnih elementov. Rezultati primerjave za nemagnetni (aluminijast) zaslon so prikazani na sliki 3.14, za magnetni (jeklen) pa na sliki 3.15. Poprečje absolutnih vrednosti relativnega odstopanja izmerjenih vrednosti od izračunanih je na sliki 3.14a $|\epsilon_\mathrm{r}|_\mathrm{sr.} \doteq 5{,}5\,\%$, na sliki 3.14b $|\epsilon_\mathrm{r}|_\mathrm{sr.} \doteq 9{,}6\,\%$, na sliki 3.15a $|\epsilon_\mathrm{r}|_\mathrm{sr.} \doteq 12{,}0\,\%$ in na sliki 3.15b $|\epsilon_\mathrm{r}|_\mathrm{sr.} \doteq 4{,}7\,\%$. Pri numeričnem izračunu je dvostranska ozemljitev zaslona privzeta kot idealna (glej razdelek 2.2). Ker sta potekala zaslon in trifazni vod vzporedno s površino zemlje, smo pri numeričnem izračunu upoštevali Greenovo funkcijo (2.6) in za specifično prevodnost zemlje smo privzeli vrednost $(1/300)\,\mathrm{S/m}$ [31, str. 291]. Izračun smo opravili tudi z Greenovo funkcijo (2.7b), vendar se rezultati niso bistveno spremenili.

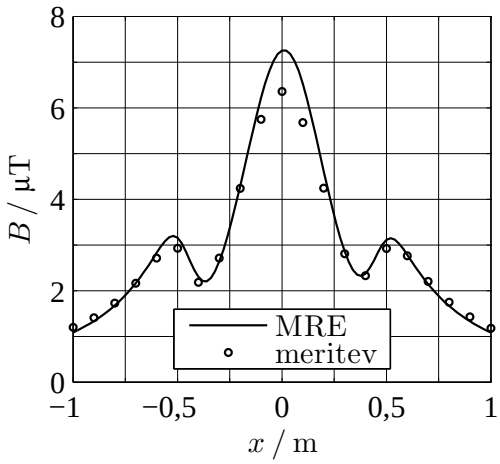

(a) $y_{\mathrm{R}} = 30\,\mathrm{cm}$

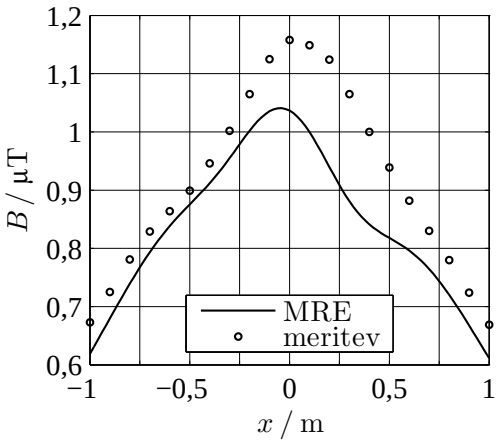

(b) $y_{\mathrm{R}} = 70\,\mathrm{cm}$

Slika 3.14: Primerjava rezultatov predlagane metode z izmerjenimi vrednostimi v primeru ravnega nemagnetnega zaslona.

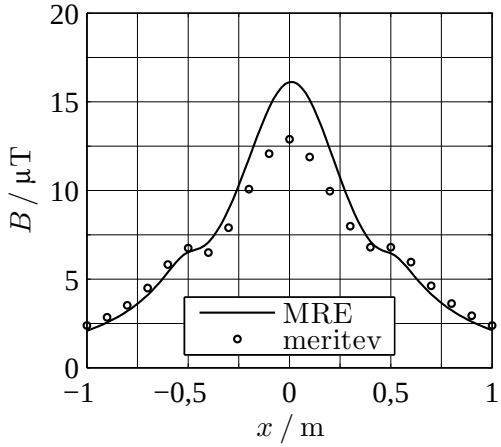

(a) $y_{\mathrm{R}} = 30\,\mathrm{cm}$

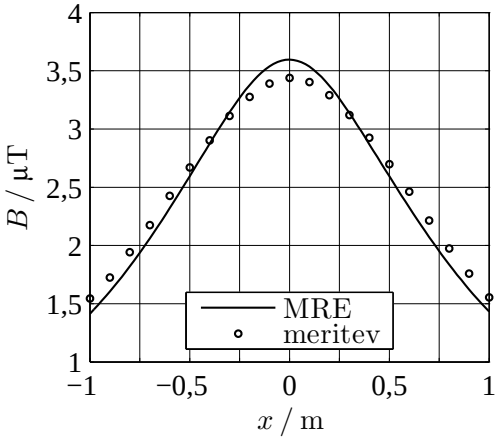

(b) $y_{\mathrm{R}} = 70\,\mathrm{cm}$

Slika 3.15: Primerjava rezultatov predlagane metode z izmerjenimi vrednostimi v primeru ravnega magnetnega zaslona.

Poglavje 4

Analiza zaslonskih struktur

Predlagana metoda robnih elementov omogoča izračun magnetnega polja pred, v in za zasloni. Z ustreznim prikazom rezultatov tega izračuna pridobimo soliden vpogled v učinke zastiranja, kar je nepogrešljivo pri dizajniranju zaslonskih struktur. Za demonstracijo takšnega prikaza rezultatov smo izbrali splošno konfiguracijo, ki je prikazana na sliki 4.1. Nad snopom vodnikov je zaslon profila U širine $l = 30\,\mathrm{cm}$ in višine $h = 20\,\mathrm{cm}$, ki naj je idealno dvostransko ozemljen. Da bi prikazani rezultati ponazorili dva različna principa zastiranja magnetnega polja, ki slonita na indukciji oziroma magnetizaciji, in učinek njunega kombiniranega vpliva, smo izbrali naslednje tri zaslone: prevodnega (nemagnetnega), $\gamma_\mathrm{C} = 10\,\mathrm{MS/m}$ in $\mu_\mathrm{C} = \mu_0$, (slabo prevodnega) magnetnega, $\gamma_\mathrm{C} = 0{,}01\,\mathrm{MS/m}$ in $\mu_\mathrm{C} = 100\mu_0$, in prevodnega magnetnega, $\gamma_\mathrm{C} = 10\,\mathrm{MS/m}$ in $\mu_\mathrm{C} = 100\mu_0$. Preostali številski podatki so: $f = 50\,\mathrm{Hz}$, $d = 6\,\mathrm{cm}$, $y_\mathrm{C} = 7\,\mathrm{cm}$ in $t = 1\,\mathrm{cm}$.

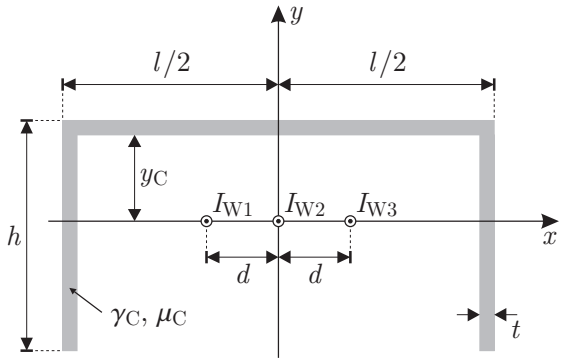

Slika 4.1: Zaslon profila U nad snopom žic.

4.1 Enofazno vzbujanje

Na sliki 4.2 so prikazane gostotnice magnetnega pretoka v trenutku 0 s za primer le srednjega tokovodnika, $I_{\mathrm{W2}} = 100\,\mathrm{A}$.

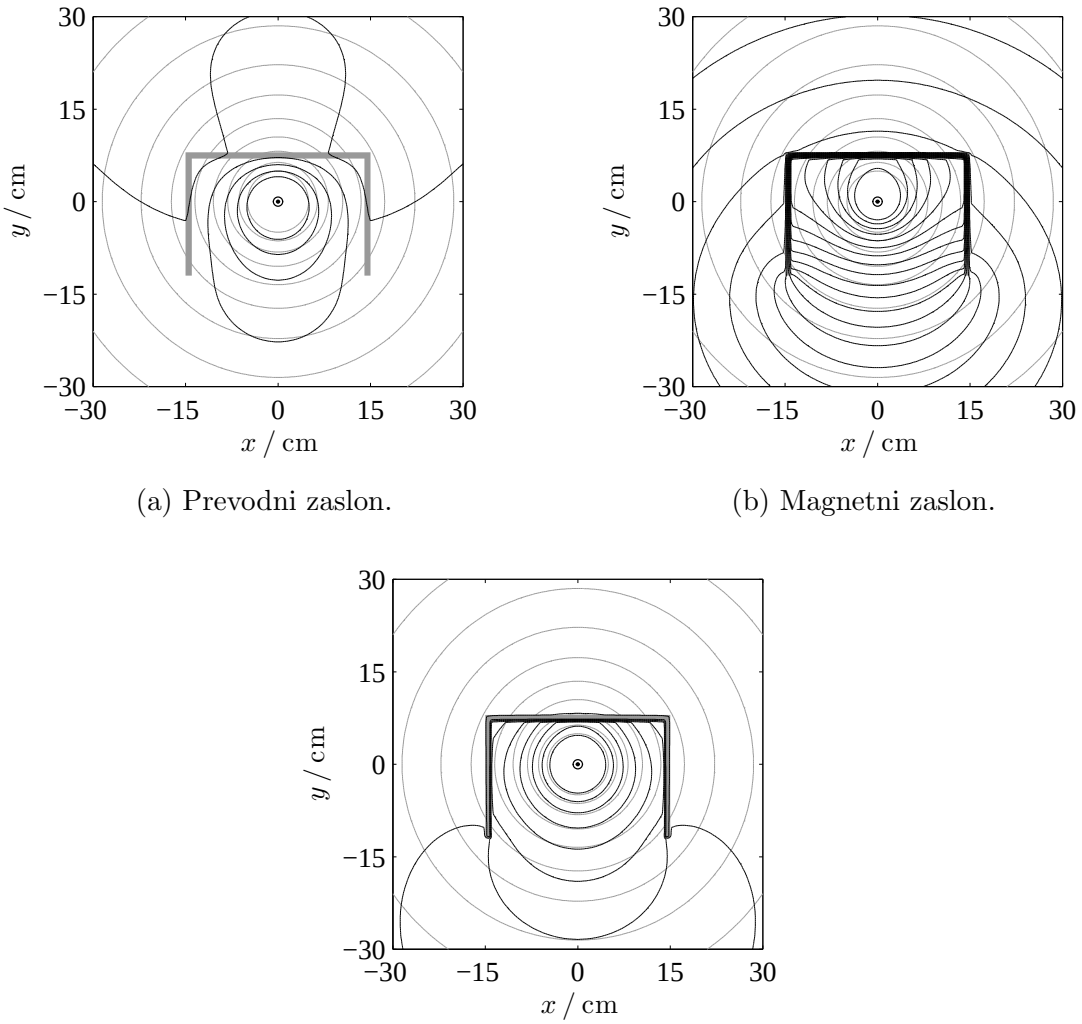

(a) Prevodni zaslon.

(b) Magnetni zaslon.

(c) Prevodni magnetni zaslon.

Slika 4.2: Sive linije prikazujejo gostotnice primarnega polja, krepke pa gostotnice rezultančnega polja.

V prevodnem nemagnetnem zaslonu se inducira tok $I_{\mathrm{C}} \doteq -(95{,}54+\mathrm{j}10{,}39)\,\mathrm{A}$, ki je skoraj nasproten toku v žici, $I_{\mathrm{C}} \approx -I_{\mathrm{W2}} = -100\,\mathrm{A}$. Ta tok kompenzira večji del primarnega polja za zaslonom, kot je razvidno na sliki 4.2a. V slabo prevodnem magnetnem zaslonu se inducira tok $I_{\mathrm{C}} \doteq -(0{,}016 + \mathrm{j}1{,}227)\,\mathrm{A}$, ki kot tak ne zmore kompenzirati primarnega polja. Ker pa se ta zaslon v polju tudi magnetizira, "ujame" precej magnetnega pretoka

('flux shunting') [61, razdelek B.1] [49, razdelka 3.1 in 3.5], kot je razvidno na sliki 4.2b. V prevodnem magnetnem zaslonu se inducira precejšen tok, $I_C \doteq -(84{,}71 + j9{,}31)\,A$, zmanjšanje gostote pretoka za zaslonom pa je zaradi magnetizacije še izrazitejše kot v obeh prejšnjih primerih (slika 4.2c).

4.2 Trifazno vzbujanje

Slika 4.3 prikazuje porazdelitev faktorja zaslanjanja okrog zaslona nad trifaznim vodom: $I_{W1} = I_0 \exp(j2\pi/3)$, $I_{W2} = I_0$ in $I_{W3} = I_0 \exp(-j2\pi/3)$, kjer je $I_0 = 100\,A$. Inducirani

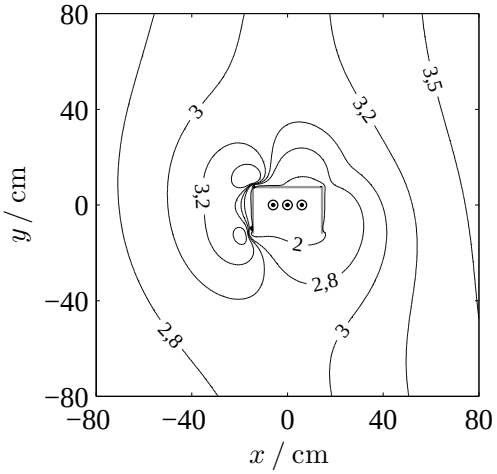

(a) Prevodni zaslon.

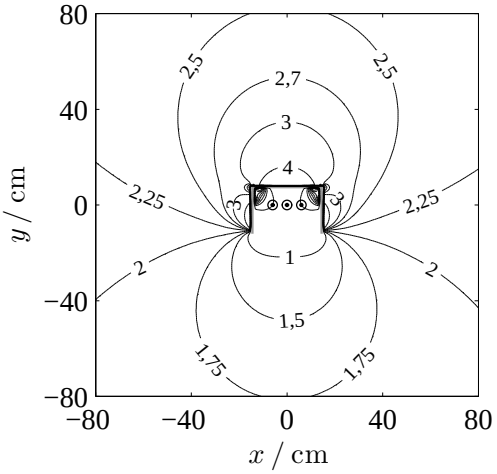

(b) Magnetni zaslon.

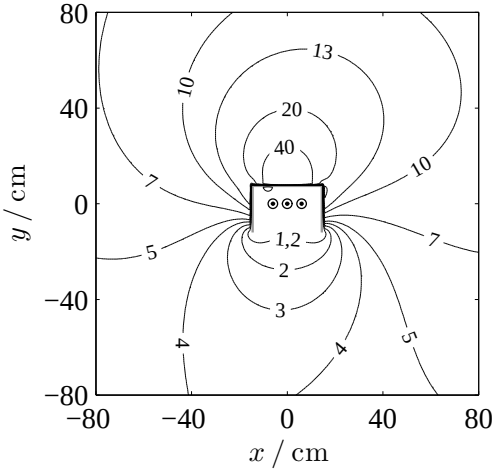

(c) Prevodni magnetni zaslon.

Slika 4.3: Porazdelitev faktorja zastiranja okrog zaslona profila U pri trifaznem vzbujanju.

tok v zaslonu je tokrat zanemarljiv: v prevodnem nemagnetnem zaslonu je $I_C \doteq (0{,}761 + \mathrm{j}0{,}324)\,\mathrm{A}$, v slabo prevodnem magnetnem je $I_C \doteq (0{,}000 + \mathrm{j}0{,}015)\,\mathrm{A}$ in v prevodnem magnetnem zaslonu je $I_C \doteq (0{,}973 + \mathrm{j}0{,}008)\,\mathrm{A}$, kar je zelo blizu primera, ko bi imel zaslon odprta konca, $I_C = 0$. Če primerjamo porazdelitev faktorja zastiranja za prevodni nemagnetni zaslon (slika 4.3a) in slabo prevodni magnetni zaslon (slika 4.3b), opazimo, da je tik za zaslonom boljši učinek magnetnega, bolj stran pa učinek prevodnega zaslona. V primeru prevodnega magnetnega zaslona, kot je razvidno na sliki 4.3c, se faktor zastiranja izdatno poveča povsod za zaslonom. Pričakovano najslabše zastiranje je pod odprtino.

4.3 Trifazno vzbujanje in dvozaslonska struktura

Da bi izboljšali zastiranje tudi na spodnji strani, smo dodali še raven zaslon, ki trifazni vod skoraj zapre. Širina tega zaslona je 32 cm, vse ostalo pa je isto kot pri zaslonu U. Širina reže med zaslonoma je 2 cm. Porazdelitev faktorja zastiranja te dvozaslonske strukture je prikazana na sliki 4.4. Pri prevodnih nemagnetnih zaslonih (slika 4.4a) in slabo prevodnih magnetnih (slika 4.4b) se je zastiranje le delno izboljšalo, pri prevodnih magnetnih zaslonih (slika 4.4c) pa se je faktor zastiranja občutno povečal povsod. Zaslanjanje je še najslabše ob reži med zaslonoma, kar je tudi pričakovano.

4.4 Analiza povratnega učinka

Kot primarni vir polja smo izbrali vodnika dvovoda polmera 2 cm s tokoma $\pm 100\,\mathrm{A}$. Osi tokovodnikov sovpadata z lego prve in tretje žice na sliki 4.1 (srednje žice tokrat ni). Na sliki 4.5 so prikazane gostotnice magnetnega polja v trenutku 0 s (sive so gostotnice primarnega polja). Pri prevodnem in magnetnem zaslonu sta (ponovno) razvidna vpliva indukcije in magnetizacije: pri prevodnem se gostotnice "stisnejo" k vodnikoma dvovoda (slika 4.5a), magnetni zaslon pa "vsrka" večino magnetnega pretoka (slika 4.5b). Pri kombiniranem zaslonu sta omenjena učinka "prepletena" (slika 4.5c).

Zaradi uravnoteženosti primarnih tokov ($\pm 100\,\mathrm{A}$) je induciran tok v kateremkoli zaslonu sicer zanemarljiv, ne pa tudi njegova gostota, zaradi katere se v cilindrih sprošča toplota. Zaslanjanje očitno ni "zastonj" in ga kaže osvetliti še s te plati. Joulska moč na dolžinskem metru j-tega cilindra je določena z enačbo (2.75). V primeru prevodnega zaslona se izgubna moč v vodnikih dvovoda poveča za 2,63 %. Ker pa je celotno povečanje izgub zaradi zastiranja 37,02 %, gre razlika povečanj na račun izgub v zaslonu. V pri-

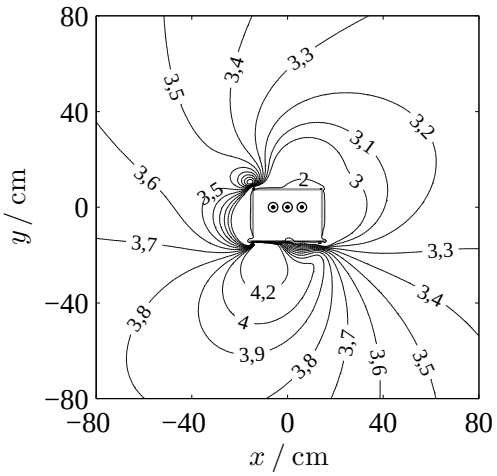

(a) Prevodni zaslon.

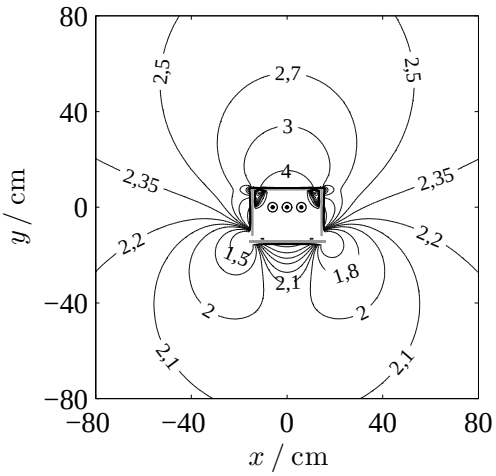

(b) Magnetni zaslon.

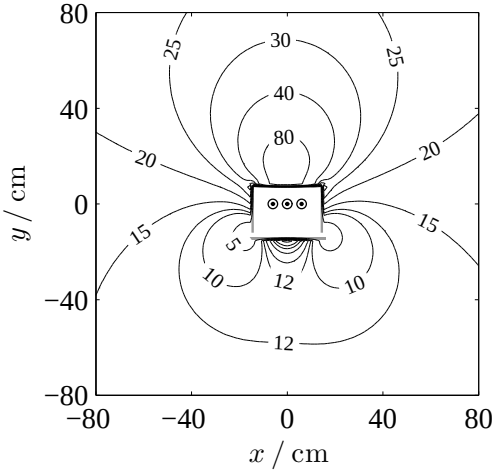

(c) Prevodni magnetni zaslon.

Slika 4.4: Porazdelitev faktorja zastiranja okrog dveh zaslonov pri trifaznem vzbujanju.

meru slabo prevodnega magnetnega zaslona se izgube v vodnikih dvovoda povečajo za 6,32 %, celotne pa le za odtenek več (6,82 %). Pri prevodnem magnetnem zaslonu sta ti povečanji približno 0,84 % oziroma 53,50 %. Celotne izgube so sicer največje, boljše pa je tudi zaslanjanje.

Izgubna moč je v neposredni povezavi z impedanco dvovoda. Impedanca/meter samega dvovoda je približno $(3{,}83 + \mathrm{j}25{,}01)\,\mathrm{m\Omega/m}$, pri prevodnem zaslonu je ta $(5{,}25 + \mathrm{j}21{,}11)\,\mathrm{m\Omega/m}$, pri magnetnem zaslonu je $(4{,}10 + \mathrm{j}29{,}39)\,\mathrm{m\Omega/m}$ in pri prevodnem magnetnem je $(5{,}89 + \mathrm{j}25{,}58)\,\mathrm{m\Omega/m}$. Razlike v rezistancah se ujemajo s predhodno podanimi povečanji izgubnih moči. Reaktanca dvovoda se najbolj poveča pri magnetnem zaslonu,

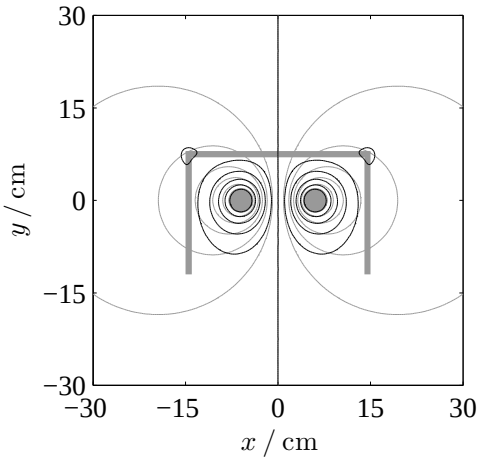

(a) Prevodni zaslon.

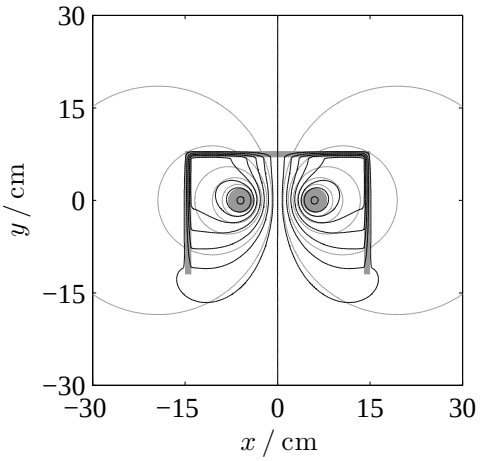

(b) Magnetni zaslon.

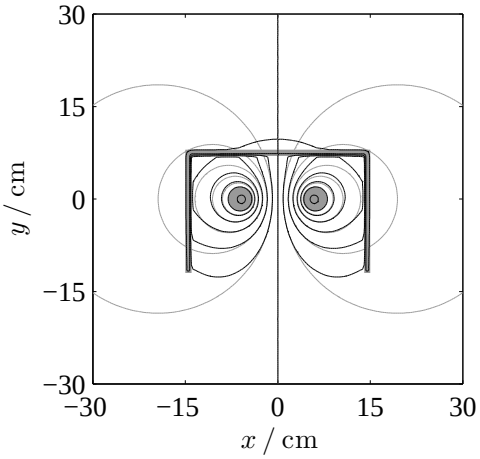

(c) Prevodni magnetni zaslon.

Slika 4.5: Gostotnice magnetnega polja dvovoda, ki je zastirano z zaslonom profila U. Sive linije prikazujejo gostotnice primarnega polja.

pri prevodnem pa se nekoliko zmanjša, kar je povsem v skladu s pričakovanji.

Poglavje 5

Sklep

Primerjave rezultatov predlagane metode z rezultati drugih metod in primeri analize zaslonskih struktur izpričujejo, da omogoča razvita metoda soliden izračun polja pred, v in za zasloni in ponuja vpogled v učinke zastiranja. Metodologija je za vse objekte zaslonske strukture enotna in omogoča analizo magnetnih, prevodnih, prevodno-magnetnih in sestavljenih zaslonov ter je primerno orodje za uspešno dizajniranje zaslonov ob snopu vzporednih tokovodnikov.

Pomanjkljivost metode je vsekakor njena omejenost na linearne snovi, kar onemogoča upoštevanje nelinearnih lastnosti feromagnetikov.

Frekvečno mejo ji teoretično določa pogoj kvazistatičnosti, praktično pa vdorna globina, kompleksnost geometrije, potrebno število robnih elementov in seveda zmogljivost računalnika. Metodo bi kazalo nadgraditi z različnimi nabori poskusnih in testnih funkcij ter analizirati natančnost in hitrost izračuna v odvisnosti od nabora funkcij in velikosti robnih elementov.

Pomanjkljivost metode je tudi njena omejenost z 2D geometrijo. Pri posplošitvi na 3D geometrijo bi se kompleksnost problema zelo povečala, saj bi oblogi enojnega in dvojnega sloja ne zadoščali. Vpeljati bi morali ekvivalentne električne in magnetne ploskovne toke na površinah zaslonov [53, razdelek 3.5], ki bi zahtevali neprimerno večje računalniške zmogljivosti.

Prispevki k znanosti

Pomembnejši izvirni prispevki k znanosti so:

1. **Uporaba potencialov enojnega in dvojnega sloja pri analizi prevodno-permeabilnih zaslonskih struktur v 2D prostoru.**
   Kvazistatično elektromagnetno polje v in ob prevodno-permeabilnih objektih je izraženo s pomočjo enojnega in dvojnega sloja oziroma oblog, ki sta porazdeljeni po površinah objektov zaslonske strukture. S pomočjo Greenove formule in lastnosti potencialov enojnega in dvojnega sloja so izpeljane robne integralske enačbe za te vire. Prednost koncepta virov je predvsem v tem, da se vprašanje polja v strukturi prevede najprej na iskanje ekvivalentnih virov po ograjah objektov, kar je numerično vsekakor manjši zalogaj, nato pa se iz njih določita še polje in učinek zastiranja.

2. **Določitev matričnega sistema robnih integralskih enačb, ki vključuje različna električna povezovanja elementov zaslonske strukture, in izračun oblog enojnega in dvojnega sloja po površinah prevodnih in permeabilnih objektov.**
   Za določitev magnetnega polja v prostoru niso pomembni le objekti kot takšni, ampak tudi načini ozemljitve in električne povezave med njimi. Te okoliščine povzemajo dodatni pogoji v obliki integralskih enačb, ki se naslavljajo na prej omenjene ekvivalentne vire. Celoten sistem robnih integralskih enačb je zatem strnjen v matrični sistem in obravnavan z momentno metodo. Pri tem je posebna pozornost posvečena numeričnim integracijam singularnih jeder robnih integralskih enačb.

3. **Analiza povratnega učinka prevodnih, magnetnih in prevodno-magnetnih zaslonov na primarne vire polja.**
   Prevodno-magnetni zasloni imajo neželen povratni vpliv na primarno strukturo, ki se kaže v spremenjenih karakteristikah. Prednost predlagane metode je ravno v tem, da obravnava vodnike in zaslone z enako metodologijo. Kot takšna že v osnovi omogoča

analizo interakcij med elementi vodniško-zaslonske strukture, zato v pogledu analize povratnega učinka ne predstavlja nadgradnje neke metode, ampak njo samo.

Izjava

Izjavljam, da sem doktorsko disertacijo izdelal samostojno pod vodstvom mentorja doc. dr. Antona R. Sinigoja. Pomoč ostalih sem navedel v zahvali.

V Ljubljani, 18. junij 2009 mag. Edi Bulić, univ. dipl. inž. el.

Zahvala

Zahvaljujem se mentorju doc. dr. Antonu R. Sinigoju za strokovno vodstvo pri delu, nepogrešljive nasvete pri izdelavi doktorske disertacije in pripombe ter izboljšave v besedilu.

Za mnoge odgovore pri postavljanju dela v sistemu LaTeX se zahvaljujem bratu Patriciu ter sodelavcema Alešu Berkopcu in Samotu Peniču.

Sodelavcem pri predmetih Osnove elektrotehnike, Elektromagnetika in Elektromagnetne strukture se zahvaljujem za prijetno delovno vzdušje ter vzpodbudo.

In nenazadnje, za veliko podporo sem hvaležen staršema Ivanu in Ivanki.

Literatura

[1] A. P. Wills. On the magnetic shielding effect of tri-lamellar spherical and cylindrical shells. *Physical Review*, vol. 9, no. 4, pp. 193–213, Oct. 1899.

[2] J. F. Hoburg. A computational methodology and results for quasistatic multilayered magnetic shielding. *IEEE Transactions on Electromagnetic Compatibility*, vol. 38, no. 1, pp. 92–103, Feb. 1996.

[3] William M. Frix and George G. Karady. A circuital approach to estimate the magnetic field reduction of nonferrous metal shields. *IEEE Transactions on Electromagnetic Compatibility*, vol. 39, no. 1, pp. 24–32, Feb. 1997.

[4] Marko Istenič. *Izpostavljenost in zaščita ljudi in naprav v okolju električnih in magnetnih polj elektroenergetskih omrežij.* Magistrska naloga, Fakulteta za elektrotehniko Univerze v Ljubljani, 2000.

[5] Massimo Guarnieri, Federico Moro, and Roberto Turri. An integral method for extremely low frequency magnetic shielding. *IEEE Transactions on Magnetics*, vol. 41, no. 5, pp. 1376–1379, May 2005.

[6] Richard B. Schulz, Vellar C. Plantz, and David R. Brush. Shielding theory and practice. *IEEE Transactions on Electromagnetic Compatibility*, vol. 30, no. 3, pp. 187–201, Aug. 1988. Originally published in *Proc. 9th Tri-Service Conf. on Electromagnetic Compatibility*, Oct. 1963.

[7] D. A. Miller and J. E. Bridges. Geometrical effects on shielding effectiveness at low frequencies. *IEEE Transactions on Electromagnetic Compatibility*, vol. 8, no. 4, pp. 174–186, Dec. 1966.

[8] J. R. Moser. Low-frequency shielding of a circular loop electromagnetic field source. *IEEE Transactions on Electromagnetic Compatibility*, vol. 9, no. 1, pp. 6–18, Mar. 1967.

[9] Peter R. Bannister. New theoretical expressions for predicting shielding effectiveness for the plane shield case. *IEEE Transactions on Electromagnetic Compatibility*, vol. 10, no. 1, pp. 2–7, Mar. 1968.

[10] Richard B. Schulz, Vellar C. Plantz, and David R. Brush. Low-frequency shielding resonance. *IEEE Transactions on Electromagnetic Compatibility*, vol. 10, no. 1, pp. 7–15, Mar. 1968.

[11] John R. Harrington and Richard B. Schulz. Design of minimum weight and maximum effectiveness of very-low-frequency shielding. *IEEE Transactions on Electromagnetic Compatibility*, vol. 10, no. 1, pp. 152–157, Mar. 1968.

[12] Robert B. Cowdell. New dimensions in shielding. *IEEE Transactions on Electromagnetic Compatibility*, vol. 10, no. 1, pp. 158–167, Mar. 1968.

[13] Peter R. Bannister. Further notes for predicting shielding effectiveness for the plane shield case. *IEEE Transactions on Electromagnetic Compatibility*, vol. 11, no. 2, pp. 50–53, May 1969.

[14] R. Yang and Raj Mittra. Coupling between two arbitrarily oriented dipoles through multilayered shields. *IEEE Transactions on Electromagnetic Compatibility*, vol. 27, no. 3, pp. 131–136, Aug. 1985.

[15] J. F. Hoburg. Principles of quasistatic magnetic shielding with cylindrical and spherical shields. *IEEE Transactions on Electromagnetic Compatibility*, vol. 37, no. 4, pp. 574–579, Nov. 1995.

[16] Yaping Du, T. C. Cheng, and A. S. Farag. Principles of power-frequency magnetic field shielding with flat sheets in a source of long conductors. *IEEE Transactions on Electromagnetic Compatibility*, vol. 38, no. 3, pp. 450–459, Aug. 1996.

[17] Leonardo Sandrolini, Antonio Massarini, and Ugo Reggiani. Transform method for calculating low-frequency shielding effectiveness of planar linear multilayered shields. *IEEE Transactions on Magnetics*, vol. 36, no. 6, pp. 3910–3919, Nov. 2000.

[18] Aldo Canova, Alessandra Manzin, and Michele Tartaglia. Evaluation of different analytical and semi-analytical methods for the design of ELF magnetic field shields. *IEEE Transactions on Industry Applications*, vol. 38, no. 3, pp. 788–796, May/June 2002.

[19] Robert G. Olsen, Marko Istenič, and Peter Žunko. On simple methods for calculating ELF shielding of infinite planar shields. *IEEE Transactions on Electromagnetic Compatibility*, vol. 45, no. 3, pp. 538–547, Aug. 2003.

[20] Marko Istenič. *Zaščita pred magnetnim poljem ekstremno nizkih frekvenc z magnetnimi zasloni končnih dimenzij*. Doktorska disertacija, Fakulteta za elektrotehniko Univerze v Ljubljani, 2003.

[21] Marko Istenič and Robert G. Olsen. A simple hybrid method for ELF shielding by imperfect finite planar shields. *IEEE Transactions on Electromagnetic Compatibility*, vol. 46, no. 2, pp. 199–207, May 2004.

[22] P. P. Silvester and R. L. Ferrari. *Finite Elements for Electrical Engineers*. Cambridge University Press, Cambridge, 1983. Reprinted 1986.

[23] Matthew N. O. Sadiku. *Numerical Techniques in Electromagnetics*. CRC Press, Boca Raton, second edition, 2001.

[24] L. Hasselgren, E. Möller, and Y. Hamnerius. Calculation of magnetic shielding of a substation at power frequency using FEM. *IEEE Transactions on Power Delivery*, vol. 9, no. 3, pp. 1398–1405, July 1994.

[25] C. Buccella, M. Feliziani, F. Maradei, and G. Manzi. Magnetic field computation in a physically large domain with thin metallic shields. *IEEE Transactions on Magnetics*, vol. 41, no. 5, pp. 1708–1711, May 2005.

[26] Aldo Canova, Giambattista Gruosso, and Maurizio Repetto. Integral methods for analysis and design of low-frequency conductive shields. *IEEE Transactions on Magnetics*, vol. 39, no. 4, pp. 2009–2017, July 2003.

[27] Miodrag Milutinov and Neda Pekarić-Nađ. Shielding effect of non -ferrous metallic plates in vicinity of three phase conductors. *Serbian Journal of Electrical Engineering*, vol. 2, no. 2, pp. 147–156, Nov. 2005.

[28] Chih-Ping Chang and Chang-Fa Yang. A moment method solution for the shielding properties of three-dimensional objects above a lossy half space. *IEEE Transactions on Electromagnetic Compatibility*, vol. 47, no. 4, pp. 723–730, Nov. 2005.

[29] Peter Silvester. AC resistance and reactance of isolated rectangular conductors. *IEEE Transactions on Power Apparatus and Systems*, vol. 86, no. 6, pp. 770–774, June 1967.

[30] Pei-bai Zhou. *Numerical Analysis of Electromagnetic Fields*. Springer-Verlag, Berlin, 1993.

[31] Anton R. Sinigoj. *ELMG polje*. Fakulteta za elektrotehniko, Ljubljana, 1996.

[32] Breda Cestnik, Primož Hrobat, Radomir Isaković, Igor Babić, Zoran Štrubel, Anton R. Sinigoj, Edi Bulić. *Možnosti za znižanje jakosti elektromagnetnega sevanja v okolju naprav in objektov distribucijskega EE-omrežja*. Referat št. 1605, Elektroinštitut Milan Vidmar, Ljubljana, 2004.

[33] Breda Cestnik, Rudi Vončina, Anton R. Sinigoj, Edi Bulić. Zaslanjanje magnetnega polja s prevodnimi in feromagnetnimi zasloni. V: Marjan Zorman (urednik), *26. posvetovanje o močnostni elektrotehniki in sodobnih električnih instalacijah Kotnikovi dnevi : izobraževalni program*, pages 1/VII–14/VII, Radenci, Slovenija, 31. marec in 01. april 2005. Elektrotehniško društvo.

[34] Edi Bulić. Izračun magnetnega polja okrog dolgih prevodnih nemagnetnih zaslonov. *Elektrotehniški vestnik*, letn. 76, št. 1-2, str. 31–37, 2009.

[35] Ibrahim Tekin and Edward H. Newman. Moment method analysis of the magnetic shielding factor of a conducting TM shield at ELF. *IEEE Transactions on Electromagnetic Compatibility*, vol. 38, no. 4, pp. 585–590, Nov. 1996.

[36] Willy P. Legros and Patrick G. Scarpa. Fast computation of magnetic field in rotationally symmetric structures. *IEEE Transactions on Magnetics*, vol. 21, no. 6, pp. 2644–2651, Nov. 1985.

[37] Piergiorgio Alotto, Massimo Guarnieri, and Federico Moro. A boundary integral formulation on unstructured dual grids for eddy-current analysis in thin shields. *IEEE Transactions on Magnetics*, vol. 43, no. 4, pp. 1173–1176, Apr. 2007.

[38] H. Igarashi, A. Kost, and T. Honma. A three dimensional analysis of magnetic fields around a thin magnetic conductive layer using vector potential. *IEEE Transactions on Magnetics*, vol. 34, no. 5, pp. 2539–2542, Sep. 1998.

[39] O. Bottauscio, M. Chiampi, D. Chiarabaglio, F. Fiorillo, L. Rocchino, and M. Zucca. Role of magnetic materials in power frequency shielding: numerical analysis and experiments. *IEE Proceedings Generation, Transmission & Distribution*, vol. 148, no. 2, pp. 104–110, Mar. 2001.

[40] Hermann A. Haus and James R. Melcher. *Electromagnetic Fields and Energy*. Prentice-Hall, Englewood Cliffs, 1989.

[41] Prem Kishore Kythe. *An Introduction to Boundary Element Methods*. CRC Press, Boca Raton, 1995.

[42] C.Pozrikidis. *A Practical Guide to Boundary Element Methods with the Software Library BEMLIB*. Chapman & Hall/CRC Press, London/Boca Raton, 2002.

[43] Roger F. Harrington. *Field Computation by Moment Methods*. IEEE Press Series on Electromagnetic Waves. IEEE Press, Piscataway, reissued edition, 1993.

[44] C. A. Brebbia. *The Boundary Element Method for Engineers*. Pentech Press, London, 1978.

[45] Julius Adams Stratton. *Electromagnetic Theory*. IEEE Press Series on Electromagnetic Wave Theory. IEEE Press, Piscataway, reissued edition, 2007.

[46] John R. Carson. Wave propagation in overhead wires with ground return. *Bell System Technical Journal*, vol. 5, pp. 539–554, Oct. 1926.

[47] Nagayoshi Morita, Nobuaki Kumagai, and Joseph R. Mautz. *Integral Equation Methods for Electromagnetics*. The Artech House Antenna Library. Artech House, Boston, 1990.

[48] George B. Arfken and Hans J. Weber. *Mathematical Methods for Physicists*. Academic Press, San Diego, fifth edition, 2001.

[49] Kenneth L. Kaiser. *Electromagnetic Shielding*. CRC Press, Boca Raton, 2006.

[50] I. N. Bronštejn, K. A. Semendjajev, G. Musiol, H. Mühlig. *Matematični priročnik*. Tehniška založba Slovenije, Ljubljana, 2. predelana in dopolnjena izdaja, 1997.

[51] J. Van Bladel. *Singular Electromagnetic Fields and Sources*. IEEE Press Series on Electromagnetic Wave Theory. IEEE Press, Piscataway, 1996.

[52] The MathWorks, Inc. *MATLAB® 7, Function Reference: Volume 2 (F-O)*, Sep. 2007. `http://www.mathworks.com/access/helpdesk/help/pdf_doc/matlab/refbook2.pdf`.

[53] Roger F. Harrington. *Time-Harmonic Electromagnetic Fields*. IEEE Press Series on Electromagnetic Wave Theory. IEEE Press, Piscataway, reissued edition, 2001.

[54] Walter Gander and Walter Gautschi. *Adaptive Quadrature – Revisited*. Technical Report 306, Departement Informatik, ETH Zürich, Aug. 1998.

[55] The MathWorks, Inc. *MATLAB® 7, Function Reference: Volume 3 (P-Z)*, Sep. 2007. `http://www.mathworks.com/access/helpdesk/help/pdf_doc/matlab/refbook3.pdf`.

[56] Anton R. Sinigoj. *Osnove elektromagnetike*. Fakulteta za elektrotehniko, Ljubljana, 1999.

[57] Heinrich Kaden. *Wirbelströme und Schirmung in der Nachrichtentechnik*. Springer-Verlag, Berlin, 1959.

[58] Lennart Hasselgren and Jorma Luomi. Geometrical aspects of magnetic shielding at extremely low frequencies. *IEEE Transactions on Electromagnetic Compatibility*, vol. 37, no. 3, pp. 409–420, Aug. 1995.

[59] James R. Wait and David A. Hill. Electromagnetic shielding of sources within a metal-cased bore hole, vol. 15, no. 2, pp. 108–112, Apr. 1977.

[60] James F. Hoburg, Bernard A. Clairmont, David W. Fugate, and Richard J. Lordan. Comparisons of measured and calculated power frequency magnetic shielding by multilayered cylinders. *IEEE Transactions on Power Delivery*, vol. 12, no. 4, pp. 1704–1710, Oct. 1997.

[61] Salvatore Celozzi, Rodolfo Araneo, and Giampiero Lovat. *Electromagnetic Shielding*. Wiley Series in Microwave and Optical Engineering. John Wiley & Sons, Hoboken, 2008.

[62] George W. Hanson and Alexander B. Yakovlev. *Operator Theory for Electromagnetics*. Springer-Verlag, New York, 2002.

[63] Constantine A. Balanis. *Advanced Engineering Electromagnetics*. John Wiley & Sons, Hoboken, 1989.

[64] M. V. K. Chari and S. J. Salon. *Numerical Methods in Electromagnetism*. Academic Press Series in Electromagnetism. Academic Press, San Diego, 2000.

[65] Jean G. Van Bladel. *Electromagnetic Fields*. IEEE Press Series on Electromagnetic Wave Theory. John Wiley & Sons, Piscataway, second edition, 2007.

[66] Endre Süli and David F. Mayers. *An Introduction to Numerical Analysis*. Cambridge University Press, Cambridge, 2003.

[67] Charles W. Steele. *Numerical Computation of Electric and Magnetic Fields*. Chapman & Hall, New York, second edition, 1997.

[68] Andrew F. Peterson, Scott L. Ray, and Raj Mittra. *Computational Methods for Electromagnetics*. IEEE/OUP Series on Electromagnetic Wave Theory. IEEE Press, Piscataway, 1998.

[69] Gabrijel Tomšič. *Izbrana poglavja iz matematike – Integralske enačbe*. Fakulteta za elektrotehniko, Ljubljana, 1998.

[70] Izrail S. Gradshteyn and Iosif M. Ryzhik. *Table of Integrals, Series, and Products*. Academic Press, San Diego, fifth edition, 1994. Alan Jeffrey, editor. Translated from the Russian by Scripta Technica, Inc.

[71] Zoya Popović and Branko D. Popović. *Introductory Electromagnetics*. Prentice-Hall, New Jersey, 2000.

[72] Clayton R. Paul. *Introduction to Electromagnetic Compatibility*. Wiley Series in Microwave and Optical Engineering. John Wiley & Sons, New York, 1992.

[73] M. H. Lean and A. Wexler. Accurate field computation with the boundary element method. *IEEE Transactions on Magnetics*, vol. 18, no. 2, pp. 331–335, Mar. 1982.

[74] Ruey-Beei Wu and Jin-Chum Yang. Boundary integral equation formulation of skin effect problems in multiconductor transmission lines. *IEEE Transactions on Magnetics*, vol. 25, no. 4, pp. 3013–3015, July 1989.

[75] Antonije R. Djordjević, Tapan K. Sarkar, and Sadasiva M. Rao. Analysis of finite conductivity cylindrical conductors excited by axially-independent TM electromagnetic field. *IEEE Transactions on Microwave Theory and Techniques*, vol. 33, no. 10, pp. 960–966, Oct. 1985.

[76] The MathWorks, Inc. *MATLAB® 7, Function Reference: Volume 1 (A-E)*, Sep. 2007. `http://www.mathworks.com/access/helpdesk/help/pdf_doc/matlab/refbook.pdf`.

An Equivalent Surface Source Method for Computation of the Magnetic Field Reduction of Metal Shields

Edi Bulić, Anton R. Sinigoj, and Breda Cestnik

***Abstract*—A numerical method for computation of the resultant quasi-static magnetic field in the vicinity of parallel wires and metal shields is presented. The primary magnetic field source is time-harmonic currents in wires. This field is modified by conducting magnetic and/or nonmagnetic shields. The material is assumed to be linear under the applied source field. The shielding effectiveness can be estimated by a comparison between the primary and the resultant field. The reaction magnetic field is expressed by a sum of fields caused by equivalent single- and double-layer sources distributed on the shield surface. Integral equations for unknown distributions of these equivalent sources are derived from the Green's second identity implemented inside and outside the shields. These equations are coupled integral equations, and are solved by the moment method. Numerical results of the resultant (shielded) magnetic field obtained with the proposed method are compared with the results of: 1) analytically solvable problems; 2) measurements; and 3) two different numerical methods.**

***Index Terms*—Boundary element methods, equivalent sources, integral equations, magnetic shielding, metal shields, moment methods, single and double layers.**

I. Introduction

In order to meet nonionizing radiation requirements and/or electromagnetic compatibility criteria, magnetic field shielding is frequently needed. The disturbing magnetic field in a particular region can be minimized by shifting field sources and/or by setting metal shields between the sources and the region. Shielding effectiveness is impacted by many of the shield parameters, such as position, size, thickness, shape, and electromagnetic properties.

To design shields efficiently, a method is needed for simulating shields of various shapes and electromagnetic properties, and for calculating the magnetic field in the shield vicinity. There are many methods proposed in literature. Analytical estimations of shielding efficiency [1]–[5] are based on various assumptions, such as extremely low frequency (ELF; 3 Hz–3 kHz [6]), flat shields, infinite planar shields, and similar, and are not suitable for general use. When using the finite-element method [7], which deals with various geometrical and material properties, there are relatively many elements required for calculating the resultant field in the shield vicinity [4]. By using integral methods, difficulties caused by the numerous elements, such as the needed computational time and computer memory consumption, are reduced. One such method is the multiconductor method (MCM) [6], [8], [9]. It is suitable for conducting nonmagnetic shields. Another one is the surface-current method (SCM) [10] used for magnetic shields. It is drawn from a magnetostatic approximation, and is therefore valid only for ultralow frequencies (ULF; below 3 Hz [6]) and conditionally for ELF.

In this paper, we propose an equivalent surface source method (ESSM) enabling calculation of the magnetic field in the vicinity of parallel wires, and conducting magnetic and/or conducting nonmagnetic shields of practically any shape, thus allowing for a wide spectrum of applicability. The ESSM is based on a quasi-static description of the field. The primary field source is time-harmonic, and as all the materials are linear, the field is time-harmonic too; therefore, the field analysis is made in the frequency space, and the field quantities are considered as phasors.

Manuscript received January 31, 2008; revised September 4, 2008. First published March 31, 2009; current version published May 15, 2009.

E. Bulić and A. R. Sinigoj are with the Faculty of Electrical Engineering, University of Ljubljana, Ljubljana 1000, Slovenia (e-mail: edi.bulic@fe.uni-lj.si; anton.sinigoj@fe.uni-lj.si).

B. Cestnik is with Milan Vidmar Electric Power Research Institute, Ljubljana 1000, Slovenia (e-mail: breda.cestnik@eimv.si).

Digital Object Identifier 10.1109/TEMC.2009.2014848

II. Equivalent Surface-Source Concept

A. Structure Geometry and Problem Presentation

The specific geometry of the problem to be examined is shown in Fig. 1. The primary magnetic field source is time-harmonic currents $I_{\mathrm{C}1}$, $I_{\mathrm{C}2}, \ldots, I_{\mathrm{C}n_{\mathrm{C}}}$ in long thin parallel conductors (wires), where n_{C} is the number of the conductors. Homogeneous conducting magnetic and/or nonmagnetic shields run parallel to the wires, and modify the primary field. The shield cross-sectional areas are $\mathcal{S}_{\mathrm{S}1}$, $\mathcal{S}_{\mathrm{S}2}, \ldots, \mathcal{S}_{\mathrm{S}n_{\mathrm{S}}}$, where n_{S} is the number of the shields. The structure length l_0 is large compared to the structure transverse dimensions so that the 2-D space can be assumed.

The other symbols in Fig. 1 denote:

1) $T_{\mathrm{C}1}, T_{\mathrm{C}2}, \ldots, T_{\mathrm{C}n_{\mathrm{C}}}$—the points on the wires axes;
2) $\mathcal{S}_0$—cross-sectional area of the shields outside;
3) $\mathcal{L}_{\mathrm{S}1}, \mathcal{L}_{\mathrm{S}2}, \ldots, \mathcal{L}_{\mathrm{S}n_{\mathrm{S}}}$—the boundaries of the shield cross-sectional areas;
4) $\gamma_{\mathrm{S}1}, \gamma_{\mathrm{S}2}, \ldots, \gamma_{\mathrm{S}n_{\mathrm{S}}}$ and $\mu_{\mathrm{S}1}, \mu_{\mathrm{S}2}, \ldots, \mu_{\mathrm{S}n_{\mathrm{S}}}$—electric conductivities and magnetic permeabilities, respectively, of the shields;
5) $\gamma_0 = 0$ and μ_0—conductivity and permeability, respectively, of the ambient medium (e.g., air);
6) $I_{\mathrm{S}1}, I_{\mathrm{S}2}, \ldots, I_{\mathrm{S}n_{\mathrm{S}}}$—the currents induced in the shields;
7) T—a point on the shield boundaries;

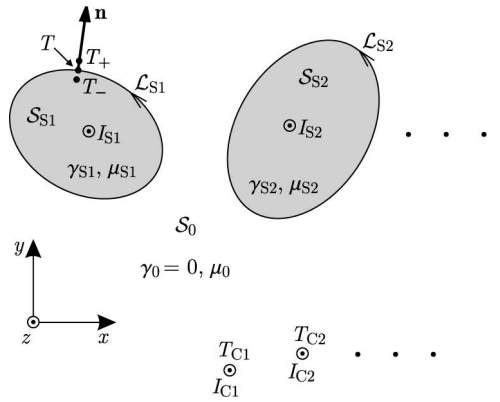

Fig. 1. Cross section of shields and wires.

8) T_-, T_+—points infinitesimally near the point T (i.e., near the shield boundaries);
9) $\mathbf{n}$—the unit normal vector of the shield boundaries pointing outward.

The union of the shield cross-sectional areas and the union of their boundaries are denoted by $\mathcal{S} = \mathcal{S}_{S1} \cup \mathcal{S}_{S2} \cup \cdots \cup \mathcal{S}_{Sn_S}$ and $\mathcal{L} = \mathcal{L}_{S1} \cup \mathcal{L}_{S2} \cup \cdots \cup \mathcal{L}_{Sn_S}$, respectively. The boundary $\mathcal{L}$ is still a part of the cross-sectional area $\mathcal{S}$, $\mathcal{L} \in \mathcal{S}$, and so the material properties on $\mathcal{L}$ (e.g., at the point T in Fig. 1) are equal to those inside $\mathcal{S}$ (e.g., at the point T_-) and not to those outside $\mathcal{S}$ (e.g., at the point T_+).

Our goal is to determine shielding factor a. In this paper, at any point T in space, it is defined as a ratio between the primary magnetic flux density magnitude $|\mathbf{B}_0(T)|$ and the resultant magnetic flux density magnitude $|\mathbf{B}(T)|$: $a(T) = |\mathbf{B}_0(T)|/|\mathbf{B}(T)|$.

B. Theory

As the primary magnetic field source and shields run parallel to the z-axis, this is also true for the induced current density $\mathbf{J}$ and for the magnetic vector potential $\mathbf{A}$ as well: $\mathbf{J} = \mathbf{e}_z J_z(x,y) \Longrightarrow \mathbf{A} = \mathbf{e}_z A_z(x,y)$. Under quasi-static conditions, the potential at some point $T(x,y)$ is governed by Poisson's equation [11]

$$\triangle A_z(T) = \begin{cases} -\mu(T) J_z(T), & T \in \mathcal{S} \\ -\sum_{i=1}^{n_C} \mu_0 I_{Ci} \delta_2\left(\overline{TT_{Ci}}\right), & T \in \mathcal{S}_0 \end{cases} \quad (1)$$

where $\overline{TT_{Ci}}$ is the distance from point T to point T_{Ci} and δ_2 is the Dirac delta function in 2-D. The current density in the shields can be expressed by the electric field intensity $\mathbf{E}$ or by the magnetic vector potential $\mathbf{A}$ and electric scalar potential V

$$J_z = \gamma E_z = -\mathrm{j}\omega\gamma A_z - \gamma\frac{\partial V}{\partial z} = -\mathrm{j}\omega\gamma A_z + \gamma\frac{U}{l_0} \quad (2)$$

where $\mathrm{j} = \sqrt{-1}$, ω is the angular frequency of the time-harmonic field, and U is the electric potential difference between the beginning and end of the shield (the direction of the z-axis defines which end of the shield is the beginning one and which is the ending one). The potential difference U is constant over the cross-sectional area of one shield, but, in general, it varies from shield to shield. Applying (2) into (1) yields

$$\triangle A_z(T) + k^2(T) A_z(T) = -\mu(T)\gamma(T)\frac{U(T)}{l_0}, \qquad T \in \mathcal{S} \quad (3a)$$

$$\triangle A_z(T) = -\sum_{i=1}^{n_C} \mu_0 I_{Ci} \delta_2\left(\overline{TT_{Ci}}\right), \qquad T \in \mathcal{S}_0 \quad (3b)$$

where $k = \sqrt{-\mathrm{j}\omega\mu\gamma}$ is the wavenumber of the (metal) shield. Equation (3a) is the Helmholtz's equation [12].

Equation (3a) is solved with the boundary element method [13]–[15]. The boundary integral equations are derived as follows. The Green's functions inside and outside the shields for the 2-D Helmholtz's and Poisson's equations, respectively, are [16]

$$g(T,T') = \frac{1}{4\mathrm{j}} H_0^{(2)}\left(k(T)\overline{TT'}\right) \quad (4a)$$

$$g_0(T,T') = \frac{1}{2\pi}\ln\frac{1}{\overline{TT'}} \quad (4b)$$

where $H_0^{(2)}$ is the zero-order Hankel function of the second kind. Inserting the Green's functions (4) and magnetic potential z-component A_z into the Green's second theorem, we obtain

$$\int_{\mathcal{S}}\Big(g(T,T')\triangle A_z(T) - A_z(T)\triangle g(T,T')\Big)\mathrm{d}s = \oint_{\mathcal{L}}\left(g(T,T')\frac{\partial A_z(T_-)}{\partial n} - A_z(T_-)\frac{\partial g(T,T')}{\partial n}\right)\mathrm{d}l \quad (5a)$$

$$\int_{\mathcal{S}_0}\Big(g_0(T,T')\triangle A_z(T) - A_z(T)\triangle g_0(T,T')\Big)\mathrm{d}s = \oint_{\mathcal{L}}\left(-g_0(T,T')\frac{\partial A_z(T_+)}{\partial n} + A_z(T_+)\frac{\partial g_0(T,T')}{\partial n}\right)\mathrm{d}l \quad (5b)$$

where T' is any point and T is the integration point. Taking (3) into consideration and the boundary conditions for tangential components of the magnetic and electric field intensities on the shield boundaries

$$-\frac{\partial A_z(T_+)}{\partial n} = -\frac{1}{\mu_r(T_-)}\frac{\partial A_z(T_-)}{\partial n} = \alpha_1(T) \quad (6a)$$

$$A_z(T_+) = A_z(T_-) = \alpha_2(T) \quad (6b)$$

where μ_r is the relative permeability, we have

$$\int_{\mathcal{S}}\left(A_z(T)\delta_2\left(\overline{TT'}\right) - \mu(T)\gamma(T)\frac{U(T)}{l_0}g(T,T')\right)\mathrm{d}s = \oint_{\mathcal{L}}\left(-\mu_r(T)\alpha_1(T)g(T,T') - \alpha_2(T)\frac{\partial g(T,T')}{\partial n}\right)\mathrm{d}l \quad (7a)$$

$$-\sum_{i=1}^{n_C} g_0(T_{Ci},T')\mu_0 I_{Ci} + \int_{\mathcal{S}_0} A_z(T)\delta_2\left(\overline{TT'}\right)\mathrm{d}s = \oint_{\mathcal{L}}\left(\alpha_1(T)g_0(T,T') + \alpha_2(T)\frac{\partial g_0(T,T')}{\partial n}\right)\mathrm{d}l. \quad (7b)$$

To find the limit of (7a) and (7b) as the point T' approaches the shield boundaries $\mathcal{L}$ from outward ($T' \to T'_+$) and from inward ($T' \to T'_-$), respectively, we take into account the results [1] from [17, Sec. 3.1]. The resulting equations are coupled integral equations for functions α_1 and α_2, which are density distributions of the single layer and double layer, respectively, on the shield boundaries

$$\alpha_2(T') + 2\oint_{\mathcal{L}} \left(\alpha_2(T)\frac{\partial g(T,T')}{\partial n} + \mu_{\mathrm{r}}(T)\alpha_1(T)g(T,T')\right)\mathrm{d}l - 2\int_{\mathcal{S}} \mu(T)\gamma(T)\frac{U(T)}{l_0}g(T,T'_+)\mathrm{d}s = 0, \qquad T' \in \mathcal{L} \tag{8a}$$

$$\alpha_2(T') - 2\oint_{\mathcal{L}} \left(\alpha_2(T)\frac{\partial g_0(T,T')}{\partial n} + \alpha_1(T)g_0(T,T')\right)\mathrm{d}l = 2\sum_{i=1}^{n_{\mathrm{C}}} g_0(T_{\mathrm{C}i},T')\mu_0 I_{\mathrm{C}i}, \qquad T' \in \mathcal{L}. \tag{8b}$$

These two layers are assumed to be equivalent surface sources of the electromagnetic field. Surface integrals over the shield cross-sectional areas can be transformed into curve integrals over their boundaries by the Gauss's theorem

$$\begin{aligned}\int_{\mathcal{S}_{\mathrm{S}j}} \mu(T)\gamma(T)\frac{U(T)}{l_0}g(T,T'_+)\mathrm{d}s &= \mu_{\mathrm{S}j}\gamma_{\mathrm{S}j}\frac{U_{\mathrm{S}j}}{l_0}\int_{\mathcal{S}_{\mathrm{S}j}} g(T,T'_+)\mathrm{d}s \\ &= \mu_{\mathrm{S}j}\gamma_{\mathrm{S}j}\frac{U_{\mathrm{S}j}}{l_0}\left(-\frac{1}{k_{\mathrm{S}j}^2}\oint_{\mathcal{L}_{\mathrm{S}j}}\frac{\partial g(T,T'_+)}{\partial n}\mathrm{d}l\right)\end{aligned} \tag{9}$$

where $U_{\mathrm{S}j}$ is the electric potential difference between the beginning and end of the jth shield and $k_{\mathrm{S}j}$ is the wavenumber of the jth shield.

Explicit expressions for the vector magnetic potential at a point inside or outside the shields are derived from (7a) or (7b), respectively

$$A_z(T' \in \mathcal{S}) = -\oint_{\mathcal{L}} \left(\alpha_2(T)\frac{\partial g(T,T')}{\partial n} + \mu_{\mathrm{r}}(T)\alpha_1(T)g(T,T')\right)\mathrm{d}l + \int_{\mathcal{S}} \mu(T)\gamma(T)\frac{U(T)}{l_0}g(T,T')\mathrm{d}s \tag{10a}$$

$$A_z(T' \in \mathcal{S}_0) = \oint_{\mathcal{L}} \left(\alpha_2(T)\frac{\partial g_0(T,T')}{\partial n} + \alpha_1(T)g_0(T,T')\right)\mathrm{d}l + \sum_{i=1}^{n_{\mathrm{C}}} g_0(T_{\mathrm{C}i},T')\mu_0 I_{\mathrm{C}i}. \tag{10b}$$

The Green's function outside the shields (4b) must be modified when the wires and shields run parallel to the ground [18]

$$g_0(T,T') \cong \frac{1}{2\pi}\ln\frac{d_{\mathrm{C}}e^{-\mathrm{j}\pi/4}}{\overline{TT'}} \tag{11}$$

where $d_{\mathrm{C}} \simeq 1.85/|k_{\mathrm{g}}|$ is the Carson's distance and k_g is the wavenumber of the ground. If the Carson's distance is much larger than the distances ($\overline{TT'}$) from the wires and shields to the observed points, the impact of the ground effect can be neglected. This condition is usually fulfiled at low frequencies when the Carson's distance is quite large.

Shields can have open ends or can be grounded for safety reasons. If the jth shield is grounded at its beginning and its end (two-sidedly grounded), an additional current path is provided for current circulation and the net-induced current $I_{\mathrm{S}j}$ in that shield is not equal to zero [5]. The current $I_{\mathrm{S}j}$ is proportional to the integral of the single-layer density over the boundary $\mathcal{L}_{\mathrm{S}j}$, according to Ampère's law, and also to $U_{\mathrm{S}j}$, according to Ohm's law (for an ac circuit)

$$I_{\mathrm{S}j} = \frac{1}{\mu_0}\oint_{\mathcal{L}_{\mathrm{S}j}} \alpha_1(T)\mathrm{d}l = \frac{U_{\mathrm{S}j}}{Z_{\mathrm{g,S}j}} \tag{12}$$

where $Z_{\mathrm{g,S}j}$ is the sum of the grounding impedances of the jth shield. This equation forms a system of equations with (8) because $U_{\mathrm{S}j}$ is also an unknown variable. If $Z_{\mathrm{g,S}j}$ is very small compared to the shield impedance, grounding can be considered ideal. In this case, $U_{\mathrm{S}j} \to 0$ and (12) does not need to join (8) because $U_{\mathrm{S}j}$ is no longer unknown. If the jth shield is grounded only at one point (one-sidedly grounded) or has open ends, no additional current path is provided and the net-induced current $I_{\mathrm{S}j}$ is equal to zero

$$I_{\mathrm{S}j} = \frac{1}{\mu_0}\oint_{\mathcal{L}_{\mathrm{S}j}} \alpha_1(T)\mathrm{d}l = 0. \tag{13}$$

Shields can also be electrically connected. If, for example, the jth and the ith shield are connected at least at their beginnings and ends, their electrical potential differences are the same, i.e., $U_{\mathrm{S}j} = U_{\mathrm{S}i}$. When they are also one-sidedly grounded, their common net-induced current is equal to zero, and the equation

$$I_{\mathrm{S}j} + I_{\mathrm{S}i} = \frac{1}{\mu_0}\oint_{\mathcal{L}_{\mathrm{S}j}\cup\mathcal{L}_{\mathrm{S}i}} \alpha_1(T)\mathrm{d}l = 0 \tag{14}$$

joins (8).

C. Numerical Method

In our paper, the system of coupled integral equations [(8) and equations like (12), (13), and/or (14)] is solved by using

[1]
$$\oint_{\mathcal{L}} \left(\mu_{\mathrm{r}}(T)\alpha_1(T)g(T,T'_+) + \alpha_2(T)\frac{\partial g(T,T'_+)}{\partial n}\right)\mathrm{d}l = \frac{\alpha_2(T')}{2} + \oint_{\mathcal{L}} \left(\mu_{\mathrm{r}}(T)\alpha_1(T)g(T,T') + \alpha_2(T)\frac{\partial g(T,T')}{\partial n}\right)\mathrm{d}l, \qquad T' \in \mathcal{L}$$

$$\oint_{\mathcal{L}} \left(\alpha_1(T)g_0(T,T'_-) + \alpha_2(T)\frac{\partial g_0(T,T'_-)}{\partial n}\right)\mathrm{d}l = -\frac{\alpha_2(T')}{2} + \oint_{\mathcal{L}} \left(\alpha_1(T)g_0(T,T') + \alpha_2(T)\frac{\partial g_0(T,T')}{\partial n}\right)\mathrm{d}l, \qquad T' \in \mathcal{L}$$

TABLE I
CPU TIME

n_{BE}	T_{ESS} (min)	T_B (s)
27	0.14	1.0
54	0.53	1.9
99	1.74	3.5
201	7.09	6.9
401	29.2	14.2
801	95.9	27.6

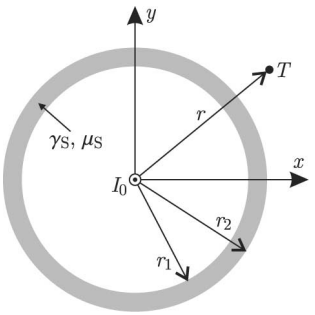

Fig. 2. Coaxial shield.

the moment method [19]. The boundaries of the shield cross-sectional areas are discretizated into short straight segments (boundary elements) of lengths $\Delta l_1, \Delta l_2, \ldots, \Delta l_{n_{\mathrm{BE}}}$, where n_{BE} is the number of the segments. The pulse functions and Dirac's delta functions are used as expansion and testing functions, respectively. The integrals of the Green's functions and their normal derivatives over the boundary elements are computed by using Simpson's rule. Solution to the system of coupled integral equations are single-layer and double-layer densities. From this solution, we first compute the vector magnetic potential in the nodes of a rectangular grid [by using (10)], and then the magnetic flux density from $\mathbf{B} = \nabla \times \mathbf{A}$ by using finite differences.

To give an idea of the computational effort for various numbers of the boundary elements, the CPU times T_{ESS} and T_B required to calculate: 1) density distributions of the single layer and double layer, and 2) magnetic flux density in one point, respectively, are shown in Table I. Computations were performed by a nonoptimized MATLAB code on a personal computer equipped with an Intel 1.83-GHz processor and 2 GB of RAM.

III. VERIFICATION OF RESULTS

The results obtained with the ESSM are compared with:
1) results of analytically solvable problems;
2) experimental results;
3) results obtained with two different numerical methods.

A. Cylindrical Shields

1) Coaxial Shield: The case in Fig. 2 corresponds to the geometry of the coaxial cable. The time-harmonic current I_0 in the inner conductor is the source of the primary magnetic field. The outer conductor plays the role of a shield and has open ends. The function of radial distribution of the induced current density $\mathbf{J} = \mathbf{e}_z J_z(r)$ in the shield, which is source-free ($\mathbf{J} = \gamma_{\mathrm{S}}\mathbf{E}$) with the wavenumber k_{S}, is governed by the Bessel's differential equation [12]

$$\triangle J_z(r) + k_{\mathrm{S}}^2 J_z(r) = \frac{\mathrm{d}^2 J_z}{\mathrm{d}r^2} + \frac{1}{r}\frac{\mathrm{d}J_z}{\mathrm{d}r} + k_{\mathrm{S}}^2 J_z(r) = 0 \quad (15)$$

and is expressed with the zero-order Bessel functions of the first and second kind

$$J_z(r) = C_1 J_0(k_{\mathrm{S}} r) + C_2 N_0(k_{\mathrm{S}} r). \quad (16)$$

The constants C_1 and C_2 result from the boundary conditions on the surfaces of the outer conductor, $H_\varphi(r_1) = I_0/(2\pi r_1)$ and $H_\varphi(r_2) = I_0/(2\pi r_2)$, and have the following values:

$$C_1 = \frac{k_{\mathrm{S}} I_0}{2\pi} \frac{N_1(k_{\mathrm{S}} r_2)/r_1 - N_1(k_{\mathrm{S}} r_1)/r_2}{J_1(k_{\mathrm{S}} r_1)N_1(k_{\mathrm{S}} r_2) - J_1(k_{\mathrm{S}} r_2)N_1(k_{\mathrm{S}} r_1)} \quad (17a)$$

$$C_2 = \frac{k_{\mathrm{S}} I_0}{2\pi} \frac{J_1(k_{\mathrm{S}} r_1)/r_2 - J_1(k_{\mathrm{S}} r_2)/r_1}{J_1(k_{\mathrm{S}} r_1)N_1(k_{\mathrm{S}} r_2) - J_1(k_{\mathrm{S}} r_2)N_1(k_{\mathrm{S}} r_1)} \quad (17b)$$

where J_1 and N_1 are the first-order Bessel functions of the first and second kind, respectively.

The net-induced current in the shield is equal to zero due to its open ends (but this does not imply that the induced current density is equal to zero). Beacuse of this and since the current density is axial-symmetrically distributed in the shield, such a shield modifies the primary field only in its own interior, where $r_1 \leq r \leq r_2$. So in this case, the shield is not to be used for shielding but is interesting only for verification of the proposed method.

A comparison of the magnetic field intensity magnitudes obtained with the ESSM and with the analytical approach is shown in Figs. 3 and 4 for a magnetically nonpermeable (Al) shield and for a magnetically permeable (Fe) shield, respectively. In the case of the Al alloy shield, the numerical data are $r_1 = 50$ mm, $r_2 = 55$ mm, $\gamma_{\mathrm{S}} = 30.5$ MS/m, $\mu_{\mathrm{S}} = \mu_0$, $I_0 = 100$ A, and $f = 5$ kHz. In the case of the steel shield, the data are changed only for conductivity, permeability, and frequency (the frequency was increased for the Al shield to avoid disturbance of the primary field to be negligible): $\gamma_{\mathrm{S}} = 10$ MS/m, $\mu_{\mathrm{S}} = 1000\,\mu_0$, and $f = 50$ Hz. In accordance with our expectations, the maximal deviation (up to 3%) from the analytical solution is detected at the shield surface, where $r \to 50$ mm or $r \to 55$ mm, i.e., at the points of the single layer and double layer.

The analytical solution in the case of the coaxial shield can be used in estimation of accuracy of the proposed numerical method. The discrepancy between the numerically and analytically computed value of the magnetic field is dependent primarily on the ratio between the length Δl of the boundary elements and the skin depth $\delta = \sqrt{2/(\omega\mu_{\mathrm{S}}\gamma_{\mathrm{S}})}$ of the shield (to allow for straightforward dependence, all the elements are of the same length). This dependence is analyzed. The numerical data were $f = 250$ Hz, $r_1 = 10$ mm, $r_2 = 20$ mm, $\gamma_{\mathrm{S}} = 10$ MS/m, and $\mu_{\mathrm{S}} = 100\ \mu_0$. Fig. 5 illustrates absolute values of the relative discrepancy in the shield at $r = 15$ mm. The discrepancy increases progressively with the ratio $\Delta l/\delta$, and at $\Delta l/\delta = 1$, it does not yet reach 1%.

2) Shielded Pair of Conductors: Consider a bifilar pair of parallel conductors, which is centered inside a cylindrical shield

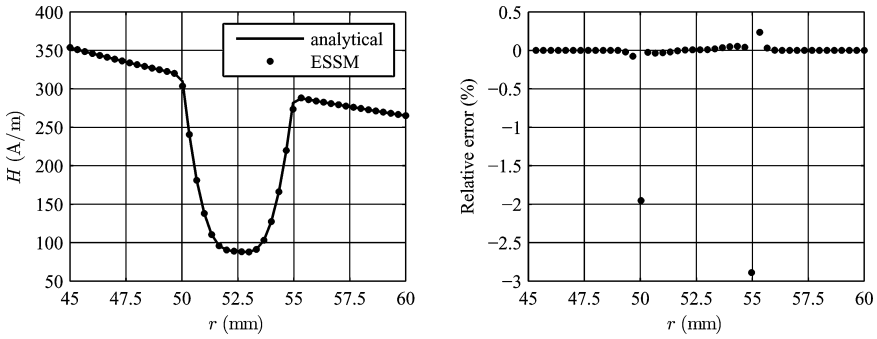

Fig. 3. Comparison with the analytical solution for the coaxial nonmagnetic-metal shield. (a) Magnetic field intensity. (b) Discrepancy.

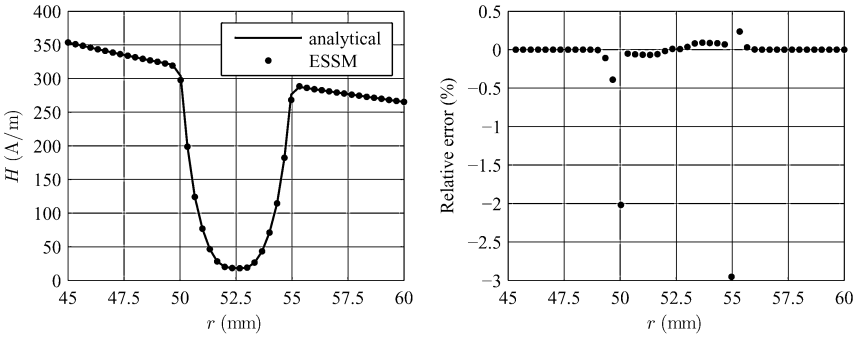

Fig. 4. Comparison with the analytical solution for the coaxial magnetic-metal shield. (a) Magnetic field intensity. (b) Discrepancy.

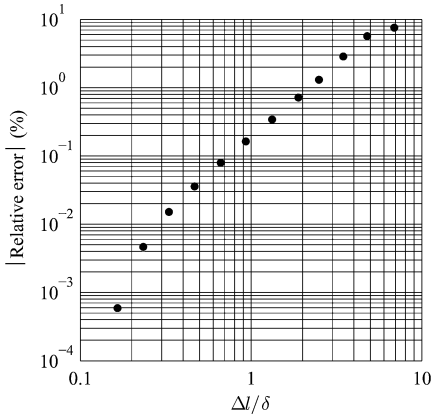

Fig. 5. Dependence of accuracy of the magnetic field intensity calculation on the ratio between the length of the boundary elements and the skin depth for the coaxial shield.

(see Fig. 6). The field in this case is analytically solvable. The analytical solution for a shield with a small thickness compared to the shield skin depth $(r_2 - r_1 \ll \delta)$ is presented in [20] and used in [7]. In the case of a line dipole source $(2d \ll r_1)$ centered inside the cylindrical shield, the analytical solution is presented in [21] and used in [22] and [23].

For the purpose of a comparison with the results of the ESSM, we used the analytical solution for a case of the shield of arbitrary thickness surrounding the arbitrarily spaced conductors [6]. This solution is derived as follows. The magnetic potential z-component A_z is governed by (3). This equation can be solved in the cylindrical coordinate system (see Fig. 6) by us-

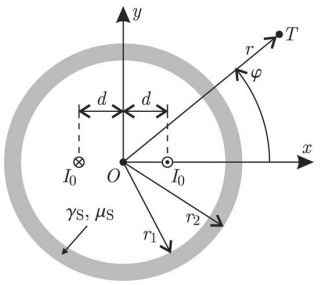

Fig. 6. Bifilar pair of conductors inside the cylindrical shield.

ing the method of separation of variables [12] and by expanding the potential $A_{0,z}$ of the unshielded conductors in the Fourier series

$$A_{0,z}(r,\varphi) = \frac{\mu_0 I_0}{\pi} \sum_{n=1}^{\infty} \cos\big((2n-1)\varphi\big) \times \frac{1}{(2n-1)2^{2n-1}} \left(\frac{2d}{r}\right)^{2n-1}. \tag{18}$$

As a general solution, we obtain

$$A_z(r,\varphi) = \sum_{n=1}^{\infty} \cos\big((2n-1)\varphi\big) \left(C_{1,n} r^{2n-1} + \frac{\mu_0 I_0}{\pi} \frac{1}{(2n-1)2^{2n-1}} \left(\frac{2d}{r}\right)^{2n-1} \right), \qquad r \le r_1 \tag{19a}$$

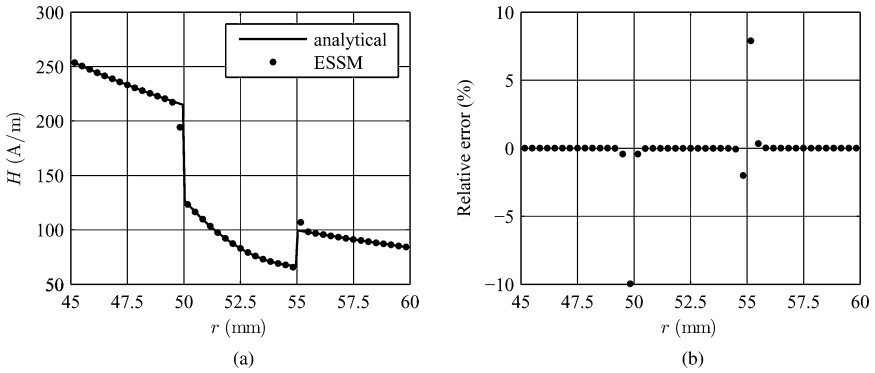

Fig. 7. Comparison with the analytical solution for a cylindrical shield surrounding a pair of conductors. $I_0 = 100\,\mathrm{A}$, $f = 50$ Hz, $2d = 30$ mm, $r_1 = 50$ mm, $r_2 = 55$ mm, $\gamma_\mathrm{S} = 10$ MS/m, and $\mu_\mathrm{S} = 10\,\mu_0$. (a) Magnetic field intensity. (b) Discrepancy.

$$A_z(r,\varphi) = \sum_{n=1}^{\infty} \cos\big((2n-1)\varphi\big)\Big(C_{2,n} H_{2n-1}^{(1)}(k_\mathrm{S} r) + C_{3,n} H_{2n-1}^{(2)}(k_\mathrm{S} r)\Big), \qquad r_1 < r < r_2 \tag{19b}$$

$$A_z(r,\varphi) = \sum_{n=1}^{\infty} \cos\big((2n-1)\varphi\big) C_{4,n} r^{-(2n-1)}, \qquad r \geq r_2 \tag{19c}$$

where $H_{2n-1}^{(1)}$ and $H_{2n-1}^{(2)}$ are the Hankel functions of the first and second kind, respectively, of order $(2n-1)$ and k_S is the wavenumber of the shield. The constants $C_{1,n}$, $C_{2,n}$, $C_{3,n}$, and $C_{4,n}$ result from the boundary conditions on the shield surfaces, which state continuity of tangential components A_z and H_φ of the magnetic vector potential and magnetic field intensity, respectively. As series in (19) converge very rapidly, only the first few summands need to be considered. We considered the first ten summands.

A comparison of the radial dependence of the magnetic field intensity magnitudes, along the straight line at $\varphi = \pi/4$, obtained with the ESSM and with the analytical approach, is shown in Fig. 7. The only significant deviation from the analytical solution is again (see Figs. 3 and 4) detected at the shield surfaces.

The analytical solution is once more used in estimation of accuracy of the proposed numerical method. The analysis of dependence of the discrepancy between the numerically and analytically computed values of the magnetic field on the ratio $\Delta l/\delta$ is made for the same shield and same frequency as in the case of the coaxial shield. The primary field source is a pair of conductors whose spacing is $2d = 10$ mm. Fig. 8 shows the results of this analysis in the point ($r = 15$ mm, $\varphi = \pi/4$). The discrepancy again increases progressively with the ratio $\Delta l/\delta$, and at $\Delta l/\delta \approx 1$, it is near 1%.

Hoburg *et al.* [24] measured the magnetic field from a pair of conductors surrounded by a cylindrical shield. Fig. 9 provides a comparison between the shielding factor values obtained: 1) analytically; 2) with the ESSM; and 3) with the experiment (in [24]) for a magnetically nonpermeable (Al) shield. Fig. 10 provides the same comparison for a magnetically permeable (low carbon steel) shield. The numerical data were: 1) for the primary field source $I_0 = 500\,\mathrm{A}$, $f = 60$ Hz, and $2d = 6$ cm; 2) for

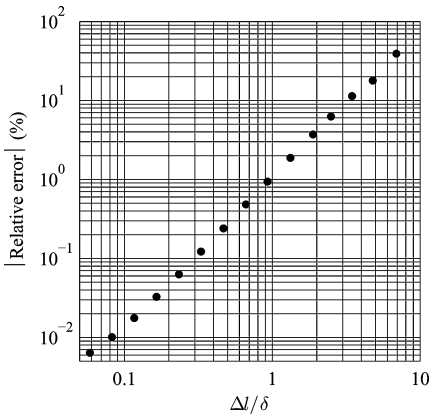

Fig. 8. Dependence of accuracy of the magnetic field intensity calculation on the ratio between the length of the boundary elements and the skin depth for a cylindrical shield surrounding a pair of conductors.

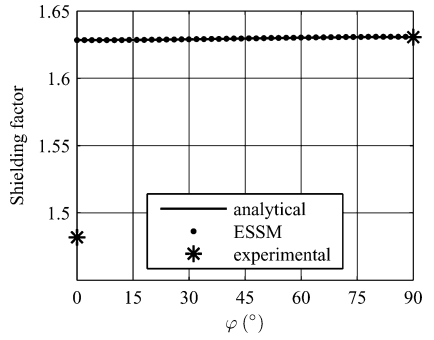

Fig. 9. Comparison with the analytical solution and experimental results for a pair of conductors inside a cylindrical nonmagnetic-metal shield.

the Al shield $r_1 = 25.435$ cm, $r_2 = 25.5$ cm, $\gamma_\mathrm{S} = 30.5$ MS/m, and $\mu_\mathrm{S} = \mu_0$; and 3) for the steel shield $r_1 = 25.43$ cm, $r_2 = 25.5$ cm, $\gamma_\mathrm{S} = 6.76$ MS/m, and $\mu_\mathrm{S} = 190\,\mu_0$[2]. The experiment

[2]In [24] it reads: "The measured initial relative permeability of the steel was $\mu_\mathrm{r} = 182.5$, and the relative permeability remained below $\mu_\mathrm{r} = 190$ for flux densities in the steel below 10^{-3} T." But the flux density in the steel shield is about 15 mT, so in calculations, we used the value of 190 for the relative permeability. The relative permeability is likely larger than 190, and this probably also causes the discrepancy between the measured and calculated results. The proposed method is applicable only to linear materials, but there are methods that can deal with the nonlinearity of ferromagnetic materials [25].

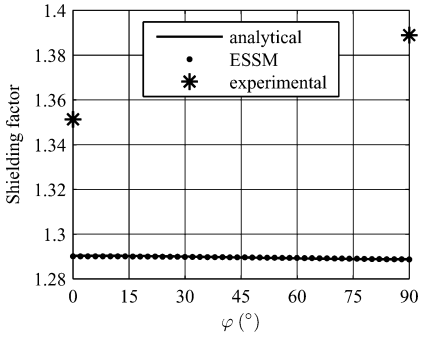

Fig. 10. Comparison with the analytical solution and experimental results for a pair of conductors inside a cylindrical magnetic-metal shield.

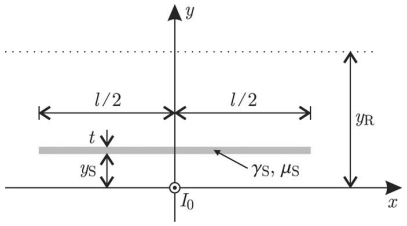

Fig. 11. Exceedingly wide flat shield above the wire.

setup is described in detail in [24]. The shielding factor is calculated at a radial distance of $r = 0.62$ m for angles $0 \leq \varphi \leq \pi/2$. It was measured at the same distance for two angles, $\varphi = 0$ and $\varphi = \pi/2$. Figs. 9 and 10 show that the ESSM yields an excellent agreement (within $0.02\,\%$) with the analytical solution. Experimental results for the Al shield deviate from the analytical one by $-9.0\,\%$ and $0.0\,\%$ for angles $\varphi = 0$ and $\varphi = \pi/2$, respectively. These deviations for the steel shield are about $4.7\,\%$ and $7.8\,\%$.

B. Exceedingly Wide Flat Shield

We deal with the case of an exceedingly wide and two-sidedly, ideally grounded shield above the wire shown in Fig. 11. The numerical data are $I_0 = 100\,\mathrm{A}$, $f = 50$ Hz, $t = 2$ mm, $y_\mathrm{S} = 5$ cm, and $l = 4\,\mathrm{m}$.

To estimate the reaction field of such shield, we use the analytical solution for the infinite planar shield [1], [18]. The analytical solution for the vector magnetic potential above the shield is expressed as the Fourier cosine transform

$$A_z(x, y > y_\mathrm{S} + t) = \int_0^\infty f(\xi) \mathrm{e}^{-\sqrt{\xi^2 - k_0^2}\, y} \cos(\xi x) \mathrm{d}\xi \quad (20)$$

where k_0 is the wavenumber of free space (or air) and the function $f(\xi)$ is obtained from the boundary conditions of the electromagnetic field on the lower and upper surface of the shield, and is given by

$$f(\xi) = \frac{I_0 \mu_\mathrm{S} \mu_0^2}{\pi} \sqrt{\xi^2 - k_\mathrm{S}^2}\, \mathrm{e}^{t\sqrt{\xi^2 - k_0^2}} \times \left(2\,\mu_\mathrm{S}\mu_0 \sqrt{\xi^2 - k_\mathrm{S}^2} \sqrt{\xi^2 - k_0^2}\, \cosh\left(t\sqrt{\xi^2 - k_\mathrm{S}^2}\right) + \left(\mu_\mathrm{S}^2 \left(\xi^2 - k_0^2\right) + \mu_0^2 \left(\xi^2 - k_\mathrm{S}^2\right)\right) \sinh\left(t\sqrt{\xi^2 - k_\mathrm{S}^2}\right)\right)^{-1}. \quad (21)$$

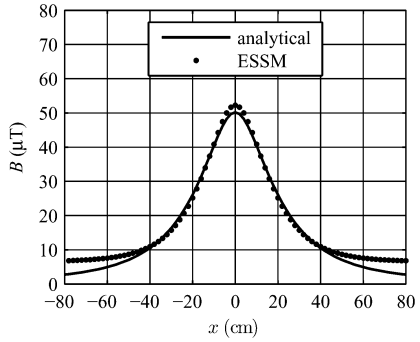

Fig. 12. Comparison with the analytical approximation for an exceedingly wide flat nonmagnetic-metal shield.

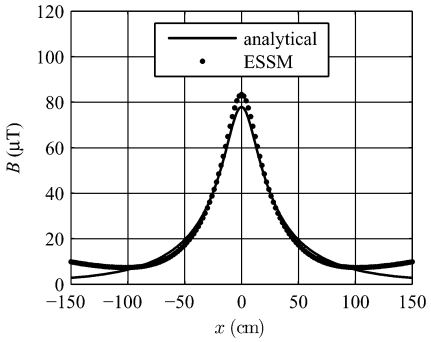

Fig. 13. Comparison with the analytical approximation for an exceedingly wide flat magnetic-metal shield.

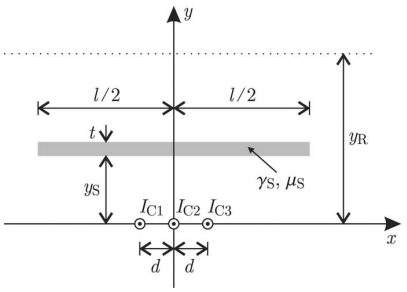

Fig. 14. Finite-width flat shield above the wires.

The integral in (20) is solved numerically.

Comparisons of the magnetic flux density magnitudes above the shield (at the height of $y_\mathrm{R} = 15$ cm above the wire) obtained with the ESSM and with analytical approximation are shown in Figs. 12 and 13 for the nonmagnetic ($\gamma_\mathrm{S} = 30.5$ MS/m and $\mu_\mathrm{S} = \mu_0$) and magnetic shield ($\gamma_\mathrm{S} = 10$ MS/m and $\mu_\mathrm{S} = 10\,\mu_0$), respectively. The wide shield resembles the infinite planar shield in the vicinity of its center. The discrepancy between the wide shield and infinte planar shield increases rapidly with the distance from the center.

C. Finite-Width Flat Shields

Our comparison between the results of several methods is made for a finite-width flat shield placed above the wires (Fig. 14).

1) Hybrid Method (HM): In [3], a method for calculating the shielding performance of a 2-D finite-width metal shield is described. It is based on an analytical approximation for the magnetic field behind the shield. This approximation combines the expressions for penetration of the field through the infinite planar shield and for leakage around the finite-width shield, and is therefore called HM.

2) Multiconductor Method (MCM): This method [6], [8], [9] is suitable only for analysis of the nonmagnetic shields. It is based on the solution of the integral equation for distribution of the induced current density $\mathbf{J} = \mathbf{e}_z J_z$ in shields. The equation is derived as follows. The sources of the magnetic field are currents in wires and shields

$$A_z(T) = \frac{\mu_0}{2\pi} \sum_{i=1}^{n_\mathrm{C}} I_{\mathrm{C}i} \ln \frac{1}{\overline{\overline{TT_{\mathrm{C}i}}}} + \frac{\mu_0}{2\pi} \int_{\mathcal{S}} J_z(T') \ln \frac{1}{\overline{\overline{TT'}}} \, \mathrm{d}s'. \tag{22}$$

If the shields and wires run parallel to the ground, the Green's functions in this equation have to be modified by means of (11). By inserting (22) in (2), the following integral equation is obtained:

$$\frac{J_z(T)}{\gamma(T)} + \frac{\mathrm{j}\omega\mu_0}{2\pi} \int_{\mathcal{S}} J_z(T') \ln \frac{1}{\overline{\overline{TT'}}} \, \mathrm{d}s' = \frac{U(T)}{l_0} - \frac{\mathrm{j}\omega\mu_0}{2\pi} \sum_{i=1}^{n_\mathrm{C}} I_{\mathrm{C}i} \ln \frac{1}{\overline{\overline{TT_{\mathrm{C}i}}}}. \tag{23}$$

The electric potential differences U between the beginning and end of the shields are also unknowns in the integral equation. Thus, to obtain its unique solution, (12) or (13) for the two-sidedly or one-sidedly grounded shields, respectively, have to be added

$$I_{\mathrm{S}j} = \int_{\mathcal{S}j} J_z(T') \mathrm{d}s' = \begin{cases} U_{\mathrm{S}j}/Z_{\mathrm{g,S}j} \\ 0 \end{cases}, \qquad j = 1, 2, \ldots, n_\mathrm{S}. \tag{24}$$

In solving numerically the acquired system of coupled integral equations (23) and (24) by using the moment method [19], the cross-sectional areas of the shields are discretizated. It is advantageous to use the MCM rather than the ESSM for thin shields (requiring less unknowns, i.e., discretization elements, for the same accuracy of results) and, inversely, for thick shields.

Frix and Karady [6] measured the magnetic field from a pair of wires ($I_{\mathrm{C}1} = I_0$ and $I_{\mathrm{C}3} = -I_0$, the central wire in Fig. 14 is absent) near a flat Al shield. The measurement was performed for two different Al shields. In the first case, the numerical data were $I_0 = 100\,\mathrm{A}$, $f = 60$ Hz, $y_\mathrm{S} = 6.35\,\mathrm{cm}$, $2d = 7.62$ cm, $l = 30.48$ cm, $t = 3.175$ mm, $\gamma_\mathrm{S} = (10^3/36.99)$ MS/m, and $\mu_\mathrm{S} = \mu_0$, the shield had open ends, and the magnetic flux density was measured at the height of $y_\mathrm{R} = 14.13$ cm above the wires. In the second case, the only changed parameters were thickness ($t = 6.35$ mm) and conductivity ($\gamma_\mathrm{S} = (10^3/45)$ MS/m) of the shield and the height of measurement points ($y_\mathrm{R} = 14.45$ cm). The experiment setup is described in detail in [6]. We made a comparison between the results obtained with the experiment, ESSM, MCM, and HM. Figs. 15 and 16 show: 1) that the ESSM yields an excellent agreement with the MCM (the average absolute value of the relative difference is $\epsilon_{\mathrm{mean\,abs.}} \doteq 0.03\,\%$) and

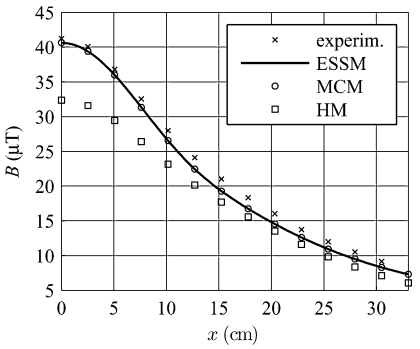

Fig. 15. Comparison with the results of the experiment, MCM, and HM for the finite-width flat Al shield of the thickness of $t = 3.175$ mm.

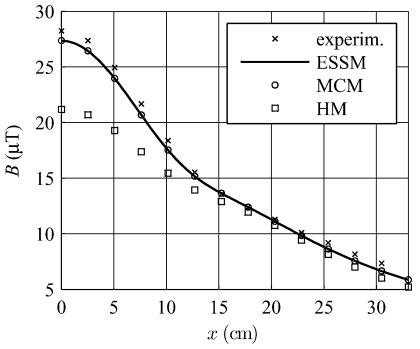

Fig. 16. Comparison with the results of the experiment, MCM, and HM for the finite-width flat Al shield of the thickness of $t = 6.35$ mm.

2) that the agreement of these two methods with the experiment ($\epsilon_{\mathrm{mean\,abs.}} \doteq 5.1\,\%$) is much better than that of the HM with the experiment ($\epsilon_{\mathrm{mean\,abs.}} \doteq 16.2\,\%$).

3) Surface-Current Method (SCM): This method is suitable only for analysis of magnetic shields. It is based on the magnetostatic approximation. On surfaces of the magnetic shields, the magnetization surface-current density $\mathbf{K}$ is proportional to the tangential component of the magnetic flux density [10]

$$\mathbf{K}(T) + \frac{2}{\mu_0} \beta(T) \mathbf{n}(T) \times \mathbf{B}(T) = \mathbf{0} \tag{25}$$

where $\beta(T) = (\mu(T) - \mu_0)/(\mu(T) + \mu_0)$. By expressing the magnetic flux density $\mathbf{B}$ in this equation as a sum of the primary field ($\mathbf{B}_0$) and contribution of the magnetization surface-current density $\mathbf{K} = \mathbf{e}_z K_z$, an integral equation for the distribution of the latter on the shield surfaces is obtained

$$K_z(T) + \frac{\beta(T)}{\pi} \oint_{\mathcal{L}} K_z(T') \frac{\mathbf{n}(T) \cdot \mathbf{P}}{P^2} \mathrm{d}l' = -\frac{2\beta(T)}{\mu_0} \mathbf{e}_z \cdot (\mathbf{n}(T) \times \mathbf{B}_0(T)) \tag{26}$$

where $\mathbf{P}$ is the distance vector between points T' and T.

A comparison between the results of the three methods, namely ESSM, SCM, and HM, is made for a two-sidedly (ideally) grounded flat magnetic-metal shield placed above wires of a three-phase system (see Fig. 14): $I_{\mathrm{C}1} = I_0 \exp(\mathrm{j}2\pi/3)$, $I_{\mathrm{C}2} = I_0$, and $I_{\mathrm{C}3} = I_0 \exp(-\mathrm{j}2\pi/3)$. Results for the magnetic flux density at the height of $y_\mathrm{R} = 40$ cm above the

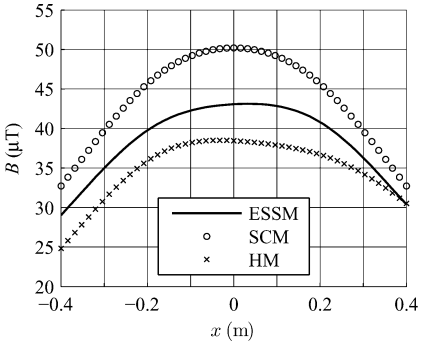

Fig. 17. Comparison with the SCM and HM for the finite-width flat magnetic-metal shield.

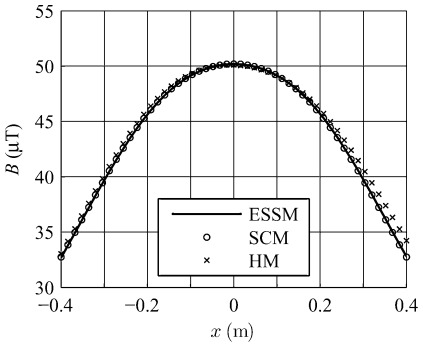

Fig. 18. Comparison with the SCM and HM for the finite-width flat magnetic-metal shield at an ULF.

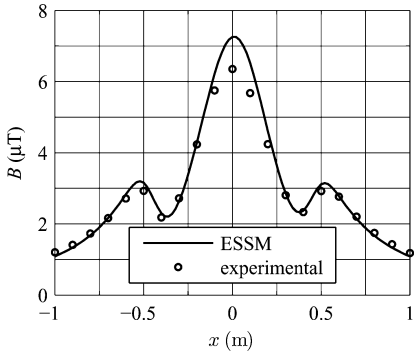

Fig. 19. Comparison with the experimental results for the finite-width flat nonmagnetic-metal shield at $y_{\mathrm{R}} = 30$ cm.

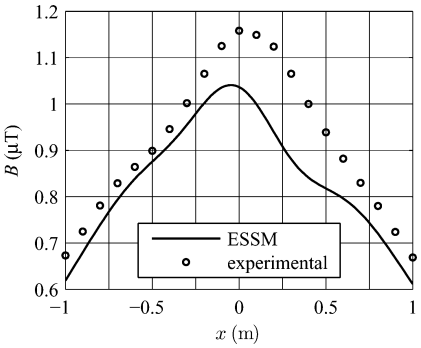

Fig. 20. Comparison with the experimental results for the finite-width flat nonmagnetic-metal shield at $y_{\mathrm{R}} = 70$ cm.

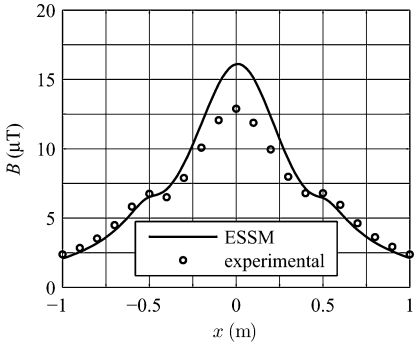

Fig. 21. Comparison with the experimental results for the finite-width flat magnetic-metal shield at $y_{\mathrm{R}} = 30$ cm.

wires are given in Figs. 17 and 18. For the case in Fig. 17, the numerical data are $I_0 = 400\,\mathrm{A}$, $f = 50$ Hz, $y_{\mathrm{S}} = 10$ cm, $d = 8$ cm, $l = 40$ cm, $t = 2$ mm, $\gamma_{\mathrm{S}} = 10$ MS/m, and $\mu_{\mathrm{S}} = 1000\,\mu_0$. The HM agreement with the ESSM is not quite good ($\epsilon_{\mathrm{mean\ abs.}} \doteq 9.5\,\%$). The SCM agreement with the ESSM is even worse ($\epsilon_{\mathrm{mean\ abs.}} \doteq 13.4\,\%$) because the magnetostatic approximation does not consider the induced eddy currents. This is why a second test (see Fig. 18) is made where only the frequency is changed ($f = 1$ Hz). This time, the SCM agreement is excellent ($\epsilon_{\mathrm{mean\ abs.}} \doteq 0.09\,\%$) and better than the HM one ($\epsilon_{\mathrm{mean\ abs.}} \doteq 1.1\,\%$). This proves that the magnetostatic approximation is justifiable only when the impact of the induced eddy currents is negligible, this being at a very low frequency [6] (or for laminated magnetic shields and ferrite shields).

4) Experimental Results: Our experiment is made for the configuration shown in Fig. 14. The two-sidedly grounded flat shield is $l = 1$ m wide and 8 m long, and is placed $y_{\mathrm{S}} = 20$ cm above the wires of a three-phase system: $I_{\mathrm{C1}} = I_0 \exp(\mathrm{j}2\pi/3)$, $I_{\mathrm{C2}} = I_0$, $I_{\mathrm{C3}} = I_0 \exp(-\mathrm{j}2\pi/3)$, $I_0 = 100\,\mathrm{A}$, $f = 50$ Hz, and $d = 8$ cm. Grounding is considered to be ideal in the numerical calculation. Two types of shields are used: 1) $t = 4$ mm thick Al shield ($\gamma_{\mathrm{S}} = 30.5$ MS/m and $\mu_{\mathrm{S}} = \mu_0$) and 2) $t = 1.6$ mm thick steel shield ($\gamma_{\mathrm{S}} = 10$ MS/m and $\mu_{\mathrm{S}} = 100\,\mu_0$). The magnetic flux density is measured by the Wandel and Goltermann EFA-3 electromagnetic (EM) field analyzer.

A comparison between the measured and calculated magnetic flux density magnitudes above the shield is made at the heights of $y_{\mathrm{R}} = 30$ cm and $y_{\mathrm{R}} = 70$ cm above the wires. Figs. 19 and 20 provide a comparison for the nonmagnetic (Al) shield, and Figs. 21 and 22 for the magnetic (Fe) shield. The average absolute values of the relative deviation of the measured results from the calculated one are $5.5\,\%$, $9.6\,\%$, $12.0\,\%$, and $4.7\,\%$ for the data on Figs. 19, 20, 21, and 22, respectively.

IV. Presentation of the Results

The ESSM enables a prominent presentation of its results. How the calculated field or how the shielding factor can be presented is demonstrated on the configuration shown in Fig. 23. The shield is two-sidedly (ideally) grounded. The numerical data are $I_0 = 400\,\mathrm{A}$, $f = 50$ Hz, $y_{\mathrm{S}} = 13$ cm, $d = 8$ cm, $l = 70$ cm, $h = 40$ cm, $t = 1$ cm, $\gamma_{\mathrm{S}} = 10$ MS/m, and $\mu_{\mathrm{S}} = 100\,\mu_0$ (steel).

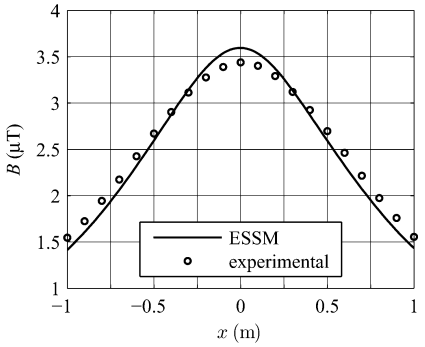

Fig. 22. Comparison with the experimental results for the finite-width flat magnetic-metal shield at $y_{\mathrm{R}} = 70$ cm.

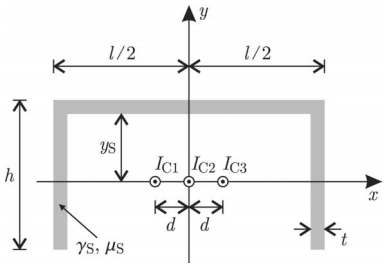

Fig. 23. Shield of a U-shape. The wires are a three-phase system: $I_{\mathrm{C}1} = I_0 \exp(\mathrm{j}2\pi/3)$, $I_{\mathrm{C}2} = I_0$, and $I_{\mathrm{C}3} = I_0 \exp(-\mathrm{j}2\pi/3)$.

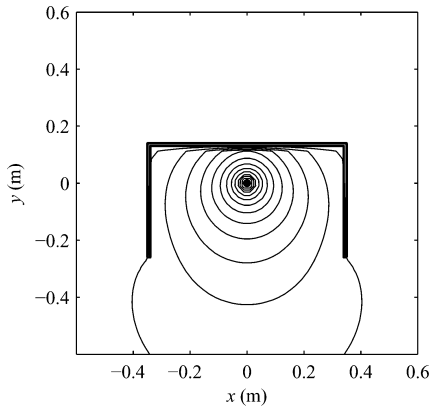

Fig. 24. Magnetic field around a U-shaped shield in the case of one-phase excitation.

Fig. 24 illustrates the magnetic flux lines in the presence of only the middle wire (one-phase excitation). It is evident that the ferromagnetic shield "catches" a lot of the magnetic flux (flux shunting).

Fig. 25 shows contours of the constant shielding factor values for the case of three-phase excitation. The reason why we here draw the contours of the shielding factor values from 1 to 20 alone is because they are sufficient to show the shielding tendency and because the contours of the higher shielding factor values are getting thicker. Attenuation of the magnetic field is evidently greater than ten times almost everywhere above the shield ($y > y_{\mathrm{S}} + t$).

Let us now add another shield. It is flat and 80 cm wide (thickness and material parameters are the same as for the first

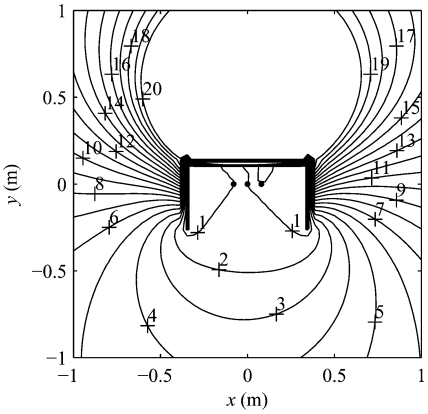

Fig. 25. Shielding factor around a U-shaped shield in the case of three-phase excitation.

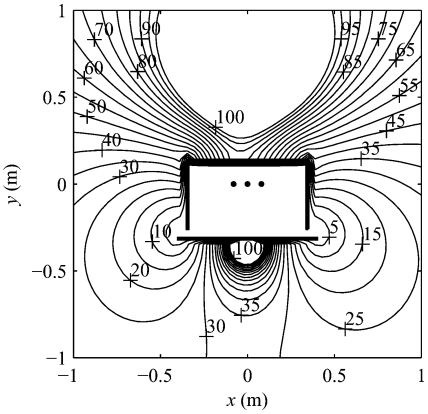

Fig. 26. Shielding factor around a two-shield structure in the case of three-phase excitation.

shield). When placing this additional shield horizontally below the first one, so that the wires are surrounded by the shields, the shielding factor is considerably increased everywhere and not only below the shields, as illustrated in Fig. 26 (showing only the contours of the shielding factor values from 5 to 100). The worst shielding effect is in the vicinity of the slots between the shields.

Presentation of the calculated field, like in Figs. 24, 25, and 26, offers an excellent insight into the shielding effect. Such analysis is found to be a very useful tool in designing shielding structures.

V. Conclusion

By comparing the ESSM with several other methods and by presenting its results, it is clear that it allows for a highly accurate calculation of the magnetic field either before, inside, or behind shields, thus providing good insight into the effectiveness of a shield we intend to choose.

The ESSM is suitable for lossy nonferrous as well as ferrous shields provided the material media are linear. Its methodology is the same for the nonmagnetic and magnetic shields meaning that structures that contain either of the two can be analyzed.

The proposed method does not impose any restrictions on the geometry of the longitudinally symmetric structures or the number of shields.

Unlike many other methods, our method is not limited to the ELF fields. Though the frequency is theoretically limited by the quasi-static field assumption, it is in practice limited by computer capability, i.e., by the number of the boundary elements the computer can deal with. This number depends on the admissible boundary element length that is related to the frequency-dependent skin depth.

Until now, none of the methods presented in literature have considered the impact of the ground vicinity, different types of grounding, and electric connections between shields.

Judging from the facts presented before, the proposed method can be considered as one of the most general and efficient 2-D calculation method for estimation of the magnetic field shielding effectiveness.

REFERENCES

[1] R. G. Olsen, M. Istenič, and P. Žunko, "On simple methods for calculating ELF shielding of infinite planar shields," *IEEE Trans. Electromagn. Compat.*, vol. 45, no. 3, pp. 538–547, Aug. 2003.

[2] R. G. Olsen and P. Moreno, "Some observations about shielding extremely low-frequency magnetic fields by finite width shields," *IEEE Trans. Electromagn. Compat.*, vol. 38, no. 3, pp. 460–468, Aug. 1996.

[3] M. Istenič and R. G. Olsen, "A simple hybrid method for ELF shielding by imperfect finite planar shields," *IEEE Trans. Electromagn. Compat.*, vol. 46, no. 2, pp. 199–207, May 2004.

[4] L. Sandrolini, A. Massarini, and U. Reggiani, "Transform method for calculating low-frequency shielding effectiveness of planar linear multilayered shields," *IEEE Trans. Magn.*, vol. 36, no. 6, pp. 3910–3919, Nov. 2000.

[5] Y. Du, T. C. Cheng, and A. S. Farag, "Principles of power-frequency magnetic field shielding with flat sheets in a source of long conductors," *IEEE Trans. Electromagn. Compat.*, vol. 38, no. 3, pp. 450–459, Aug. 1996.

[6] W. M. Frix and G. G. Karady, "A circuital approach to estimate the magnetic field reduction of nonferrous metal shields," *IEEE Trans. Electromagn. Compat.*, vol. 39, no. 1, pp. 24–32, Feb. 1997.

[7] L. Hasselgren and J. Luomi, "Geometrical aspects of magnetic shielding at extremely low frequencies," *IEEE Trans. Electromagn. Compat.*, vol. 37, no. 3, pp. 409–420, Aug. 1995.

[8] P. Silvester, "AC resistance and reactance of isolated rectangular conductors," *IEEE Trans. Power App. Syst.*, vol. PAS-86, no. 6, pp. 770–774, Jun. 1967.

[9] A. Canova, G. Gruosso, and M. Repetto, "Integral methods for analysis and design of low-frequency conductive shields," *IEEE Trans. Magn.*, vol. 39, no. 4, pp. 2009–2017, Jul. 2003.

[10] W. P. Legros and P. G. Scarpa, "Fast computation of magnetic field in rotationally symmetric structures," *IEEE Trans. Magn.*, vol. MAG-21, no. 6, pp. 2644–2651, Nov. 1985.

[11] H. A. Haus and J. R. Melcher, *Electromagnetic Fields and Energy*. Englewood Cliffs, NJ: Prentice-Hall, 1989.

[12] R. F. Harrington, *Time-Harmonic Electromagnetic Fields*. New York: Wiley Interscience, 2001.

[13] P. K. Kythe, *An Introduction to Boundary Element Methods*. Boca Raton, FL: CRC Press, 1995.

[14] C. Pozrikidis, *A Practical Guide to Boundary Element Methods with the Software Library BEMLIB*. London, U.K./Boca Raton, FL: Chapman & Hall/CRC Press, 2002.

[15] P. Zhou, *Numerical Analysis of Electromagnetic Fields*. Berlin, Germany: Springer-Verlag, 1993.

[16] M. V. K. Chari and S. J. Salon, *Numerical Methods in Electromagnetism*. San Diego, CA: Academic Press, 2000.

[17] N. Morita, N. Kumagai, and J. R. Mautz, *Integral Equation Methods for Electromagnetics*. Boston, MA: Artech House, 1990.

[18] J. R. Carson, "Wave propagation in overhead wires with ground return," *Bell Syst. Tech. J.*, vol. 5, pp. 539–554, Oct. 1926.

[19] R. F. Harrington, *Field Computation by Moment Methods*. Piscataway, NJ: IEEE Press, 1993.

[20] H. Kaden, *Wirbelströme und Schirmung in der Nachrichtentechnik*. Berlin, Germany: Springer-Verlag, 1959.

[21] J. R. Wait and D. A. Hill, "Electromagnetic shielding of sources within a metal-cased bore hole," *IEEE Trans. Geosci. Electron.*, vol. 15, no. GE-2, pp. 108–112, Apr. 1977.

[22] J. F. Hoburg, "Principles of quasistatic magnetic shielding with cylindrical and spherical shields," *IEEE Trans. Electromagn. Compat.*, vol. 37, no. 4, pp. 574–579, Nov. 1995.

[23] J. F. Hoburg, "A computational methodology and results for quasistatic multilayered magnetic shielding," *IEEE Trans. Electromagn. Compat.*, vol. 38, no. 1, pp. 92–103, Feb. 1996.

[24] J. F. Hoburg, B. A. Clairmont, D. W. Fugate, and R. J. Lordan, "Comparisons of measured and calculated power frequency magnetic shielding by multilayered cylinders," *IEEE Trans. Power Del.*, vol. 12, no. 4, pp. 1704–1710, Oct. 1997.

[25] O. Bottauscio, M. Chiampi, D. Chiarabaglio, F. Fiorillo, L. Rocchino, and M. Zucca, "Role of magnetic materials in power frequency shielding: Numerical analysis and experiments," in *Proc. Inst. Elect. Eng. Gener. Transmiss. Distrib.*, Mar. 2001, vol. 148, pp. 104–110.

Edi Bulić was born in Pula, Croatia, in 1973. He received the B.Sc. and M.Sc. degrees in electrical engineering from the University of Ljubljana, Ljubljana, Slovenia, in 1997 and 2000, respectively.

Since 1997, he has been an Assistant Professor of electromagnetics and basics in electrical engineering in the Faculty of Electrical Engineering, University of Ljubljana. His current research interests include numerical computation of the electromagnetic field.

Anton R. Sinigoj was born in Ljubljana, Slovenia, in 1955. He received the B.Sc., M.Sc., and Ph.D. degrees in electrical engineering from the University of Ljubljana, Ljubljana, in 1978, 1982, and 1989, respectively.

Since 1989, he has been an Assistant Professor in the Faculty of Electrical Engineering, University of Ljubljana. His current research interests include electromagnetic fields, numerical methods in electromagnetics, antennas and propagations in optical fibers, electric and magnetic shielding, and induction warming. He has authored or coauthored the books *Fundamentals of Electrical Engineering* and *Electromagnetic Fields* (Ljubljana, Slovenia: FE and FRI Publishing, 1994 and 1996, respectively).

Breda Cestnik was born in Slovenia in 1967. She received the B.Sc. and M.Sc. degrees in electrical engineering from the Faculty of Electrical Engineering, University of Ljubljana, Ljubljana, Slovenia, in 1990 and 1999, respectively.

Since 1990, she has been a Researcher at Milan Vidmar Electric Power Research Institute, Ljubljana. Her current research interests include effects of electric devices on the environment.